POLITECNICO DI MILANO

Scuola di Ingegneria dei Processi Industriali

Dipartimento di Chimica, Materiali e Ingegneria Chimica "G. Natta"

Master of science in Materials engineering and Nanotechnologies

PROBABILITY OF STAINLESS STEEL CORROSION: EXPERIMENTAL VALIDATION OF THE MARKOV'S CHAINS MATHEMATICAL MODEL

Tutor: **Prof. Marco ORMELLESE**

Co-tutor: **Ing. Andrea BRENNA**

Chiara DE ANGELIS

Matr. 770400

Anno accademico 2012-2013

CONTENTS

CONTENTS OF FIGURES

CONTENTS OF TABLES

CONTENTS OF PLOTS

ABSTRACT

Stainless steels are widely used in industrial application for their corrosion resistance; nevertheless, in presence of chloride ions, they may be subject of localized corrosion attack, as pitting and crevice, which, once initiated, rapidly propagates and leads to equipment failure. Due to the stochastic nature of pitting phenomenon and, in particular, of its initiation, a statistical approach is mandatory for initiation time prediction and, then, for materials selection in engineering application. In this work is proposed a Markov chain's mathematical model which assumes that pitting retains no memory of its past history and is characterized by two absorbing conditions (pitting and repassivation) and three transitional states (metastable, metapassive, metapitting); the model takes into account metallurgical and environmental factors, as material composition (PREN), chlorides concentration, pH, temperature, fluidodynamic condition and oxidant power of the system, with the aim to calculate the corrosion probability of stainless steels in different industrial and natural environments. The proposed equations, which relate input parameters and transitional probabilities were, initially, empirical expressions based on engineering knowledge of corrosion behavior of stainless steels; aim of this thesis is to validate and confirm these mathematical expressions: electrochemical tests (potentiostatic, potentiodynamic and linear polarization resistance tests) were carried out and the experimental results, in addition of literature corrosion data, were carefully elaborated in order to propose new revised equations of Markov model.

INTRODUZIONE

Gli acciai inossidabili sono utilizzati negli impianti industriali per la loro elevata resistenza a corrosione; tuttavia, in presenza di cloruri, possono essere soggetti a pericolose forme di attacco localizzato come pitting e crevice. Nella corrosione per pitting si distinguono due stadi: l'innesco del pit e la sua propagazione; poiché una volta innescato il pit propaga velocemente, molte risorse sono state impiegate, sia in passato che nel presente, nel tentativo di trovare modelli che permettano la previsione del tempo d'innesco; il pitting è un fenomeno intrinsecamente stocastico, il cui innesco è caratterizzato da una variabilità sia temporale che spaziale: la sua previsione deve essere effettuata, quindi, secondo un approccio probabilistico. In questo scenario si inserisce la proposta di un modello matematico che utilizza delle matrici di Markov per la previsione della probabilità d'innesco del pitting e che risulta particolarmente utile per la classificazione della resistenza a pitting dei diversi acciai inossidabili. Caratteristica di un processo stocastico markoviano è l'assenza di memoria: la sua evoluzione temporale dipende, quindi, solo dal suo stato attuale. Per la descrizione del fenomeno del pitting è stato proposto un modello a catene di Markov a cinque stadi che prevede due stati assorbenti, quello di pitting e di ripassivazione, e tre stati di transizione, quello matastabile, di metapitting e di metapassività, come mostrato in figura.

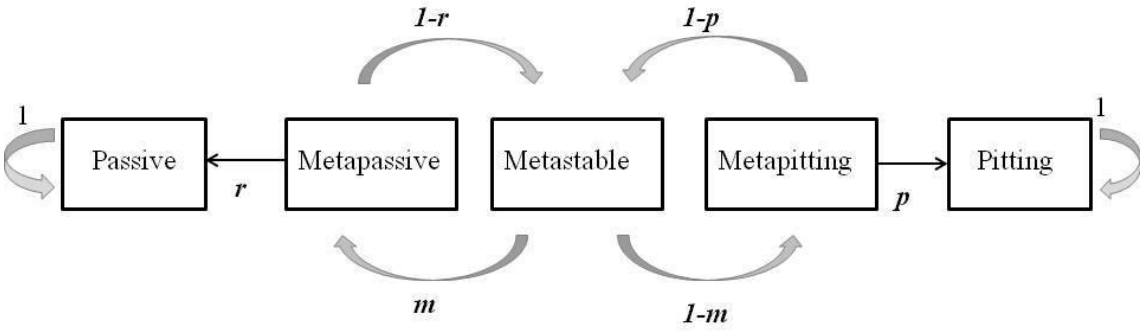

Modello di Markov a 5 stadi.

Le probabilità *r*, *m* e *p* sono state inizialmente definite mediante relazioni empiriche in funzione dell'acciaio inossidabile (PREN) e di parametri operativi, come contenuto di

cloruri, pH, temperatura, condizioni fluidodinamiche e potere ossidante del sistema, tarate sulla base della conoscenza ingegneristica del comportamento degli acciai inossidabili. Questo lavoro di tesi si propone l'obbiettivo di validare queste equazioni tramite elaborazione di dati di letteratura ed esperimenti di laboratorio. Sono state effettuate delle prove potenziostatiche con tre acciai inossidabili (PREN 17, 18 e 24) in diverse condizioni definite dal potenziale di polarizzazione, dalla temperatura e dal contenuto di cloruri; le prove hanno permesso di ottenere valori sperimentali di probabilità di corrosione che sono stati confrontati con quelli previsti dal modello di Markov esistente: è stata osservata una differenza rilevante tra i risultati di laboratorio e quelli del modello, soprattutto per le condizioni sperimentali meno aggressive. Tenendo comunque sempre presente i limiti delle prove di corrosione accelerate e la difficoltà dell'interpretazione dei loro risultati, sono state effettuate prove elettrochimiche (potenziodinamiche e di polarizzazione lineare) volte alla modifica delle equazioni della probabilità *p* e *m*: la struttura matematica del modello e i fattori d'influenza delle probabilità sono rimasti invariati ma si sono apportate delle modifiche nelle relazioni tra i parametri di input e le probabilità.

La tesi è strutturata in sei capitoli: nel primo viene descritto il fenomeno della corrosione localizzata degli acciai inossidabili e i suoi fattori d'influenza; nel secondo si sottolinea l'importanza dell'approccio probabilistico per la descrizione dello stadio d'innesco del pitting e si propongono le equazioni esistenti del modello di Markov a cinque stadi; il terzo capitolo descrive le prove di polarizzazione potenziostatica effettuate e propone, tramite tabelle e istogrammi, il confronto tra le probabilità di corrosione sperimentali e quelle del modello. Il capitolo quattro è incentrato sulla probabilità *p*: tramite la rielaborazione di dati di letteratura sono proposte due nuove equazioni che vengono validate per mezzo di prove sperimentali (potenziodinamiche). Nel capitolo cinque vengono descritte le prove di polarizzazione lineare effettuate a diversi pH e temperature, i cui risultati, rielaborati, permettono di modificare due delle equazioni che definiscono la probabilità *m*. Le nuove equazioni delle probabilità *p* e *m* sono state quindi sostituite nel modello e le risultanti probabilità di corrosione, calcolate tramite Matlab®, sono state confrontate nel capitolo sei con quelle sperimentali e del vecchio modello.

Chapter 1

CORROSION OF STAINLESS STEEL: AN OVERVIEW

1.1 STAINLESS STEELS

Stainless steels are iron-chromium or iron-chromium-nickel alloys containing a minimum of approximately 11% chromium; this amount of chromium allows the formation on the metal surface of a thin protective oxide film (thickness in the order of 1 to 10 nm) which reduces steel corrosion rate in several environments, as neutral electrolytes without chlorides. In order to be protective from corrosion, the oxide film must be stable in the environment where the metal works, it must be compact, uniform and non-porous over the entire surface of the metal.

In addition to chromium, other alloying elements provide specific properties or ease of fabrication. The most beneficial elements to increase corrosion resistance are chromium, molybdenum, tungsten, nitrogen and nickel; otherwise, sulfur and manganese are considered detrimental [1].

Commercial stainless steels are divided into three groups according to the metallurgical structure: austenitic, ferritic and martensitic. The American Iron and Steel Institute (AISI) designates standard grades of stainless steels by three digit numbers. The austenitic grades are designated by codes in the 200 and 300 series, whereas the ferritic and martensitic grades are designated in the 400 series. Duplex stainless steels, precipitation hardening stainless steels and cast stainless steels are generally known by other designations [1].

The Schaeffler diagram (Fig.1.1) relates the metallurgical structure with the composition of stainless steels, conveniently expressed in terms of either nickel equivalent (austenite stabilizer) or chromium equivalent (ferrite stabilizer) on a weight percentage basis. It is not an equilibrium diagram because it indicates the structure obtained after rapid cooling at room temperature from 1050°C. The alloying elements commonly found in stainless steels are divided either as austenite stabilizer (nickel, cobalt, carbon, nitrogen, manganese, copper) or ferrite stabilizer (chromium, silicon, molybdenum, vanadium, aluminum, niobium, titanium). Austenite stabilizers extend the γ-domain of the steel equilibrium

diagram, chromium, instead, acts by closing the γ-region increasing whose of ferrite. However, when chromium is added to a steel containing nickel it retards the kinetics of the $\gamma \rightarrow \alpha$ transformation, thus making it easier to retain austenite at room temperature [1].

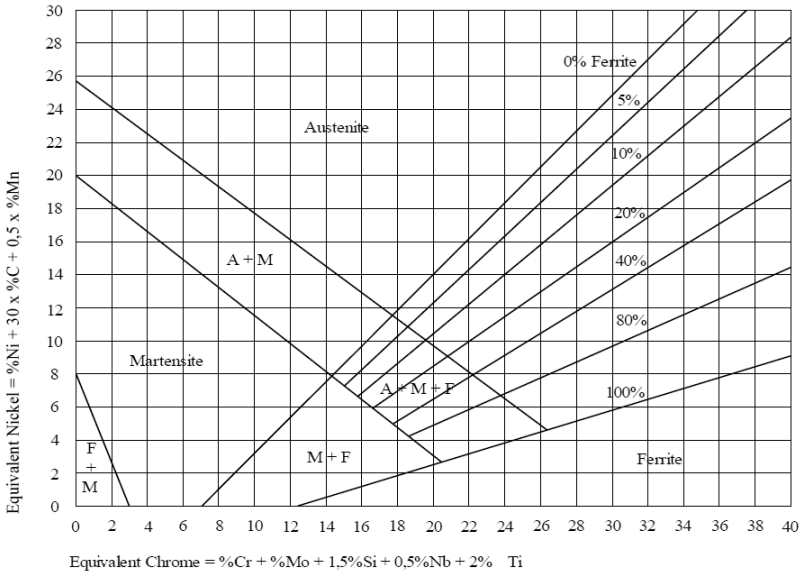

Figure 1.1- Schaeffler diagram [1].

1.1.1 Austenitic stainless steels

As name suggests, austenitic stainless steels show an austenitic microstructure with a faced centered cubic lattice. This structure makes them extremely formable and weldable; they can be successfully used from cryogenic temperatures to the red-hot temperatures of furnaces and jet engines. They contain chromium in the range from 16 to 25%, nickel in the range of 5-15% and other elements in solution, as shown in Table 1.1. The addition of molybdenum improves pitting and crevice corrosion resistance; a low carbon content and/or the addition of titanium reduce intergranular corrosion in welded materials; nickel and chromium are added to improve high temperature oxidation resistance, strength and stress corrosion resistance [1].

Stainless steel type 304, the general purpose grade is widely used in applications requiring a good combination of corrosion resistance and formability and is one studied in this work.

Table 1.1- General chemical composition of austenitic stainless steels available on the market.

AISI grade	C %	Mn %	P %	S %	Si %	Cr %	Ni %	Mo %
201	0,15	5,5÷7,5	0,045	0,015	1	16÷18	3,5÷5,5	-
202	0,15	7,5÷10,5	0,045	0,015	1	17÷19	4÷6	-
301	0,05÷0,15	2	0,045	0,015	2	16÷19	6÷9,5	0,8
304	0,07	2	0,045	0,015	1	17÷19,5	8÷10,5	-
304L	0,03	2	0,045	0,015	1	18÷20	10÷12	-
316	0,07	2	0,045	0,015	1	16,5÷18,5	10÷13	2÷2,5
316L	0,03	2	0,045	0,015	1	16,5÷18,5	10÷13	2÷2,5
330	0,15	2	0,045	0,015	1÷2	15÷17	33÷37	-

1.1.2 Ferritic stainless steels

Stainless steels with ferritic microstructure have a body centered cubic lattice structure: they are less ductile than austenitic stainless steels and not hardenable by heat treatment as martensitic steels; some examples are shown in Table 1.2. They resist corrosion and oxidation and are also resistant to stress corrosion cracking; ferritic stainless steels are used for decorative trim, sinks and automotive applications, particularly exhaust system. The most popular ferritic grade is type 430, with a range of chromium content between 12 and 18%: a low chromium content (12-13%) improves weldability, impact resistance, strength and hardness, but implies loss in corrosion resistance; an high chromium content (16-18%) involves gain in corrosion resistance but loss in mechanical properties [1].

Table 1.2- General chemical composition of ferritic stainless steels available on the market.

AISI grade	C %	Mn %	P %	S %	Si %	Cr %	Ni %	Mo %
405	0,08	1,0	0,04	0,015	1	12÷14	-	-
409	0,03	1	0,04	0,015	1	10,5÷12,5	0,3÷1	-
430	0,08	1	0,04	0,015	1	16÷18	-	-
439	0,05	1	0,04	0,015	1	16÷18	-	-
446	0,15÷0,2	1	0,04	0,015	1	26÷29	-	-

1.1.3 Martensitic stainless steels

Martensitc stainless steels have an austenitic structure at elevated temperatures which can be transformed into martensite by a proper cooling (quenching) to room temperature. After quenching they show a martensitic structure characterized by a body centered tetragonal lattice, high hardness and mechanical strength. In martensitic stainless steels chromium lies in the range from 11,5 to 18%, with the lower limit being governed by corrosion resistance and the upper limit by the requirement for the alloy to convert fully to austenite during heating. After rapid cooling, the steels hardened by transformation martensite must be tempered (heated at a temperature such as to achieve hardness reduction) in order to obtain mechanical properties suitable for engineering applications [2]. Martensitic grades (some example in Table 1.3) are used when, in addition to moderate corrosion resistance, hardness, strength and wear resistance are required, so for istance for turbine components, valve parts, cutlery, fasteners and machinery parts.

Table 1.3- General chemical composition of martensitic stainless steels available on the market.

AISI grade	C %	Mn %	P %	S %	Si %	Cr %	Ni %	Mo %
403	0,08÷0,15	1,5	0,04	0,015	1	11,5÷13,5	0,75	-
416	0,08÷0,15	1,5	0,04	0,015÷0,025	1	12÷13,5	-	0,6
420	0,16÷0,25	1,5	0,04	0,015	1	12÷14	-	-
440A	0,65÷0,75	1	0,04	0,015	0,70	14÷16	-	0,5

1.1.4 Duplex stainless steels

Duplex stainless steels show a two-phases microstructure consisting of ferritic and austenitic grains, roughly 50% austenite and 50% ferrite. Duplex stainless steels show a mechanical strength which is twice higher than austenitic or ferritic stainless steels; they have significantly better toughness and ductility than ferritic grades although they don't reach the excellent values of austenitic grades.

Duplex stainless steels also improved resistance to localized corrosion, particularly pitting, crevice corrosion and stress corrosion cracking. They are characterized by high chromium (up to 32%) and molybdenum (4-5%) and lower nickel contents than austenitic stainless

steels (Table 1.4). They are widely used in chemical process industry, not only in chlorides containing environments, where they are more resistant to stress corrosion cracking than austenitic grades, but also in strongly alkaline chlorides-bearing solution, in caustic fluids and high temperature application.

Table 1.4- General chemical composition of duplex stainless steels available on the market.

AISI grade	C %	Mn %	P %	S %	Si %	Cr %	Ni %	Mo %
329	0,05	2	0,035	0,015	1	25÷28	4,5÷6,5	1,3÷2
S31803	0,03	2	0,035	0,015	1	21÷23	4,5÷6,5	2,5-3
S32550	0,03	2	0,035	0,015	0,7	24÷26	5,5÷7,5	2,7÷4
S32760	0,03	1	0,035	0,015	1	24÷26	6÷8	3÷4

1.2 CORROSION FORMS OF STAINLESS STEEL

1.2.1 General corrosion

Uniform (or general) corrosion is a corrosion attack uniformly distributed over the entire surface of a metal. Corrosion proceeds at approximately the same rate over the metal surface. The material becomes thinner as it corrodes until its thickness is reduced to the point at which failure occurs. Failures by general corrosion are less feared than those by localized corrosion because they are more predictable [1].
Stainless steels can exhibit general corrosion in strong acids, as in chemical plants [1].

1.2.2 Localized corrosion

The most dangerous corrosion form of stainless steels is localized corrosion; it proceeds corresponding to small areas on the metal surface in contact with a corrosive environment. This corrosion form starts with the localized breakdown of the passive film corresponding to surface defects of the metal (as inclusions, welding) or in correspondence of heterogeneity of the electrolyte (area with higher temperature, higher concentration of

aggressive chemicals or with lower pH). Once the passive film is damaged, corrosion propagates into the bulk material with high corrosion rate, up to some mm/year.
Pitting, crevice, stress corrosion cracking, corrosion fatigue and intergranular corrosion are the most frequent causes of failure of stainless steel components.
This work will focus on pitting and crevice corrosion which will be described in the following.

1.3 PITTING CORROSION

Pitting is a form of localized corrosive attack that leads to the creation of localized anodic area (pits) on the metal surface (Fig. 1.2); due to the high corrosion rate corresponding to the formed pits, their depth can affect in a short time the whole thickness of metal walls [4]. As every localized corrosion form, pitting is considered detrimental for the engineering use of stainless steels and must be correctly prevented.

Figure 1.2- Typical shape of pitting corrosion attack [4].

1.3.1 Pitting corrosion mechanism

Pitting corrosion attack can be divided in two stages: initiation and propagation. Pitting initiation is related to interaction between chloride ions and the passive film, whose inclusions, second phases and areas of compositional heterogeneity, which are always present in commercially produced stainless steels, are preferential sites for pits nucleation; pits may also nucleate in regions where the environment is more aggressive, due, for example, to temperature or chlorides concentration increase or pH decrease [4].

The pit propagation process is illustrated schematically in Fig.1.3 for a stainless steel in neutral aerated sodium chloride solution.

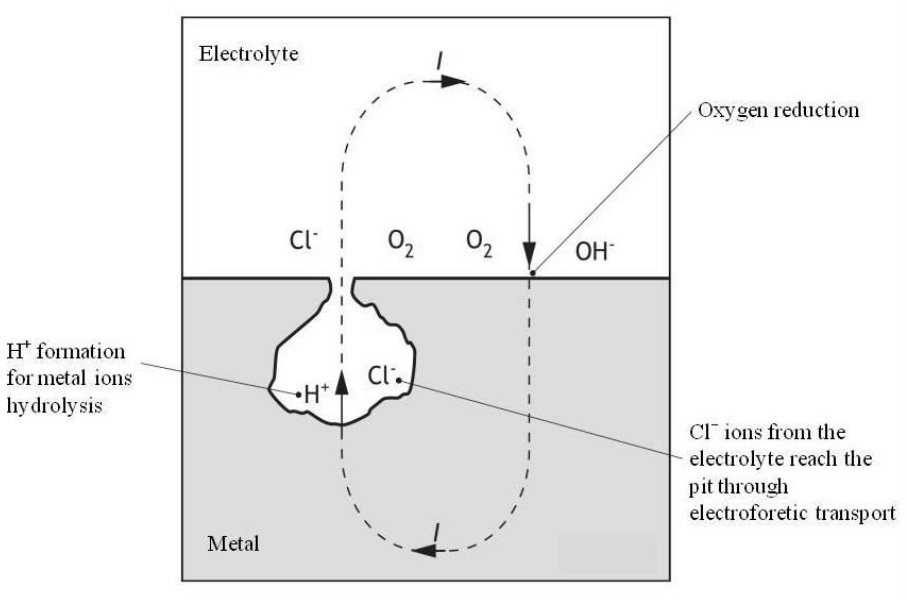

Figure 1.3- Pitting corrosion attack mechanism [4].

Once pits are initiated they may continue to grow by a self sustaining mechanism [1]: pit propagation involves the creation of a macrocouple current between the anodic area (pit), where dissolution of the metal occurs ($M \rightarrow M^+ + e^-$), and the cathodic area (adjacent metal), where oxygen reduction occurs ($O_2 + 2H_2O + 4e^- \rightarrow 4OH^-$). The anodic current density can be very high compared to the cathodic one, because the ratio between cathodic area and anodic area can also reach values higher than 1000 [4]: then, to gain electrons balance, the anodic current must be much greater than the cathodic one.

During propagation stage, the solution inside the pit becomes gradually more aggressive due to the hydrolysis reactions of metal ions ($M^{z+} + zH_2O \rightarrow M(OH)_z + zH^+$), which determine a progressive acidification; meanwhile, the pH of the bulk solution remains neutral or increases thank to cathodic oxygen reduction. Furthermore, the circulation of the macrocouple current favors the increase of chlorides ions concentration within the pit [4]. Consequently, pitting corrosion attack propagates with increasing speed (autocatalytic mechanism) and does not tend to spread to the surface of the material, but to penetrate inside. Corrosion rate can reach high values, in many cases of the order of few millimeters per year [4].

1.3.2 Thermodynamic and kinetic aspects of pitting corrosion

In order to understand the thermodynamic corrosion behavior of stainless steels, the chromium potential-pH diagram (Pourbaix diagram) should be considered. Pourbaix diagram enables the determination of condition (pH and potential intervals) for immunity, where no corrosion is possible, passivation, where a corrosion product film forms and may confer protection against corrosion, and for corrosion, where corrosion is expected [2]. Figure 1.4 shows chromium Pourbaix diagram, main element of the stainless steel protective film: in a large range of pH (neutral and passive) and potential, the protective chromium oxides film, which lowers stainless steel corrosion rate to negligible values, is stable. As already explained, passive film stability decreases in chlorides containing environment; Figure 1.5 shows chromium Pourbaix diagram in solutions containing chlorides: the stability region of chromium oxide in dramatically reduced.

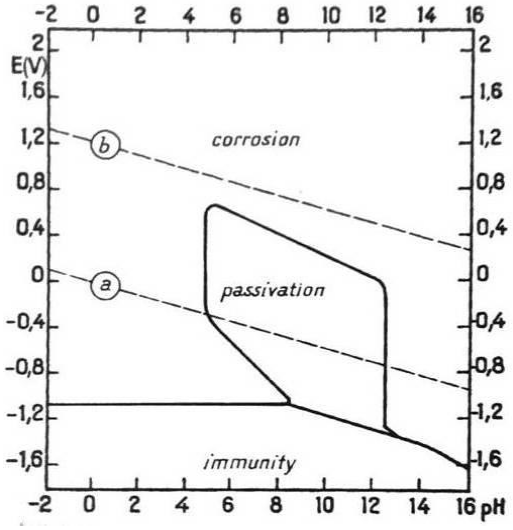

Fig. 1.4- Chromium Pourbaix diagram [5].

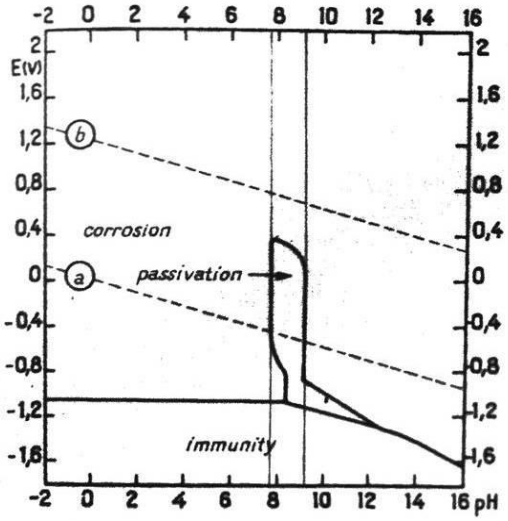

Fig. 1.5- Chromium Pourbaix diagram in solution containing chlorides [5].

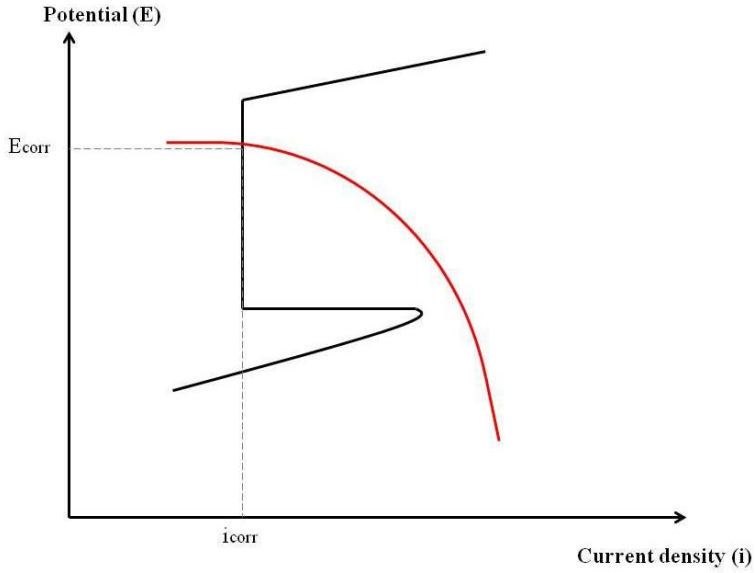

Fig. 1.6- Evan's diagram: anodic curve of a passive metal and cathodic curve (red line) arising from oxidizing condition.

Passivity of stainless steels can be studied by means of the potential-current curves (Evan's diagram) which represent cathodic and anodic partial reactions constituting the overall corrosion process. Figure 1.6 shows the intersection of the anodic curve of stainless steel and the cathodic curve resulting from oxidizing condition. The intersection point defines the corrosion potential E_{corr} and the corrosion current i_{corr}.

Figure 1.7 shows the general features of a passive material (as stainless steel) anodic curve: the current initially increases with an increase in potential until the potential reaches E_p (passivating potential); the current density than decreases markedly to the passive current density i_p, signaling the onset of passivity. When the potential reaches the value E_{bd} (breakdown potential or pitting potential) the current density increases above i_p and corrosion starts [2]. In the transpassive region oxygen evolution and possibly increased corrosion is observed. It's important to point out that, at potentials far below E_{bd}, and during the induction time before the onset of stable pitting at potentials above the pitting potential, metastable pits can form; metastable pits are pits that initiate and grow for a limited period before repassivating: they are typically considered to be those of µm size at most with a lifetime on the order of seconds or less [6]. The effect of chloride ions on the anodic curve of stainless steel (section 1.3.6) is that of reducing pitting potential and then the passivity region (Fig.1.8).

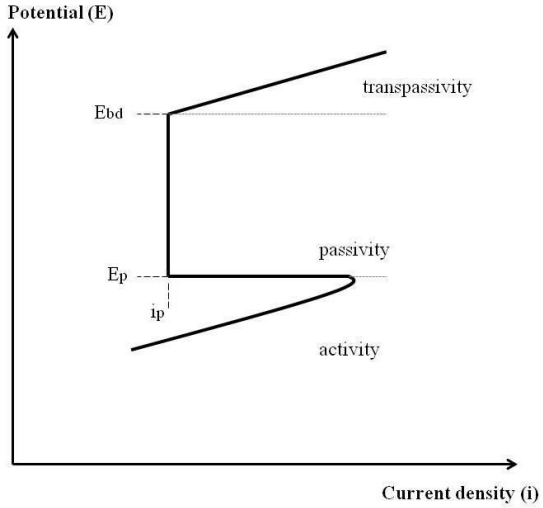

Fig. 1.7- Anodic curve of stainless steel.

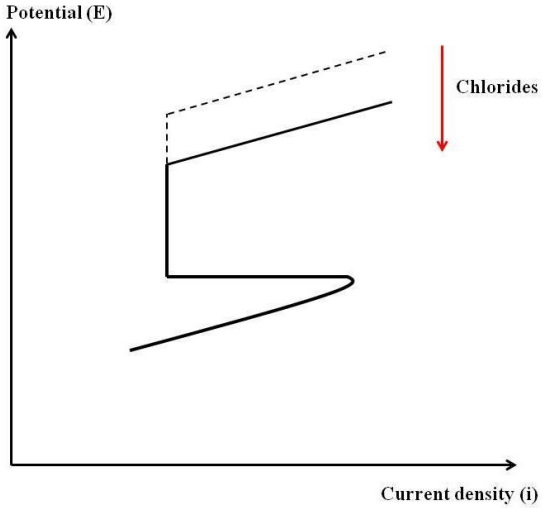

Fig. 1.8- Effect of chlorides of anodic curve of stainless steel.

Another anodic curve feature of great interest is the repassivation potential, E_{rp} (or protection potential, E_{prot}), shown in Figure 1.9. In general, once initiated, localized corrosion sites can propagate only at some potential more positive than the protection potential [7] ; in other words, even after pitting initiation, repassivation will occur at more negative potential. Therefore, the more positive E_{prot} is, the less likely localized corrosion will propagate. At potential between E_{bd} and E_{prot}, sites that have initiated can propagate.

The Pedeferri diagram (Fig.1.10) shows conditions for immunity, passivity and corrosion in terms of chlorides concentration and potential and is commonly used to evaluate initiation condition of reinforced concrete in presence of chlorides. Carbon steel rebars are passive because concrete pH is around 12; but, if the chloride concentration reaches the critical threshold, pitting corrosion can start. In the Pedeferri diagram four regions can be identified [4]: the region A is characterized by the conditions that cause the initiation and propagation of the pit; region B provides the conditions that do not allow new pit initiation, but only the propagation of those already started; region C gives the conditions which allow neither the initiation of new pits nor the propagation of already started pits; region D determines the immunity conditions.

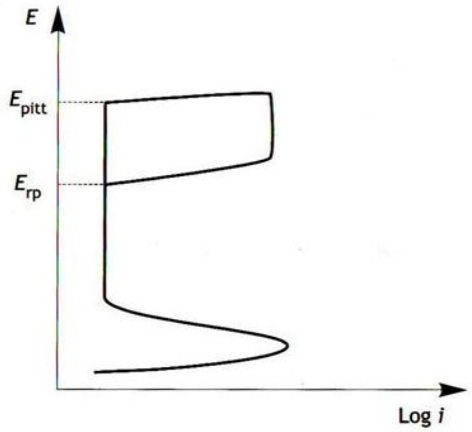

Figure 1.9- Anodic curve of a passive metal: pitting and repassivation potential definition [4].

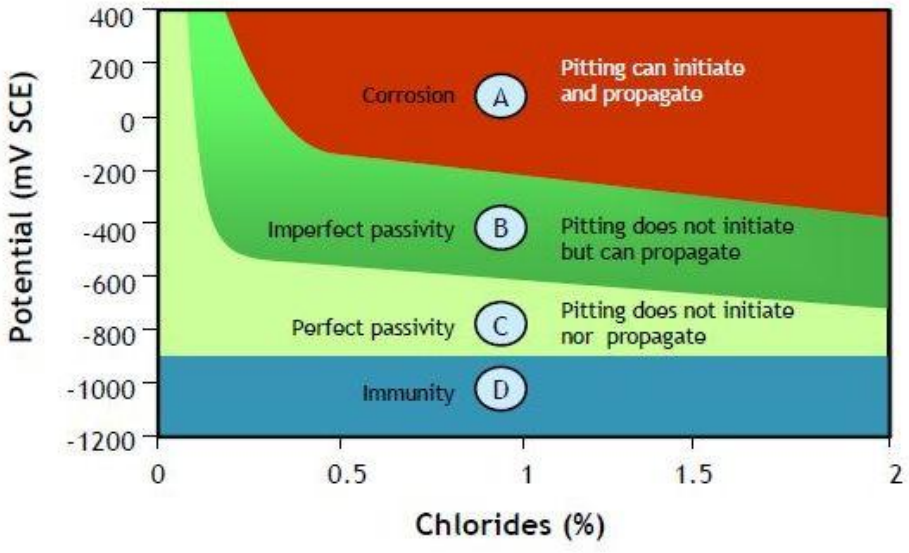

Figure 1.10- Pedeferri diagram [4].

1.3.3 Effect of stainless steels composition on pitting resistance

The corrosion resistance of stainless steels can be increased by modification of the chemical composition of the alloy by introducing some metallic or non metallic elements which improve the corrosion behavior [4]. Generally, alloying elements increase the ability of the metal to form a stable and resistant passive film. Figure 1.11 summarizes the effect of some alloying elements on the anodic curve of stainless steel. In particular, the presence of chromium shifts E_{pitt} towards more noble value and i_c, i_p, which are a measure of the susceptibility to passivation, towards lower values [8]; the addition of molybdenum

increases the strength of the passive film; nitrogen increases corrosion resistance of austenitic stainless steels but can be detrimental for ferritic grade; nickel, although does not interfere with pitting initiation, slows the propagation and favors the repassivation. Niobium and titanium are "stabilizers" because they are able to prevent sensitization phenomena and intergranular corrosion. Otherwise, manganese is affine to sulfur and tends to form sulfides which are sites for pits initiation [9]. Boron, carbon and copper can have a variable effect. Boron is beneficial if it is in solid solution, but detrimental when precipitated as intermetallic compound. Carbon has no effect on pitting resistance if it is in solid solution but is detrimental when precipitated as carbide. Copper has no effect in the absence of molybdenum, but a slightly detrimental effect in its presence [1].

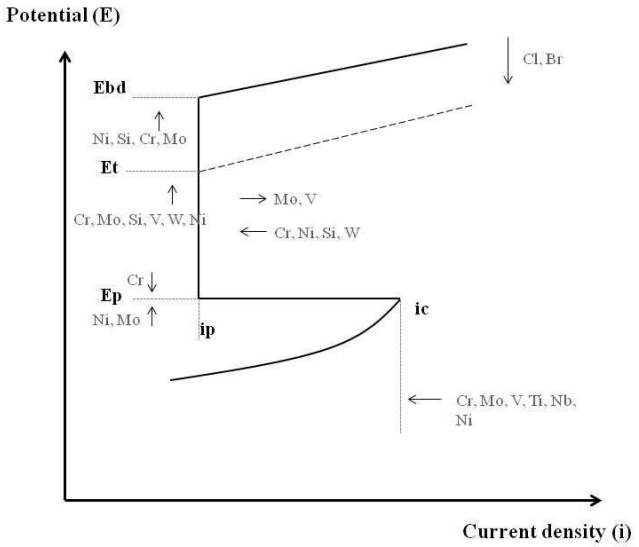

Figure 1.11- Effect of some alloying elements on the anodic polarization curve of stainless steel (adapted from [10]).

The effect of stainless steel composition on pitting corrosion resistance is commonly described by means of the "Pitting Resistance Equivalent Number" (PREN) which takes into account chromium, molybdenum, tungsten and nitrogen concentration by the formula:

Eq. 1.1 $$PREN = [\%Cr] + 3{,}3([\%Mo] + 0{,}5[\%W]) + X[\%N]$$

With X=0 for ferritic stainless steels, X=16 for austenitc and X=30 for duplex stainless steels [11].

This index is used to rank and compare the pitting corrosion resistance of different types of stainless steels. In general the higher is the PREN, the higher will be the chloride concentration tolerable in the solution, the higher will be the breakdown potential [4].
Figure 1.12, 1.13 and 1.14 show the effect of Cr, Mo and Ni, respectively, on pitting potential of different stainless steels in 0,1 N NaCl solution at 25°C (3500 ppm Cl^-).

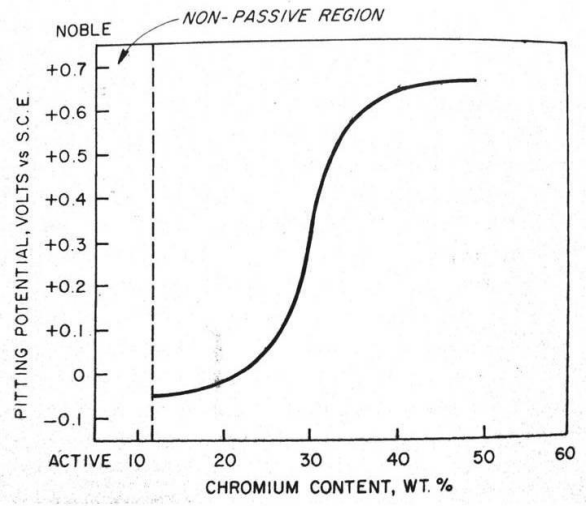

Figure 1.12- Effect of chromium content on pitting potential of iron-chromium alloys in deareated 0.1 N NaCl solution at 25 °C [1].

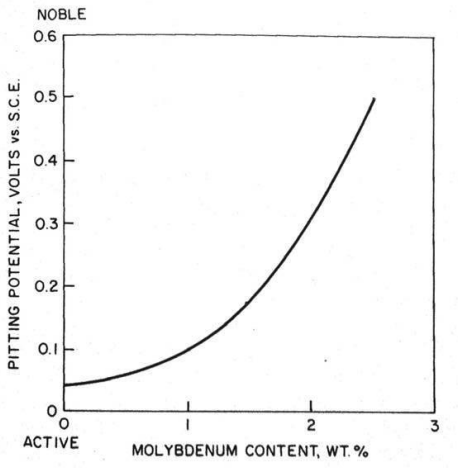

Figure 1.13- Effect of molybdenum content on pitting potential of Fe-15% Cr-13% Ni alloys in a deareated 0.1 N NaCl solution at 25°C [1].

As already explained in section 1.1, a chromium content lower than 12% is not enough to form a stable passive film on the metal surface. Increasing chromium content, stainless steel pitting resistance improves: as shown in Fig. 1.12, up to 20% there is only a small variation of the pitting potential which, instead, increases dramatically for chromium concentration between 25 and 35% and stabilizes to noble value for high chromium content. As shown in Fig. 1.13, the effect of molybdenum content on stainless steel pitting potential is quite strong: molybdenum weight percentage variation from 1 to 2% involves an increase of 200 mV of the pitting potential. The increase of nickel content also improves pitting corrosion resistance, but less dramatically: in particular, as shown in Fig.1.14, every 10% increase of nickel content involves an increase of 5 mV of stainless steel pitting potential.

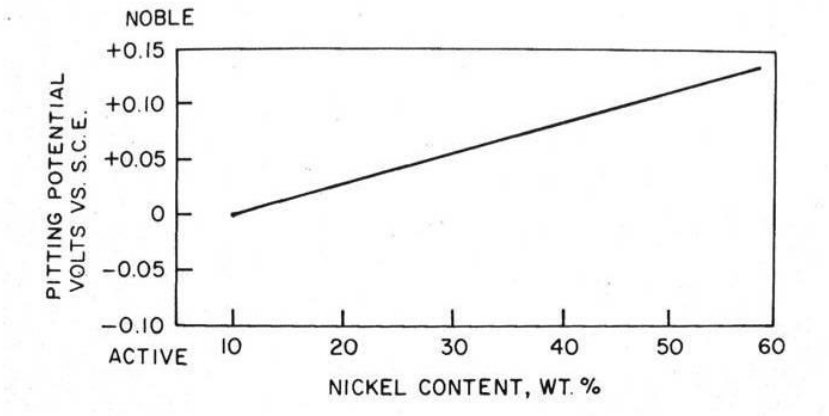

Figure 1.14- Effect of nickel content on pitting potential of Fe-15% Cr alloys in a deareated 0.1 N NaCl solution at 25 °C [1].

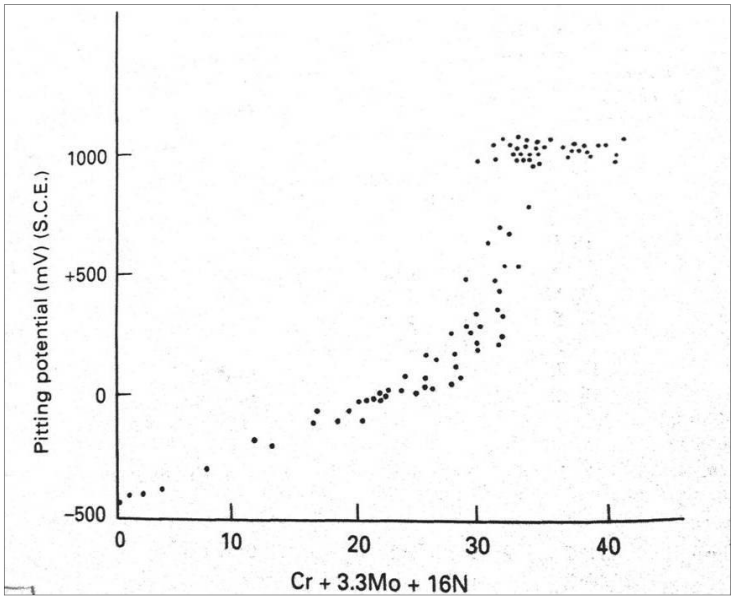

Figure 1.15- Effect of PREN on pitting potential of stainless steel in a 0.6 M NaCl solution at 25°C (21000 ppm Cl^-). [3]

Figure 1.15 displays the relationship between pitting potential and PREN. Pitting potential increases linearly as PREN increases up to 30, then sharply reaches values of the order of 1 V SCE and stabilizes for PREN higher than 35. It is worth to point out the statistical distribution of pitting potential due to the intrinsic stochastic nature of pitting corrosion (see section 2.1) and to the fact that stainless steels with different chemical composition have the same PREN.

1.3.4 Effect of microstructure on pitting behavior of stainless steel

Steel microstructure plays an important role in determining pitting resistance. Phases such as sulfides, δ-ferrite, α-prime, σ-phase, the strengthening precipitates in precipitation hardening stainless steels, sensitized grain boundaries, and welds, can have an effect on pitting resistance [1].

Studies of the role of manganese sulfide inclusions in the pitting behavior of stainless steels have led to a recognition of the importance of the composition of these inclusions: high chromium content manganese sulfide inclusions could improve pitting resistance [1].

δ-ferrite in austenitic stainless steels is generally considered detrimental to pitting resistance; σ-phase is also detrimental, even if it contains higher chromium and molybdenum than the austenitic matrix and exhibits more noble potential in chloride solutions than austenite: some chromium or molybdenum depletion is occurring within the austenite immediately adjacent to the precipitating sigma, and the pits sites may be associated with such depleted region [1], as in intergranular corrosion form.

1.3.5 Effect of surface finish on pitting behavior of stainless steel

A factor in determining pitting potential for a given alloy/environment system is the surface finish of the material. Comparing the pitting tendencies of different alloy having different surface finishes can yield non significant results [1]. Anyway, the consensus is that smoother surfaces have higher pitting resistance than rough surfaces [12,13]: peaks and valley structure of rough surfaces makes easy the chloride ions accumulation; furthermore, surface defects and discontinuity may act as preferential site for pits initiation or play the role of crevice. Among chemical surface treatments aimed at improving pitting resistance, "passivation" is a well known one and consists of immersing the stainless steel in a 20% HNO_3 solution [1,12]. The main effect of this treatment is to clean the stainless steel by dissolving surface inclusions and contaminants, such iron and steels particles embedded in the surface during fabrication. This treatment also removes from the surface manganese sulfide particles which can act as pit initiation sites.

1.3.6 Effect of environmental parameters on pitting resistance of stainless steel

From a practical viewpoint most equipment failures due to pitting corrosion are caused by chloride and chlorine containing ions [1]. In general, whatever the conditions considered, the presence of chloride ions tends to promote the passive film breakdown. Increasing the chloride concentration of a solution significantly increases pitting corrosion probability. The effect of chloride ions on the anodic curve of stainless steel, shown in Fig.1.16, are the decrease of pitting potential and the increase of the passivity current. Figure 1.17 shows the decrease of pitting potential of AISI 316 and 304 stainless steels as chlorides content of the solution increase. For example, the pitting potential of AISI 304 goes from 200 mV SCE at 3500 ppm Cl^- to -200 mV SCE at 35000 ppm Cl^-.

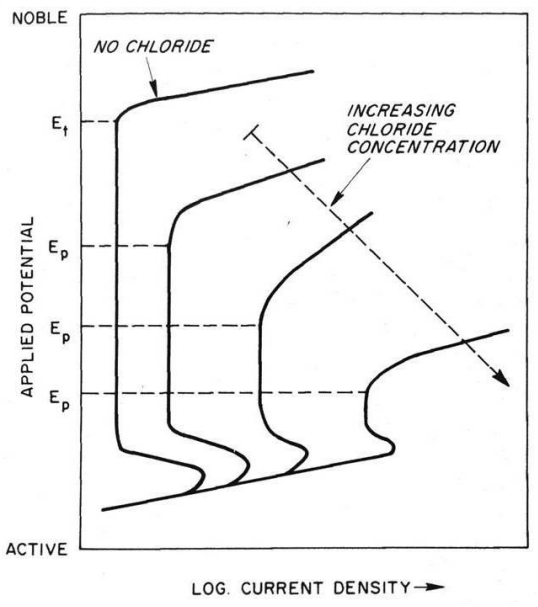

Figure 1.16- Effect of chloride ions on the polarization curve of stainless steel [2].

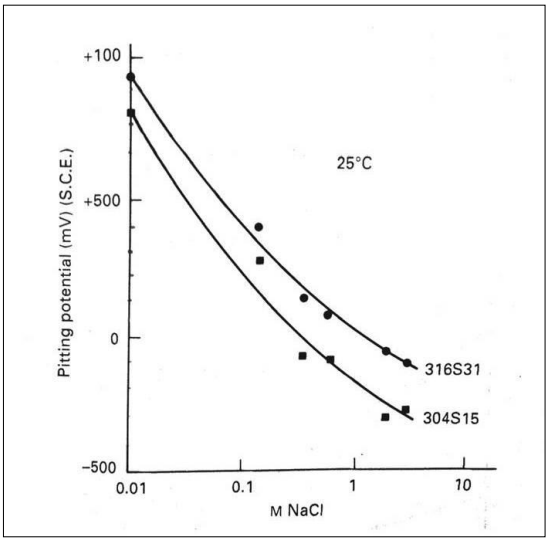

Figure 1.17- Effect of chlorides concentration on the pitting potential of AISI 316 and 304 at room temperature in a 3% NaCl solution [1].

The effect of temperature on pitting corrosion resistance is reported in Figure 1.18: pitting potential decreases by increasing the temperature. Nevertheless, the effect of temperature on pitting potential also depends on the composition of the alloy [1]: as seen from Fig.

1.18, for the molybdenum containing type AISI 316 at temperature above 70°C, the pitting potentials become largely independent of temperature.

Figure 1.19 shows the relationship between stainless steels pitting potential and the pH of the solution: pitting potential increases slightly with pH up to pH 8 when a stronger passive film forms. Thus, at low pH stainless steels approach the region of active corrosion indicated in Pourbaix diagrams where the stability of the passive layers are reduced; on the contrary, an increase in the pH value favors the existence of more stable passive films, and therefore, the pitting potential increases and the corrosion rates lowers [14].

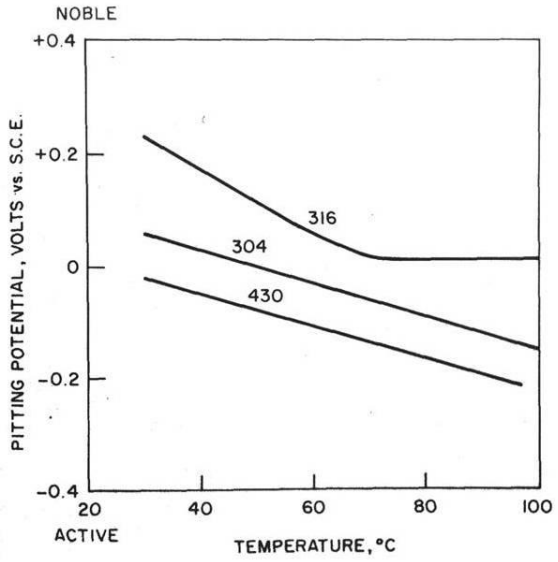

Figure 1.18- Effect of temperature on the pitting potential of various stainless steels in a 3% NaCl solution. [1]

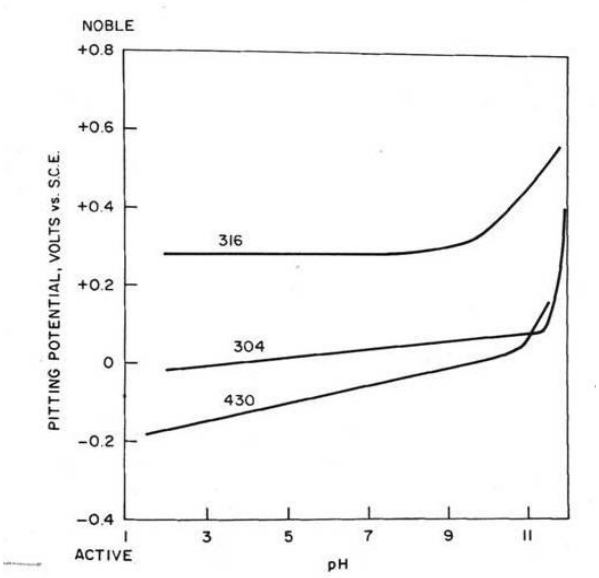

Figure 1.19-Effect of pH on pitting potential of various stainless steels in a 3% NaCl solution. [1]

Also solution velocity has an effect on pitting corrosion resistance of stainless steels [1]. Pit initiation is more difficult in fluids with higher flow velocities and pit is suppressed by increasing flow velocity in the turbulent regime [15]. At sufficiently high velocity the chemical species within the pit are dislodged from the pit thus interfering with the growth of metastable pit and ultimately hindering stable pit formation. The pitting potential is then shifted in the noble direction and the pit formation is suppressed [15].

1.4 CREVICE CORROSION

Crevice corrosion is a form of localized corrosion that may occur within crevices or at shielded surfaces where a stagnant solution is present [1]. The crevice must be wide enough to permit the solution to enter, but sufficiently narrow to maintain a stagnant zone of solution within the crevice so that the removal of the reaction products is very slow and occurs only by diffusion and migration [11].

Such crevices may be formed by the geometry of the structure, e.g. gaskets, rivets, welded fabrications, threaded joints; crevices can also arise from the contact between the metal and non-metallic solids, e.g. plastics, rubber, glass. Corrosion can also take place under deposits of sand, dirt or permeable corrosion products on the metal surface (under deposit corrosion) [11].

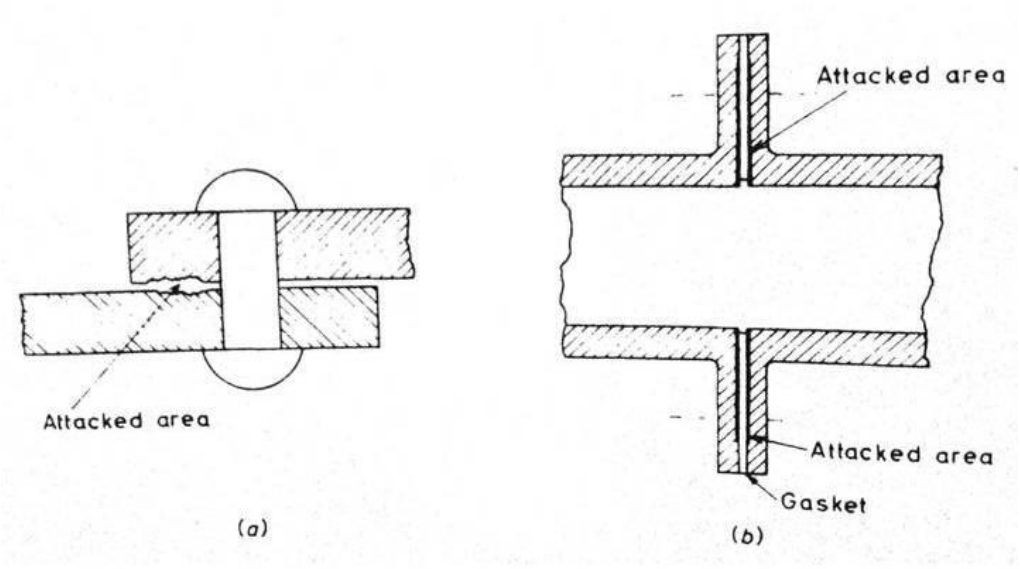

Figure 1.20- Crevice corrosion: (a) crevice resulting from the joining of the two plates of steel; (b) crevice due to a gasket between two flanged pipes [11].

Crevice corrosion mechanism for a stainless steel in an aerated sodium chloride solution is very similar to that proposed for pitting [1]. The main difference is that the location of a possible crevice corrosion initiation is predictable: the obvious method of controlling crevice corrosion is to avoid crevices in the design of the structure, or at least to keep them as open as possible, and to avoid geometrical conditions that lead to the formation of deposits on the metal surface.

Figure 1.21 is a schematic illustration of the crevice corrosion mechanism: initially anodic and cathodic reactions take place uniformly over the entire metal surface, including the surface within the crevice. Nevertheless, inside the crevice the oxygen consumed by the cathodic reaction is not replenished with the subsequent formation of an occluded cell where oxygen concentration is lower than outside the crevice. The anodic process occurs inside the crevice but the cathodic reactions only outside, where oxygen is present: the high ratio beween cathodic and anodic area involves an high corrosion rate. The current flowing between the anodic and cathodic areas leads to an increase of the chlorides concentration in the crevice [4]. At the same time, metal ions hydrolysis results in a sharp drop in pH. When the acidity and the chlorides concentration reach a critical threshold, which depends on the stainless steel corrosion resistance, there is the breakdown of the passive film. At this point begins the propagation phase: in a first time, corrosion rate increases because current circulation between anodic and cathodic areas makes the environment inside the crevice more aggressive. The growth then ceases when the current reaches a value such that the ohmic drop consumes all the work available for the occurrence of the process [4].

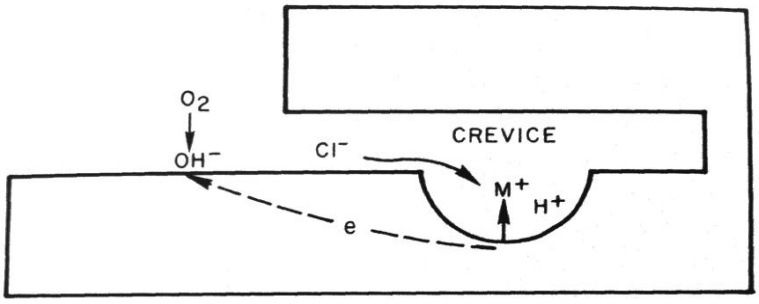

Figure 1.21- Schematic illustration of the crevice corrosion mechanism [1].

As regard stainless steels, the major alloying elements, nickel and chromium, increase resistance to crevice corrosion; the beneficial effect is attributable to the fact that chromium and nickel rise the pitting potential of the material in the more noble direction. Another important alloying element which increase crevice resistance of stainless steels is molybdenum which increases difficulty in breaking down the passive film and raises E_{pitt} in the noble direction [11].

ASTM G48 and ASTM G78 cover procedures for the determination of the resistance of stainless steels crevice corrosion when exposed to oxidizing chloride environments and provide a basis for assessing the relative resistance of various alloys to crevice corrosion under certain specified conditions. Also in the case of crevice corrosion the PREN index (Eq. 1.1) is used to rank stainless steels; at equal environmental conditions, in order to prevent crevice corrosion, stainless steels with higher PREN than that used to prevent pitting corrosion are needed [8].

For the elaboration of the Markov model used in this work of thesis, the crevice is simply considered a more aggressive form of pitting [16]; if the stainless steel is immersed in an environment particularly narrow and aggressive, the corrosion phenomena is more critic and occurs as crevice corrosion.

Chapter 2

MARKOV MODEL: STATE OF ART

2.1 INTRODUCTION

Pitting corrosion is a stochastic phenomenon and its initiation is characterized by an intrinsic variability [17]. It follows that pitting corrosion cannot be explained without statistical and stochastic methods [18]: the experimental data concerning the occurrence of pitting corrosion (initiation time, corrosion current, pitting potential), obtained from a set of measurements under the same experimental or field conditions, are scattered for a given metal [19]. The breakdown potential, for example, is typically observed to be a significantly "statistically distributed" property [7, 13, 19, 20]. These distribution have been attributed to the stochastic nature of pitting [7] and to the inherent randomness of the corrosion system [21]. From a microstrustural point of view, metals are generally polycrystalline materials consisting of grains of different forms and orientations, on the boundaries of which various chemical elements are concentrated. In addition, cracks, inclusions, voids, etc., occur within metals. These microstructural features cause metals to be susceptible to random variations in physical properties and, consequently, in their corrosion behavior. Likewise, local variations in flow conditions, temperature, pH, etc., are some of the environmental parameters to be considered. Thus the inherent randomness of the corrosion system can be viewed from the high degree of complexity of the metal-protection-environment combination [21].

Anyway, it is important to be able to determine the extent of pitting, either to select the most pitting-resistant materials for service, or to predict the remaining life of a metal structure [22]. Then, the two stages of pitting (initiation and propagation) must be considered: probabilistic methods for prediction of initiation time and propagation time have been developed in the last decades. ASTM G16 and G46 standardize statistical analysis of pitting corrosion data, as, for example, extreme value statistics (section 2.5), or methods to rate pits in terms of density, size, and depth as, for example, standard charts (Fig. 2.1).

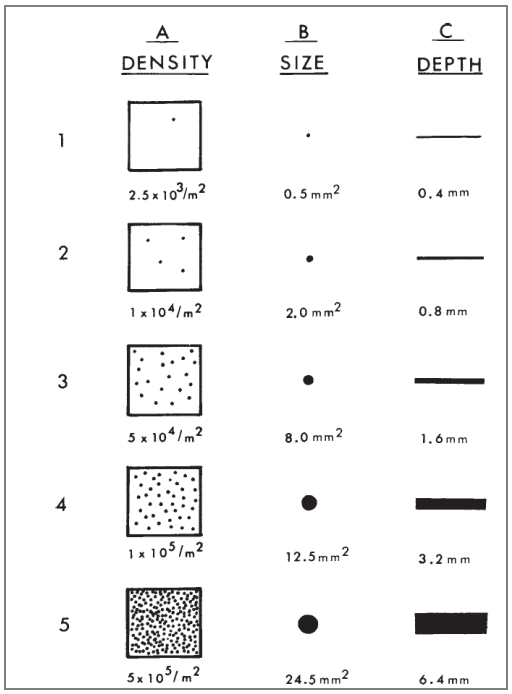

Figure 2.1- Standard rating charts for pits [22].

From an engineering point of view it's of practical interest the prediction of the initiation time, because, once pit starts, its propagation is very fast and generally unstoppable; the major effort, then, must be focused on materials selection and plants design and maintenance. An analytic method to evaluate system reliability, or, in other words, to calculate corrosion probability, is a stochastic model based on Markov chains [23]: a five-steps Markov model for pitting prediction is described in the following sections of the chapter.

2.2 MARKOV CHAINS

In this thesis the pitting corrosion phenomena is described by a Markov process which assumes that pitting corrosion retains no memory of the past, so only the current state of the damage influences its future development [24]. Some basics of Markov chains mathematical concepts follow.

A stochastic process is a phenomenon that varies to some degree unpredictably as time goes on [25]. In defining such a process it is necessary to specify the time set T involved, that can be continuous (Eq. 2.1) or discrete (Eq. 2.2):

Eq. 2.1 $T = \{t : t \geq 0\}$

Eq. 2.2 $T = \{0, 1, 2, 3, ...\}$

Suppose that at each point of the time set T, a measure of the random variable X can be observed. Thus, a given experiment is assumed and for each sample point or experimental outcome there corresponds not a single number but an entire function X_t. If the sample point or the outcome is denoted by *x*, this function can be properly denoted by $\{X_t(x) \;\; t \varepsilon T\}$. The probability structure of the stochastic process is completely defined provided that the probability density function of this set of variable is determined. Basically, the analysis of a stochastic process involves determining the density function, $f_{X_{t_n}, \ldots, X_{t_1}}(t_n, \ldots, t_1)$, and using it to predict the behavior of the process in the future, given a certain behavior in the past [25].

Classes of stochastic process can be defined by imposing suitable restriction on the n-dimensional density function [25]:

Stationary processes: their probability density functions are invariant to time translation.

Gaussian, or normal, processes: their density functions are multivariate normal.

Markov processes: their density functions are function only of the immediate past of the story and not of its entire history.

A Markov chain is a system which starts in one of the states defined by Eq. 2.3 and successively moves from one state to another [26]; each move is called a *step*.

Eq. 2.3 $T = \{s_1, s_2, s_3, ..., s_k\}$

The probability $p_{ij}(n)$ that the chain from the state s_i moves to state s_j at the next step does not depend upon which states the chain was in before the current state. The probabilities $p_{ij}(n)$ are called *transition probabilities.* The process can remain in the state it is in, and this occurs with probability p_{ii}. An initial probability distribution, denoted on *S*, specifies the starting state. Usually this is done by specifying a particular state as the starting state [26].
Let *P* be the transition matrix of a Markov chain, its ij^{th} entry $p_{ij}^{(n)}$ gives the probability that the Markov chain, starting in state s_i, will be in state s_j after *n* steps.
Consider, now, the long-term behavior of a Markov chain when it starts in a state chosen by a probability distribution on the set of states, which is called a *probability vector*. If u_0 is a probability vector which represents the initial state of a Markov chain, the i^{th} component of u_0 represents the probability that the chain starts in state s_i.
Let P^n be the *transition matrix* of a Markov chain, and let u_0 be the probability vector which represents the starting distribution. Then the probability that the chain is in state s_i after *n* steps is the i^{th} entry in the vector [26]:

Eq. 2.4 $$\overline{u_n} = \overline{u_0} \cdot \overline{\overline{P^n}}$$

As depicted in Equation 2.4, the transition matrix and its powers are the keys to define the whole Markov process, knowing the initial probability distribution.
The Chapman-Kolmogrov equation is always valid for a Markov process; let be $P_{ij}(n)$ the probability that the system go from s_i to s_j in *n* steps, for $r < n$ [26]:

Eq. 2.5 $$P_{ij} = \sum_k P_{ik}(r) \cdot P_{kj}(n-r)$$

The Chapman-Kolmogrov equation involves a new condition that the transition probabilities must satisfy:

Eq. 2.6 $$P_{ij}(0,0) = \begin{cases} 0 & i=j \\ 1 & i \neq j \end{cases}$$

A state s_i of a Markov chain is called *absorbing* if it is impossible to go away from it (i.e., $p_{ii} = 1$). A Markov chain is *absorbing* if it has at least one absorbing state, and if from

every state it is possible to go to an absorbing state (not necessarily in one step). In an absorbing Markov chain, a state which is not absorbing is called *transient* [26].
Consider an arbitrary absorbing Markov chain. Renumber the states so that the transient states come first. If there are *r* absorbing states and *t* transient states, the transition matrix will have the following *canonical form* [26]:

Eq. 2.7 $$P = \begin{bmatrix} Q & R \\ 0 & Id \end{bmatrix}$$

Here *Id* is an *r*-by-*r* identity matrix which represents the probability to move from an absorbing state to another, *0* is an *r*-by-*t* zero matrix because the probability to go from an absorbing state to a transient state is zero, *R* is a nonzero *t*-by-*r* matrix which represents the probability to move from a transient state to an absorbing one, and *Q* is an *t*-by-*t* matrix which includes all the transition probabilities from a transient state to another [16].
As discussed before, the entry $p_{ij}(n)$ of the matrix $P^{(n)}$ is the probability of being in the state s_j after *n* steps, when the chain is started in state s_i. A standard matrix algebra argument shows that $P^{(n)}$ is of the form [34]:

Eq. 2.8 $$P^n = \begin{bmatrix} Q^n & * \\ 0 & Id \end{bmatrix}$$

Where the asterisk * stands for the *t*-by-*r* matrix in the upper right-hand corner of P^n:

Eq. 2.9 $$\left(Id + \sum_{k=1}^{n-1} Q^k\right) \cdot R$$

The form of P^n shows that the entries of Q^n give the probabilities for being in each of the transient states after *n* steps for each possible transient starting state. The probability of being in the transient states after *n* steps approaches zero. Thus every entry of Q^n must approach zero as *n* approaches infinity (i.e, $Q^n \rightarrow 0$). In other words, in an absorbing Markov chain, the probability that the process will be absorbed is 1 (i.e. $Q^n \rightarrow 0$ as $n \rightarrow 1$) [26].

For an absorbing Markov chain *P* the matrix *Id-Q* has an inverse *N* and $N = I + Q + Q^2 + \ldots$ is called the *fundamental matrix* for *P*. The *ij*-entry n_{ij} of the matrix *N* is the expected number of times the chain is in the transient state s_j, given that it starts in state transient state s_i [26].

Let t_i be the expected number of steps before the chain is absorbed, given that the chain starts in state s_i, and let *t* be the column vector whose i^{th} entry is t_i. Then,

Eq. 2.10 $$t = N \cdot c$$

Where *c* is a column vector all of whose entries are 1.

Eq. 2.11 $$t = \begin{bmatrix} t_1 \\ t_2 \\ \ldots \\ t_3 \end{bmatrix} = N \cdot \begin{bmatrix} 1 \\ 1 \\ \ldots \\ 1 \end{bmatrix}$$

Let b_{ij} be the probability that an absorbing chain will be absorbed in the absorbing state s_j if it starts in the transient state s_i. Let *B* be the matrix with entries b_{ij} . Then *B* is an *t*-by-*r* matrix [26]:

Eq. 2.12 $$B = N \cdot R$$

where *N* is the fundamental matrix and *R* is as in the canonical form.

Knowing the expressions of the quantities calculated in the previous equations, the computation of the probability distribution vector u_n can be performed by computer programs, like MATLAB®, imposing a reasonably big number of steps *n*.

2.3 THREE STEPS MARKOV MODEL

As already pointed out, a statistical approach is mandatory for the material selection in engineering application due to the stochastic nature of pitting phenomenon and to the several feature that affect pitting corrosion (initiation and propagation). In recent years, important advances have been made in modeling pitting corrosion through Markov processes: Rodriguez in 1986 [25] and Provan and Rodriguez [21] used a non-homogenous Markov process to model pit depth growth for the first time; Hong [27] proposed a model in which the pit generation process is represent by the Poisson process, and the pit depth growth process by the Markov process; Valor et al. [28, 29] proposed a new stochastic model in which pit initiation is modeled as a Weibull process, while pit growth is modeled using a non-homogenous, linear growth Markov process.

The issue of all these models is the difficulty in the correlation of their specific parameters with environmental, geometrical and metallurgical factors of real corrosion systems [30]. With the aim of proposing a model for practical application, Lazzari, Bolzoni et al. [30, 31] used a continuous-time, three-state Markov process (Fig. 2.2) to model the first stages of localized corrosion considering three possible states of the metal surface: two absorbing states, passivity and localized corrosion, and one transient state, metastability. The passivity state is characterized by a very small current density, the metastability by oxidation phenomena of short duration (a few seconds to some minutes), and the localized corrosion state by the formation of stable occluded cells.

Figure 2.2- Schematization of the three steps Markov model.

The three states model has been resulted to be too simple and not adequate in describing a lot of corrosion systems because not able to deal with conditions, for example, of turbulence of the fluid, of cathodic protected system, of presence of biofilms or oxidizing species [16]; a five step model has been then developed [16] and in this work of thesis an attempt to validate it is moved.

2.4 FIVE STEPS MARKOV MODEL

Generally, the pitting corrosion phenomenon can be represented by a Markov process with two absorbing states [16]: the pitting state, characterized by the formation of occluded cells, and the passive state characterized by small corrosion currents. Thus, after a finite but reasonably high number of transitions, the system will be absorbed necessarily by one of these two states. The higher the probability to move to the passive absorbing state, the higher the tendency of the material to resist pitting corrosion.

Three transient states, called metastability, metapitting and metapassivity, are defined to take into account the presence of instability phenomena, the metastable pits formation and repassivation [16]: indeed, before moving to an absorbing state, a passive metal as stainless steel is generally subjected to micro-breakdown of the passive film which could, in a short time, repassivate, or lead to pits formation.

In the five steps Markov model, represented in Fig. 2.3, the system, from the metastable condition (initial condition), moves to an absorbing state step by step and with a defined probability.

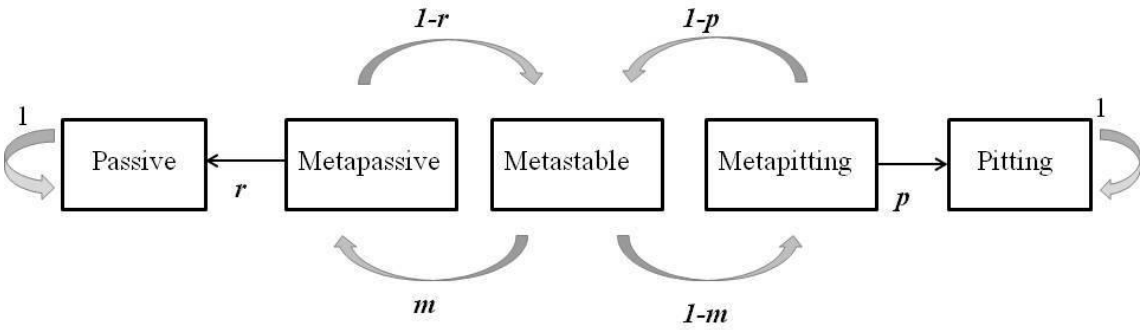

Figure 2.3- Schematization of the five steps Markov model.

The initial state is the metastable state from which the system has a probability to move to the metapassive condition (probability *m*) and to the metapitting state (probability *1-m*). The metapassive state shows a probability *r* to be absorbed by the passive state and *1-r* to go back to the metastable state; at the same time, the metapitting state has probability *p* to move to pitting and *1-p* to revert to the metastable condition. The probability *m*, *r* and *p* are logically independent from each other [16].

The transition matrix (Eq. 2.13) and the distribution vectors (Eq. 2.14 and 2.15) are expressed by:

Eq. 2.13
$$P = \begin{bmatrix} 1 & 0 & 0 & 0 & 0 \\ r & 0 & 1-r & 0 & 0 \\ 0 & m & 0 & 1-m & 0 \\ 0 & 0 & 1-p & 0 & p \\ 0 & 0 & 0 & 0 & 1 \end{bmatrix}$$

Eq. 2.14
$$u_0 = \begin{bmatrix} 0 \\ 0 \\ 1 \\ 0 \\ 0 \end{bmatrix}$$

Eq. 2.15
$$u_n = \begin{bmatrix} R \\ 0 \\ 0 \\ 0 \\ 1-R \end{bmatrix}$$

Where *R* is the repassivation probability and *1-R* the final corrosion probability.

Some considerations to discuss the transitional probabilities should be done. The introduction of the metapassive and the metapitting states, with respect to the three steps model, lead to the tendency of the final distribution vector to the passive state (if *r* increases) or to the pitting condition (if *p* increases). If *p* is equal to *r*, the five steps model becomes identical to the three steps one. If the initial state is the metastability and if *m* is equal to 0,5, the final distribution vector would depend only on the ratio between *p* and *r* .

In the case that a transitional probability is zero, the system would not evolve to the subsequent step: if *p* is zero, with *r* and *m* between 0 and 1, it would be impossible to have pitting. Vice versa, if *p* is equal to one, once the system is in the metapitting condition, it would evolve to pitting; but, considering that the starting condition is the metastable one (Fig. 2.3), the system has some probability not to move to metapitting and can repassivate.

The same reasoning remains valid for the *r* probability. If *m* will be equal to zero (or to one), the passive state (or the pitting state) would be impossible to reach.

2.4.1 Transitional probabilities relation with input parameters

In order to obtain R and 1-R probabilities (Eq. 2.15), needed for Markov model practical applications, the mathematical expressions of transitional probabilities *r*, *m* and *p*, and their relations with pitting corrosion influence factors, are required.
Environmental, geometrical and metallurgical parameters which affect pitting corrosion behavior of stainless steels are the following:

- Chlorides concentration
- Temperature
- pH
- PREN
- Fluidodynamic condition of the system
- Oxidant power of the system

Figure 2.4 shows the influence of these factors on the transitional probabilities. The *m* probability depends mainly on the ratio between the solution chloride concentration and critical chloride concentration for the material. As discussed before, if *p* is zero, pitting would be avoided: this condition occurs only under cathodic protection condition and the probability *p* then depends on the difference between the potential of the material in a specific environment and the protection potential. The probability *r* expresses the tendency of the system to repassivate and is considered dependent on the PREN and on the system fluidodynamic condition.
On the basis of experimental results and corrosion engineering experience, equations, which relates these parameters to transitional probabilities, have been proposed and discussed in the following sections.

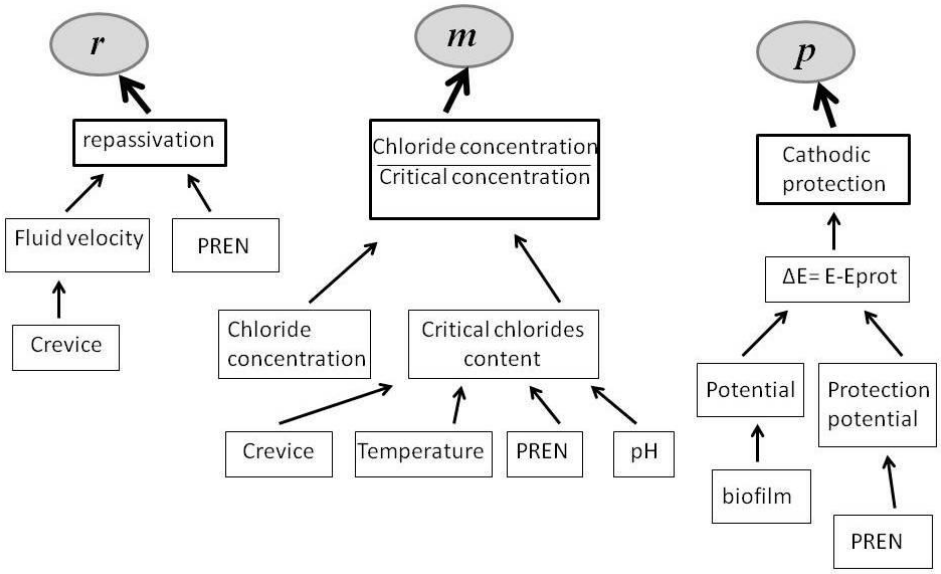

Figure 2.4- Scheme of the influence factors of the transitional probabilities.

2.4.2 Transitional probability m: meta-stable to meta-passive transition

The transitional probability *m* is the probability that a stainless steel in a specific environment moves from the initial state of metastability to the condition of metapassivity. This probability depends on the factor k, defined as the ratio between the chlorides concentration in the solution $[Cl^-]$ and the critical chloride threshold $[Cl^-]_{cr}$. This dependence, expressed by Eq. 2.16, is an exponential one, as shown in Figure 2.5: if the chlorides concentration of the solution increases, the pitting susceptibility of stainless steel also increases (see section 1.3.6): the repassivation probability will decrease.

Eq. 2.16 $$m = 1 - \exp\left(-\frac{2{,}8}{k}\right)$$

Eq. 2.17 $$k = \frac{[Cl^-]}{[Cl^-]_{cr}}$$

In particular, two cases can be well recognized:

- When $[Cl^-] < [Cl^-]_{cr}$ or k<1, m-probability tends to one: the material tends to repassivate.

- When $[Cl^-] > [Cl^-]_{cr}$ or k>1, m-probability rapidly decreases because the environment becomes more aggressive; in particular, for k>10 *m*-probability becomes rapidly less than 20%

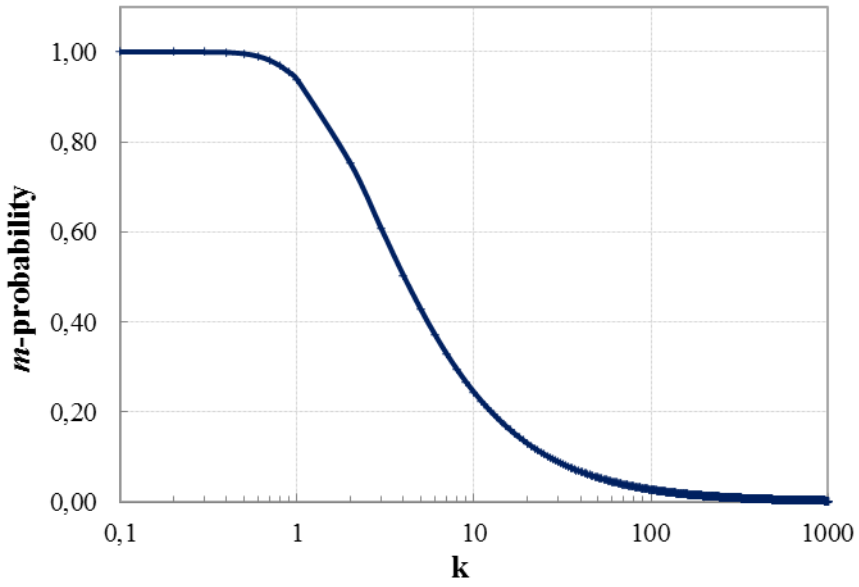

Figure 2.5- k dependence of *m*-probability.

The concept of critical chloride content is widespread, for instance, in the study of reinforced concrete structure: corrosion initiates corresponding to a critical chlorides content reached at carbon steel rebar surface (in the range from 0,4 to 1% vs. cement in aerated concrete); the main difficulty is that this parameter is not a unique value and depends on several variables [32].

At the same way the breakdown of the passive film of stainless steel is more likely to occur as the chloride concentration of the solution approaches the critical chloride content.

Equation 2.18 shows the relationship between the critical chloride threshold and metallurgical, environmental and geometrical factors:

Eq. 2.18
$$Log\left[Cl^-\right]_{cr} = \left[\frac{PREN}{9} - \frac{7 - pH}{3{,}5} - \frac{T - 20}{20\left(1 - \frac{1}{4}k_{crevice}\right)} - 0{,}3k_{crevice}\right]$$

As shown in paragraph 1.3.3, it is common to describe the pitting corrosion resistance of stainless steel in terms of PREN. Materials with higher PREN are less susceptible to pitting and can tolerate higher chloride concentration than lower PREN stainless steels, because they have a stronger protective film. In corrosion engineering it is widespread the use of the equation:

Eq. 2.19 $$Log\left[Cl^{-}\right]_{cr} \propto \frac{PREN}{9}$$

Where PREN depends on the chemical composition of the metal (Eq. 1.1)
Increasing the solution pH, the critical chloride thershold increases: an increase of the pH favors the existence of more stable passive films, and therefore, the pitting resistance increases; on the contrary, increasing the acidity of the electrolyte, materials approach the region of active corrosion indicated in Pourbaix diagrams where the stability of the passive layers are reduced. It has been chosen the value pH=2 as the limit under which stainless steels will be subjected to general corrosion. The relation between the critical chlorides threshold and pH (Eq. 2.20) is linear in semi-logarithmic scale as shown in Fig. 2.6.

Eq. 2.20 $$Log\left[Cl^{-}\right]_{cr} \propto \frac{pH-7}{3{,}5}$$

It's worth to point out that the contribution of Eq. 2.20 to Eq. 2.18 becomes zero at neutral pH. Figure 2.6 shows some theoretical curves obtained by using Eq. 2.20 for different stainless steels (PREN from 18 to 40) at 20°C. At pH 7 the critical chlorides content for AISI 304 is 100 ppm which decreases of an order of magnitude at pH 3. A PREN 40 duplex stainless steel has a critical threshold of about 30000 ppm at pH 7 which increases up to 300000 ppm at pH 14.

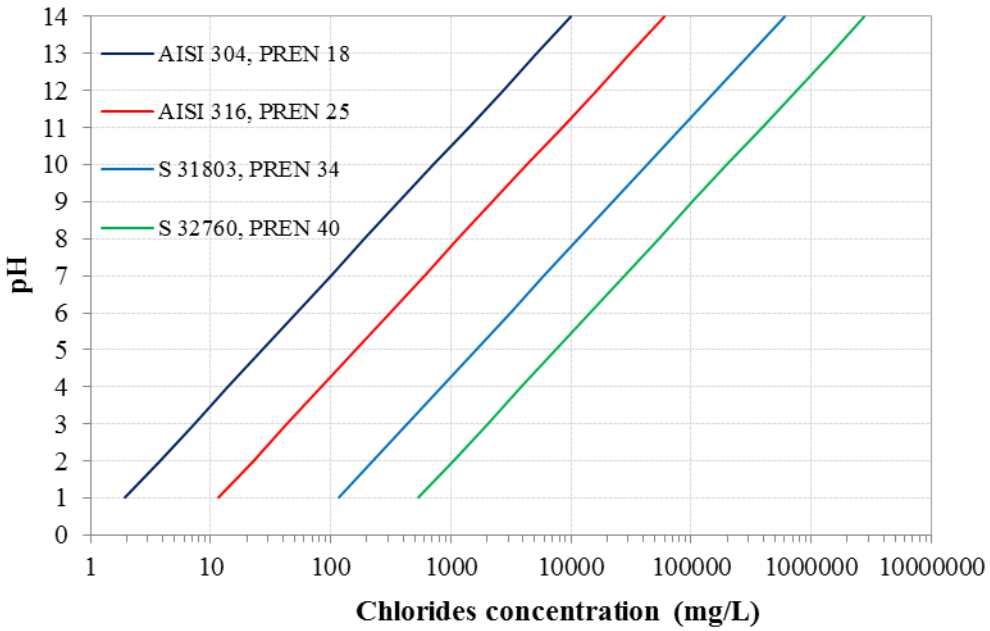

Figure 2.6- Critical chlorides threshold dependence of pH.

As widely known, the pitting corrosion resistance decreases by increasing temperature: the kinetic of electrochemical reactions is faster and the material more susceptible to pitting corrosion. Also the relation between critical chloride threshold and temperature is linear in semi-logarithmic scale:

Eq. 2.21 $$Log\left[Cl^{-}\right]_{cr} \propto \frac{20-T}{20}$$

Also in this case, at room temperature the contribution of Eq. 2.21 to Eq. 2.18 is zero. Indeed, at 20°C the critical chlorides content for AISI 304 is 100 ppm; raising the temperature up to 40°C the critical threshold becomes 10 ppm.

The effect of system geometry is taken into account in equation 2.22 by a correction factor equal to 1 in the presence of discontinuity, gaskets and any crevices on the metal surface; if only pitting corrosion is expected $k_{crevice}$ is equal to 0. Fig. 2.7 shows the temperature-critical chlorides concentration trend and the effect of crevice: for example, the critical threshold for AISI 316 at 40°C is about 60 ppm which decreases to 30 ppm in the presence of crevices.

Eq. 2.22 $$Log\left[Cl^{-}\right]_{cr} \propto 0{,}3k_{cr} + \frac{20-T}{20(1-0{,}25k_{cr})}$$

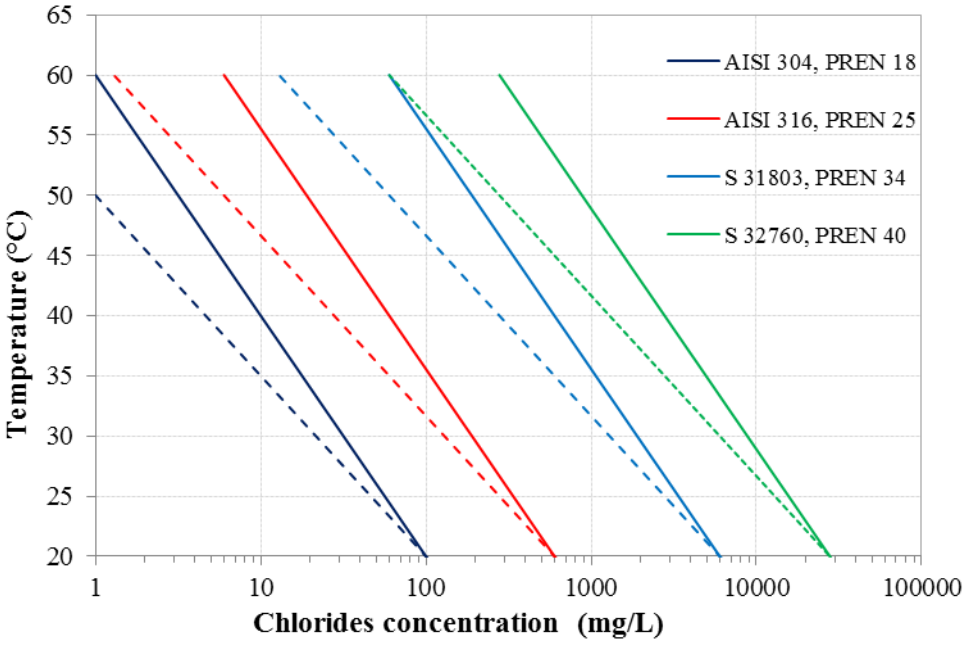

Figure 2.7- Critical chlorides threshold dependence of temperature and effect of crevice (dashed lines).

2.4.3 Transitional probability r: meta-passive to passive transition

The probability *r* is the probability that a stainless steel in a specific environment moves from the metapassive condition to the absorbing state of passivity. It takes into account the tendency of the material to repassivate: stainless steels with higher PREN and stronger passive film have an higher probability of repassivate their metastable pits. Furthermore, the fluidodynamic condition of the system play an important role: in agitation conditions, with respect to stagnant, more oxygen, needed for oxide layer repassivation, arrive to the metal surface by diffusion or convection and chloride ions can be moved away from the pit; the high velocity of the electrolyte results in washout of the aggressive pit chemistry (acidic solution by hydrolysis of metal ions), making pit propagation more difficult.
It should be pointed out that, even if r =1, there is always a probability of pitting different from 0 if the material is not under adequate cathodic protection ($p < 1$).

The expression of *r* (Eq. 2.23) is derived from the known trend of R: the repassivation probability increases slowly with fluid velocity until 0,5 m/s, at 1-1,5 m/s increases dramatically, then stabilizes and for velocity higher than 25 m/s erosion corrosion can occur [16].

Eq. 2.23 $$r = 1 - (1 - r_{\min}) \exp(-0{,}2v^4)$$

Where *v* is the fluid velocity and r_{min} (eq. 2.24) is a parameter which depends on the stainless steel composition.

Eq. 2.24 $$r_{\min} = \left(\frac{PREN}{50}\right)^{3,2}$$

High PREN stainless steel are more able to repassivate than low PREN metals. In stagnant condition this difference is large but increasing fluid velocity it vanishes (Fig. 2.8) because of the large oxygen supply. This consideration is taken into account imposing r_{min} equal to zero for PREN higher than 49: fluid velocity does not affect the pitting corrosion behavior of high PREN stainless steels and *r*, then, becomes equal to one (Eq. 2.23).

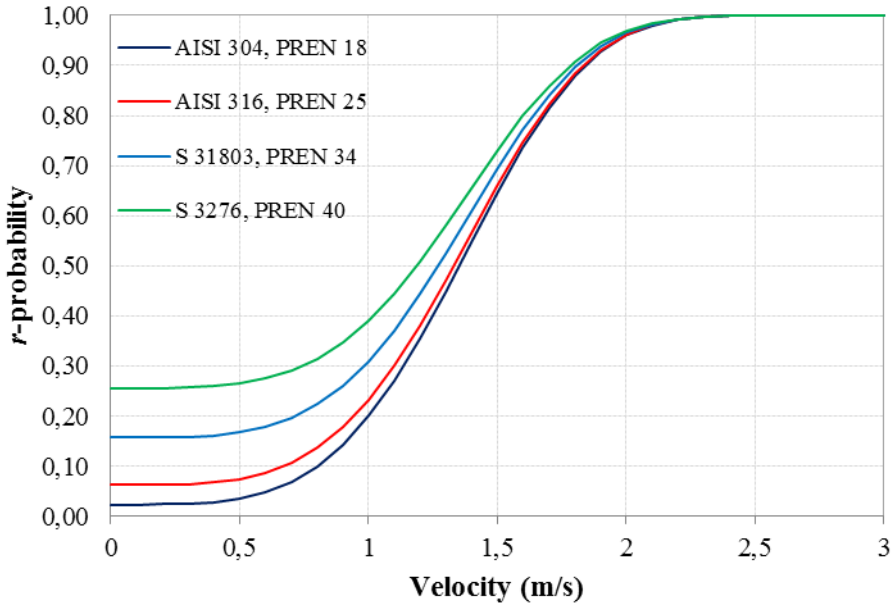

Figure 2.8- Velocity dependence of *r* probability.

2.4.4 Transitional probability p: meta-pitting to pitting transition

The *p*-probability is the probability that a stainless steel in a specific environment moves from the metapitting condition to the pitting absorbing state. If the metal is in cathodic protection (if the potential E of the material in a specific environment is lower than the protection potential E_{prot}) *p* is zero because corrosion is not thermodynamically possible.
It follows that:

Eq. 2.25
$$\begin{cases} p=0 & \text{if } E \leq E_{prot} \\ p=(E-E_{prot})^{3/2} & \text{if } E \geq E_{prot} \end{cases}$$

Figure 2.9 shows the potential dependence of *p*-probability for different stainless steels: for example, at potential of 400 mV SCE *p*-probability of AISI 304 stainless steel is 70% which decreases to 20% considering a PREN 40 duplex stainless steel.

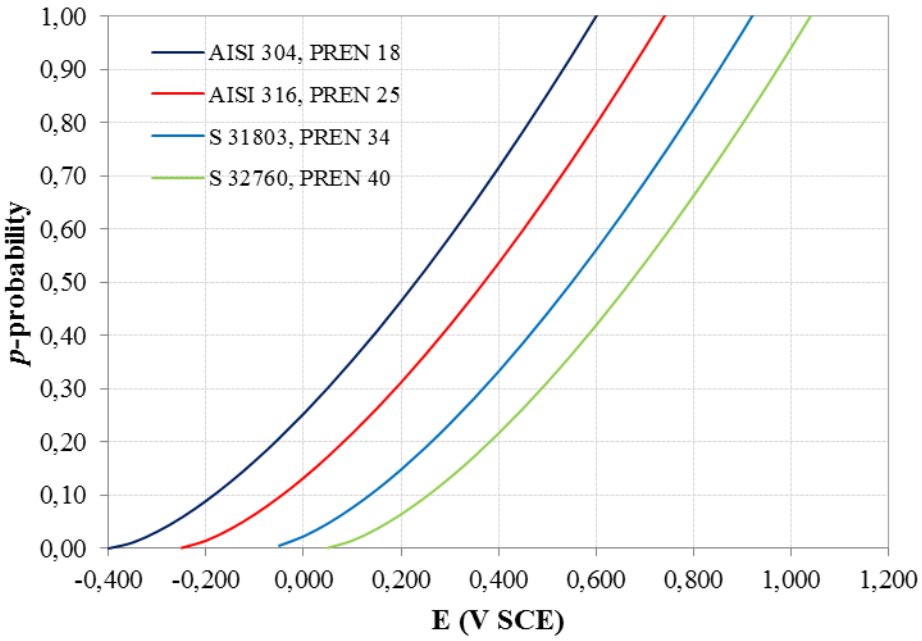

Figure 2.9- Potential dependence of *p* probability.

The protection potential is considered independent from chlorides concentration (this could be too restrictive) and a linear dependence from PREN is assumed (Fig. 2.10):

Eq. 2.26 $$E_{prot} = -0{,}760 + \frac{PREN}{50}$$

The potential is expressed in Volt vs SCE and 0,760 V SCE is the protection potential of carbon steel, considered as a zero PREN stainless steel.

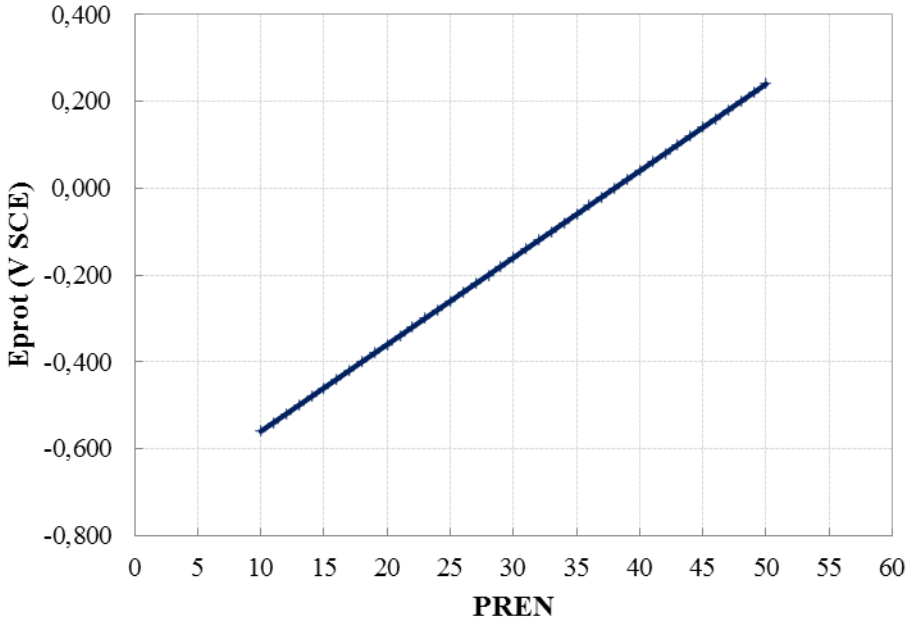

Figure 2.10- PREN dependence of protection potential.

2.4.5 Example of R calculation

In the following tables are reported the results (expressed by R and transitional probabilities) obtained from the MATLAB® implementation of the five-steps Markov model with different input data in terms of temperature, chlorides concentration, pH and fluid velocity. Two materials are considered: AISI 304 (PREN 18) and AISI 316 (PREN 24); the free corrosion potential is set equal to 0 V SCE for stainless steel AISI 304, and equal to 0,100 V SCE for AISI 316. Figure 2.11 shows the MATLAB® window with transitional probabilities, transition matrix and transition vector after input data

implementation: as example AISI 304 stainless steel at pH 7, 20°C , fluid velocity of 0,5 m/s and default corrosion potential is considered.

The results are plausible on the basis of plant experiences and empirical considerations [17]. From this recognition the need of laboratory tests aimed to validate the model.

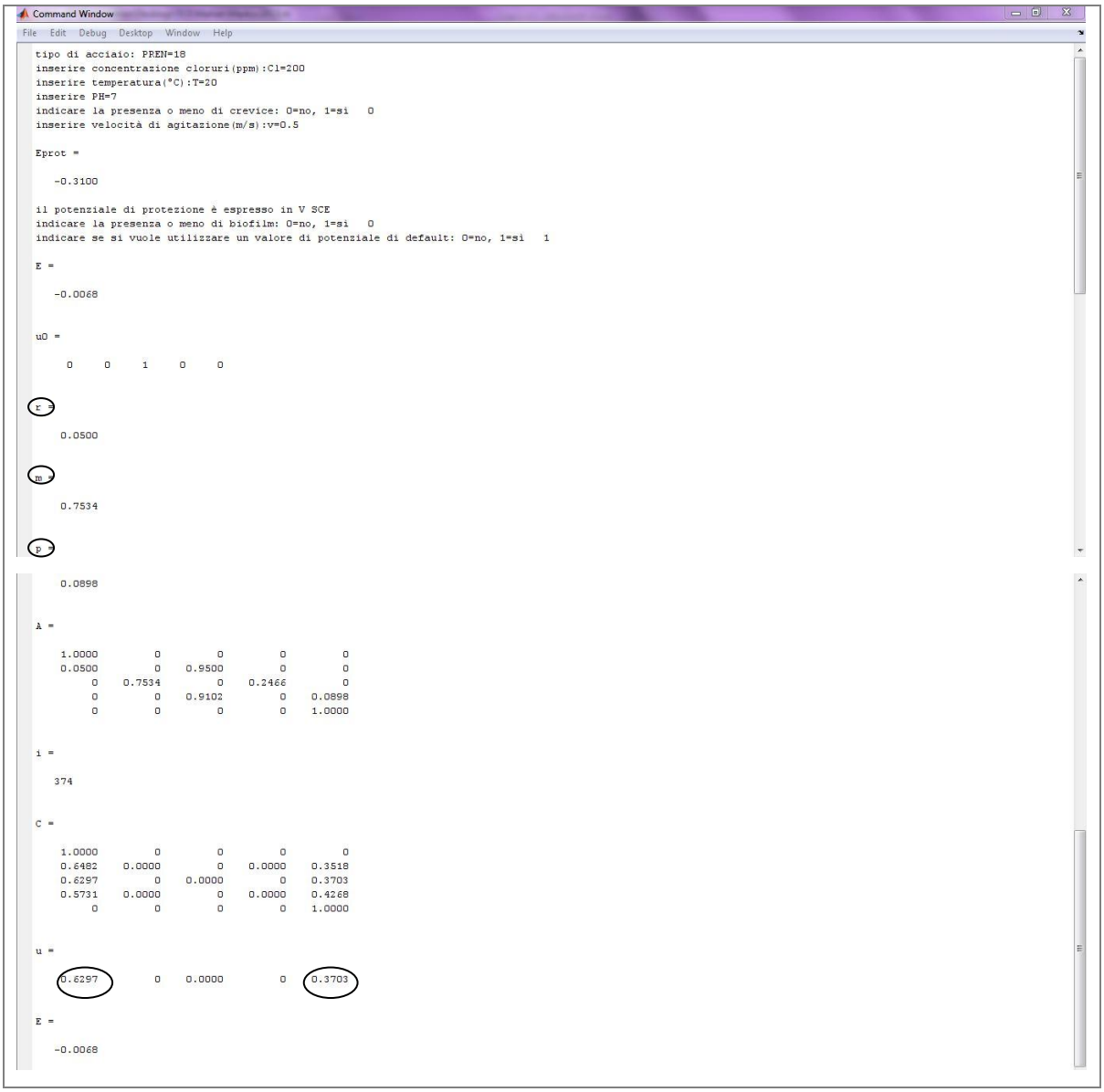

Figure 2.11- Matlab implementation of the Markov model.

Table 2.1- AISI 304, pH= 7, E= 0 V SCE

[Cl] ppm	V (m/s)	r	p	20°C		30°C		50°C	
				m	R	m	R	m	R
10	0	0,04	0,23	1	**1**	1	**1**	0,63	**0,25**
	0,5	0,05			**1**		**1**		**0,29**
	2	0,96			**1**		**1**		**0,88**
200	0			0,75	**0,42**	0,39	**0,11**	0,05	**0,01**
	0,5				**0,48**		**0,14**		**0,01**
	2				**0,94**		**0,73**		**0,18**
500	0			0,47	**0,14**	0,18	**0,04**	0,02	**0**
	0,5				**0,18**		**0,05**		**0**
	2				**0,79**		**0,48**		**0,8**

Table 2.2- AISI 304, E= 0 V SCE, *v*= 1,5 m/s, T=20 °C

pH	r	p	50 ppm		200 ppm		1000 ppm		5000 ppm	
			m	R	m	R	m	R	m	R
3	0,65	0,22	0,35	**0,62**	0,10	**0,26**	0,02	**0,06**	0,01	**0,01**
5			0,80	**0,93**	0,33	**0,60**	0,08	**0,20**	0,02	**0,05**
7			1	**1**	0,78	**0,91**	0,26	**0,52**	0,06	**0,16**
8			1	**1**	0,95	**0,98**	0,44	**0,71**	0,11	**0,27**
10			1	**1**	1	**1**	0,88	**0,96**	0,36	**0,72**
12,6			1	**1**	1	**1**	1	**1**	0,91	**0,97**

Table 2.3- AISI 316, pH=7, E= 0,100 V SCE

[Cl] ppm	V (m/s)	r	p	20°C		30°C		50°C	
				m	R	m	R	m	R
200	0	0,11	0,21	1	**1**	0,89	**0,81**	0,20	**0,11**
	0,5	0,12			**1**		**0,82**		**0,12**
	2	0,96			**1**		**0,97**		**0,53**
1000	0			0,75	**0,61**	0,36	**0,22**	0,04	**0,02**
	0,5				**0,63**		**0,24**		**0,03**
	2				**0,93**		**0,72**		**0,17**
5000	0			0,24	**0,14**	0,08	**0,05**	0,01	**0**
	0,5				**0,16**		**0,05**		**0**
	2				**0,60**		**0,30**		**0,04**

Table 2.4- AISI 316, E= 0,100 V SCE, *v*=1,5 m/s, T=20°C

pH	R	p	200 ppm		1000 ppm		5000 ppm		25000 ppm	
			m	R	m	R	m	R	m	R
3	0,68	0,21	0,39	**0,68**	0,10	**0,26**	0,02	**0,06**	0,01	**0,01**
5			0,84	**0,95**	0,31	**0,60**	0,07	**0,20**	0,02	**0,05**
7			1	**1**	0,75	**0,91**	0,24	**0,51**	0,05	**0,16**
8			1	**1**	0,93	**0,98**	0,41	**0,70**	0,10	**0,27**
10			1	**1**	1	**1**	0,86	**0,95**	0,33	**0,62**
12,6			1	**1**	1	**1**	1	**1**	0,89	**0,96**

2.4 STATISTICAL EVALUATION OF CORROSION DATA

As already discussed in section 2.1, pitting corrosion phenomena are intrinsically stochastic and, in order to describe them, a statistical approach is mandatory. Follows a summary of the basics of statistical evaluation of corrosion data aimed to the description of the propagation stage of pitting corrosion.

The use of probability concepts in describing the corrosion phenomena was first introduced by Evans, Mears, and Queneua in 1933: they designed an experiment for demonstrating the concept of corrosion probability [33]. As illustrated in Figure 2.12, wax lines were drawn on the surface of an iron plate, dividing the surface area in N sections, which were then covered with a thin film of water. This procedure was equivalent to preparing N separated specimens exposed to an identical corrosion condition. After exposure for a fixed time under a mixed gas atmosphere consisting of oxygen and nitrogen, n squares were corroded. The corrosion probability was calculated as:

Eq. 2.12 $$P = \frac{n}{N}$$

The sample survival probability is, then, calculated as:

Eq. 2.13 $$P_s = 1 - \frac{n}{N}$$

The pitting probability test can be conducted to determine the susceptibility of metals to pitting, but it will not provide information about the rate of propagation, and the results are only applicable to the exposure conditions [22].

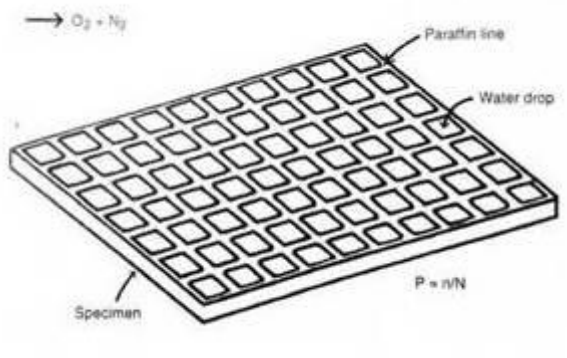

Figure 2.12- Demonstration of the concept of corrosion probability by Mears and Evans [33].

2.4.1 Corrosion data distributions

The distribution of corrosion data can be reduced to several basic probability distributions, listed in Table 2.5.

Table 2.5- Examples of probability distribution in corrosion [33].

Probability distribution	**Examples in corrosion**
Normal distribution	Pitting potential
Log-Normal distribution	SSC-failure time
Exponential distribution	Induction time for pit generation
	SCC and hydrogen embrittlement failure time
Extreme value distribution	
Gumbel distribution	Maximum pit depth
Weibull distribution	SCC failure time
Generalized extreme values distribution	Maximum pit depth
	Fatigue crack depth

The various breakdown potentials obtained for the same material from different identical tests are not considered as univocal but as distributed potentials [20]. All distributions obey the normal (Gaussian) distribution [18, 20, 33].

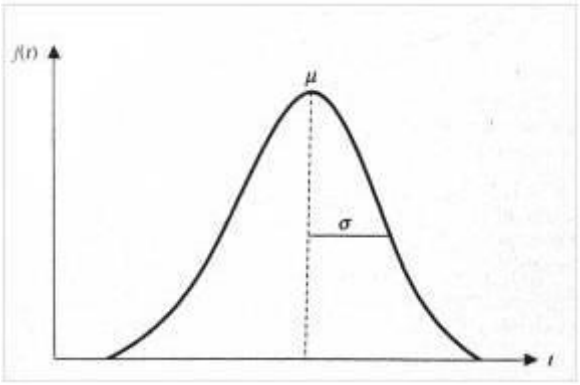

Figure 2.13- Normal (Gaussian) distribution [23].

The normal distribution is a bell shaped curve (Fig. 2.13) which fits the histogram of most corrosion data [33]. The curve is described by the probability density function, *f(x)*:

Eq. 2.14 $$f(x)=\left(\frac{1}{\sigma\sqrt{2\pi}}\right)\exp\left[-\frac{(x-\mu)^2}{2\sigma^2}\right]$$

Where μ and σ are the mean and standard deviation, respectively, which determine the shape of the curve. The area under the curve gives the probability of occurrence, calculated by the cumulative probability function, *F(x)*:

Eq. 2.15 $$F(x)=\int f(x)dx=\frac{1}{\sigma\sqrt{2\pi}}\int\exp\left[-\frac{(x-\mu)^2}{2\sigma^2}\right]dx$$

Each set of [*x*, *F(x)*], for the pitting potential and the corresponding cumulative probability, can be plotted on normal probability paper. The straight line fitting the points, shown in Figure 2.14, indicates that the measured data obey the normal probability distribution [18, 33].

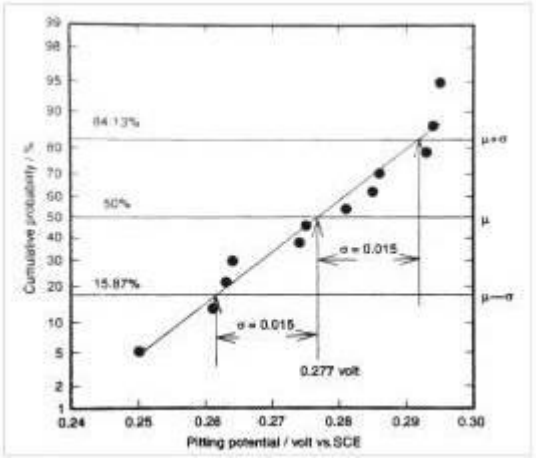

Figure 2.14- Probability plot for the distribution of pitting potential on normal probability paper [33].

The Poisson distribution is used to describe random phenomena observed in rare events [33]. Pits generation is a good example of a random process that can be described using the Poisson distribution [18, 27, 33], expressed as:

Eq. 2.16 $$P(x)=\left[\frac{m^{x}}{x!}\right]\exp(-m)$$

Where *P(x)* is the probability of occurrence of *x* pits in unit area and *m* is the mean or expected value of *x*. Figure 2.15 shows distribution curves of pits obeying the Poisson distribution.

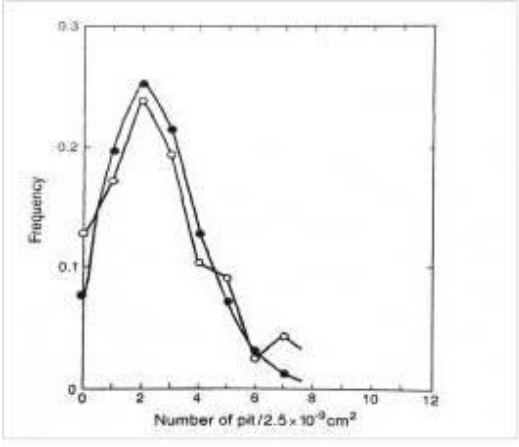

Figure 2.15- Distribution curves of pits obeying the Poisson distribution. [33]

2.4.2 Extreme value statistics

When the required corrosion data are not available, corrosion engineers design a laboratory test that simulates field operating conditions. In some cases, they may also be asked to predict the remaining life of apparatus in operation. The size of the coupon and the duration of testing may change over a wide range depending on the purpose of the test and the requirements of the client. In the laboratory test, coupons of relatively small area (e.g. 1 cm^2) are used and tested in a relatively short time (hours, days or weeks depending on the test type) under accelerating conditions, whereas larger coupon, several times 10 cm^2, are required in pilot plant tests that typically last for at least a few months [33]. Difference in size as well as in duration between the laboratory test and the field examination are extremely large; a method for bridging these large differences is provided by the statistical theory of extreme values [18, 33]. The extreme value distribution can be reduced to three types of asymptotic distributions for an infinite number of samples, and which of the three types applies in a given situation depends on the initial distribution:

Eq. 2.17 $F(x) \sim \exp[-\exp(-x)]$ Type I, Gumbel distribution

Eq. 2.18 $F(x) \sim \exp(-x)^{-k}$ Type II, Caucy distribution

Eq. 2.19 $F(x) \sim \exp\left[-(w-x)^{k}\right]$ Type III, Weibull distribution

When corrosion data for the maximum and the minimum value are collected, one must decide which type of extreme value distribution should be fitted the observed data.
The Gumbel distribution is used to analyze pit depth distribution. It is not the overall corrosion rate or the number of pits that are of interest, but the deepest pits because they cause the failure of the system [21].
In order to estimate the maximum depth of pits over the larger surface area from which specimens of small area are extracted, the Gumbel distribution is expressed as [33]:

Eq. 2.20 $$F(x) = \exp\left[-\exp\left(-\frac{x-\lambda}{\alpha}\right)\right]$$

Where *F(x)* is the cumulative probability of pit depth, *x*, and λ and α are the location and scale parameters, respectively. The probability density function, *f(x)* is given by:

Eq. 2.21 $$f(x) = \left(\frac{1}{\alpha}\right)\exp\left[-\frac{x-\lambda}{\alpha}\exp\left(-\frac{x-\lambda}{\alpha}\right)\right]$$

The maximum pit depth is obtained from experimental results and tabulated. An example of plotting the pit depth data is shown in Figure 2.16 [20]. The Gumbel probability is constructed with values of *y* scaled on the vertical axis and the associated cumulative probabilities (Eq. 2.22).
The reduced variable *y* is defined as:

Eq. 2.22 $$y = \frac{x-\lambda}{\alpha}$$

Then,

Eq. 2.23 $$y = -\ln\{-\ln[F(y)]\}$$

Eq. 2.24 $$F(y) = 1 - \frac{i}{1+N}$$

Where *i* is the i^{th} position of the ordered values of *x*, in descending order, and *N* is the total number of samples. Plotting *y* as a function of *x* (Fig.2.16) yields a straight line, and its slope is $1/\alpha$, and the intercept at y=0 gives λ.

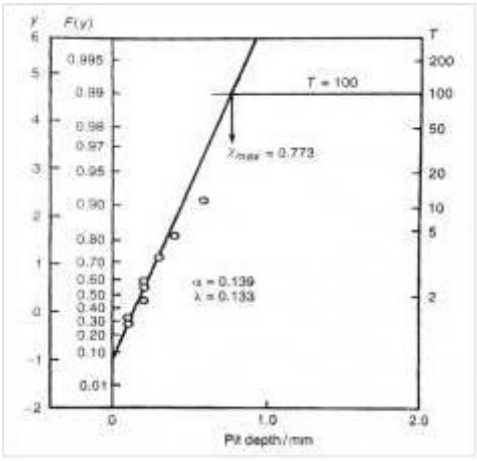

Figure 2.16- Probability plot of the distribution of pit depth in samples of small area on Gumbel probability paper, from which the maximum pit depth for the larger surface area can be extimated [33].

The third type of extreme value distribution for the minimum value, the Weibull distribution, is used often in reliability engineering to analyze failure life distribution in stress corrosion cracking situations [18, 33]:

Eq. 2.25 $$F(t) = 1 - \exp\left[-\left(\frac{t-\gamma}{\eta}\right)^{m}\right]$$

Where γ, η and m are the location, scale and shape parameters, respectively.
The shape parameter is an important parameter because it controls the shape of the probability density function *f(t)*, and also the failure time $\lambda(t)$:

Eq. 2.26 $$f(t) = \frac{dF(t)}{dt} = m(t-\gamma)^{m-1}(\eta)^{-m}\exp\left[-\left(\frac{t-\gamma}{\eta}\right)^{m}\right]$$

Eq. 2.27 $$\lambda(t) = \frac{f(t)}{1-F(t)} = m(\eta)^{-m}(t-\gamma)^{m-1}$$

Without going deeper into this topic, some graphs are reported [33] which show probability plots of the SCC failure time on Weibull probability paper (Fig. 2.17, 2.18).

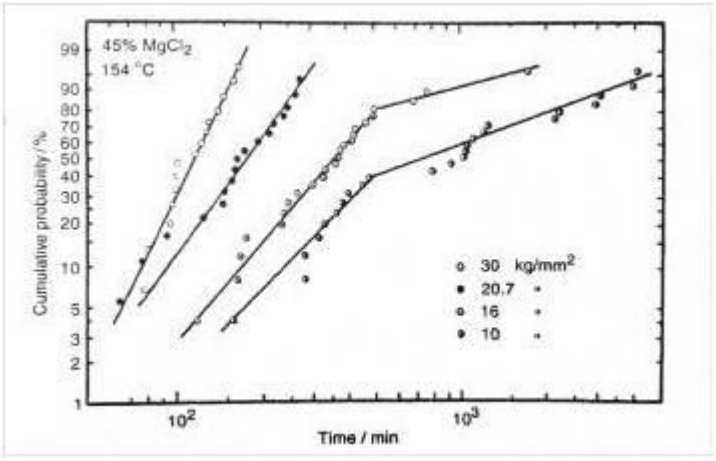

Figure 2.17- Probability plots on Weibull probability paper of the SCC failure time of austenitic stainless steel in boiling $MgCl_2$ solution [33].

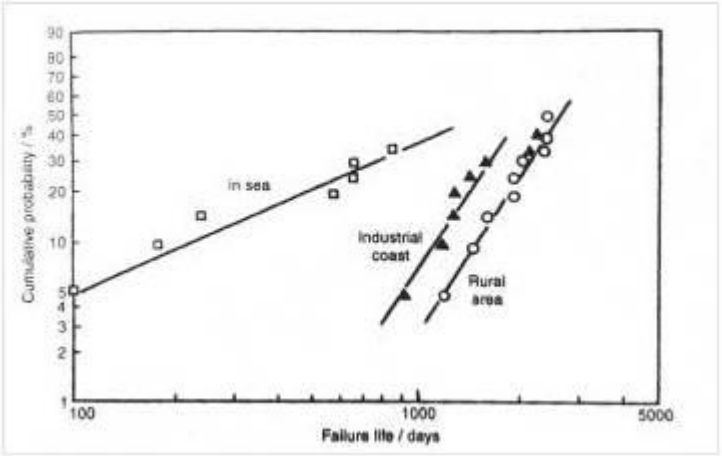

Figure 2.18- Weibull probability plots of the SCC failure time of high strength steel bolts exposed under various environmental conditions. [33]

The extreme value statistical theory is a powerful tool to analyze localized corrosion quantitatively but limited in analysis of the time-dependent probabilistic aspects of pitting corrosion, which would be very useful in assessing the reliability of a corroding system [18, 25]. Since the initiation time prediction plays a critical role for engineering application, the attention has been focused on the experimental validation of the five-steps Markov model.

Chapter 3

VALIDATION OF THE PROPOSED MARKOV MODEL: POTENTIOSTATIC POLARIZATION TEST

3.1 AIM OF THE TEST

The results obtained from MATLAB® implementation of the five steps Markov model, which are summarized in tables of section 2.4.5, are considered reasonable on the basis of engineering knowledge of stainless steels behavior [16, 17]. Despite that, they require the design and set up of experimental tests aimed to their validation.

The first step of the Markov model validation work has implied the run of potentiostatic polarization tests on stainless steels with different PREN, progressive increasing the content of chlorides in solution at pH 7 obtained with distilled water and addition of sodium chloride (NaCl). Table 3.1 reported the chemical composition of the test materials.

Table 3.1- Chemical composition of the test materials.

AISI grade	EN grade	PREN	C %	Mn %	P %	S %	Si %	Cr %	Ni %
430	1.4016	17	0,08	1	0,04	0,015	1	17	-
304	4.4301	18	0,07	2	0,045	0,015	1	18	9
470LI	1.4613	24	0,03	1	-	0,015	1	24	-

3.2 POTENTIOSTATIC POLARIZATION TEST

Potentiostatic and potentiodynamic polarization tests are electrochemical techniques commonly used for corrosion testing. Electrochemical tests require an electrochemical cell (Fig. 3.1) which includes, in addition to the metal to study (working electrode, W), a counter electrode (CE), a reference electrode (EF) and a source of electric work: the reference electrode has a well known standard potential and is used to measure the potential of the working electrode (the sample); the counter electrode is used to make a connection with the electrolyte so that the current can be applied to the working electrode;

the source of electric work is, in the case of potentiostatic tests, the potentiostat, an instrument that applies a current to the specimens which enables the potential to be controlled in a desired way.

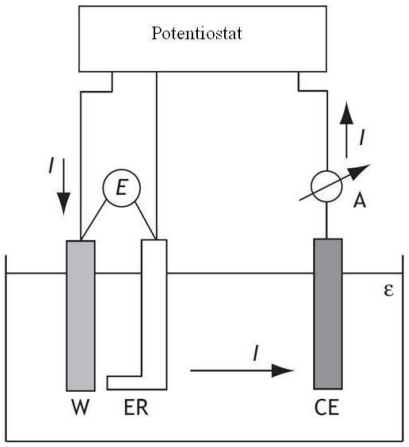

Figure 3.1- Schematic representation of an experimental set up [4].

Each test material was polarized through the potentiostat to +50 mV and +150 mV with respect to the free corrosion potential. For each polarization potential the chlorides concentration is varied from 100 to 1000 mg/L. For each chlorides content (100, 300 and 1000 mg/L), the number of corroded sample is registered after a week.
The tests is carried out at two different temperatures, 25° C and 40° C, in stagnant conditions.

3.3 EXPERIMENTAL SET UP

3.3.1 Samples preparation

For each material, samples of size 3 x 3 cm (Fig. 3.2) were cut from provided sheets of dimensions 18 x 27 x 0.1 cm. They are electrically connected to an insulated copper cable by spot welding of the back surface (Fig. 3.3).
The final surface to be exposed to the solution was 2 x 2 cm: the back surface and lateral edges of the sample were coated with an insulating polymer resin with high covering power (Fig. 3.4). A commercial product consisting of a bi-component epoxy resin with thixotropic properties was used, which guarantees high coverage of the surface also in

correspondence of angular points of the plate, as the edges. As the final surface exposed to the test solution should not undergoing any treatment which would affect its roughness (must not be blasted or mechanically abraded), it was only cleaned with acetone.

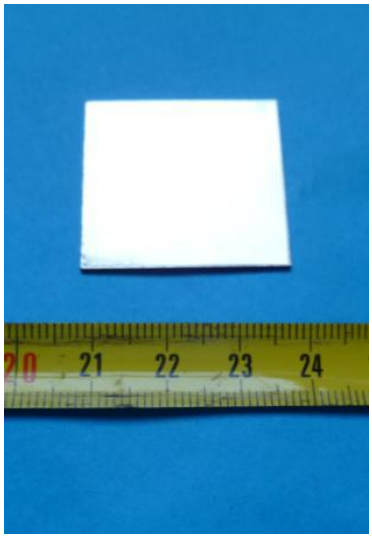

Figure 3.2- Stainless steel sample 3x3 cm.

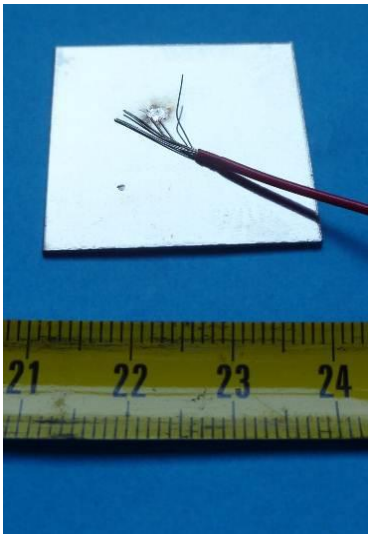

Figure 3.3- Welded cable on the sample back surface.

Figure 3.4- Coated back surface.

Figure 3.5- Exposed surface (2x2 cm).

3.3.2 Electrochemical cells assembly

In order to ensure that the ratio between the test solution volume and the sample surface is at least 0,2 mL/mm^2, according to the standard which rules corrosion immersion tests [34], 20 L of solution are placed into tanks of dimensions 40 x 40 x 20 cm and capacity 30 L.
The test cell consist of 20 stainless steel samples electrically connected, a Ti-MMO counter electrode and a SSC_{sat} reference electrode (silver-silver chloride in KCl saturated solution, +0,200 V SHE), which is placed in the tank equidistant from all the samples. Figure 3.6 shows a scheme of the test cells. For each material, twenty samples were positioned in the tank along a circle drawn on tank cover so as to ensure homogeneous distribution of current (Fig. 3.7 and 3.8). They were short-circuited and connected to the Working (W) of the potentiostat. Each sample is series connected to an electrical resistance of 10 kΩ which is required for voltage measurement, in order to calculate the circulating current. Also counter electrode and reference electrode are connected to the potentiostat (Fig. 3.9).

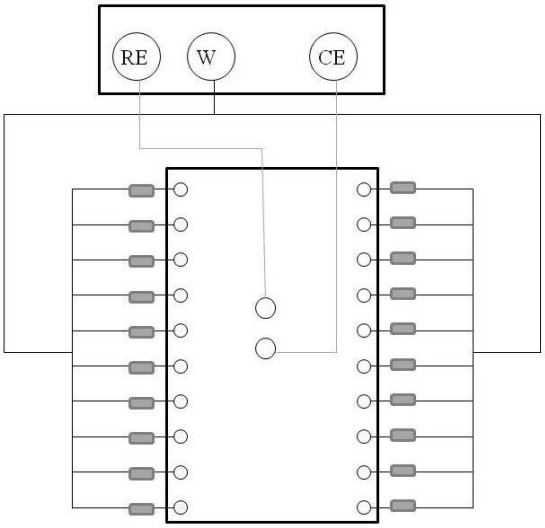

Figure 3.6- Scheme of the test cell and electrical connections.

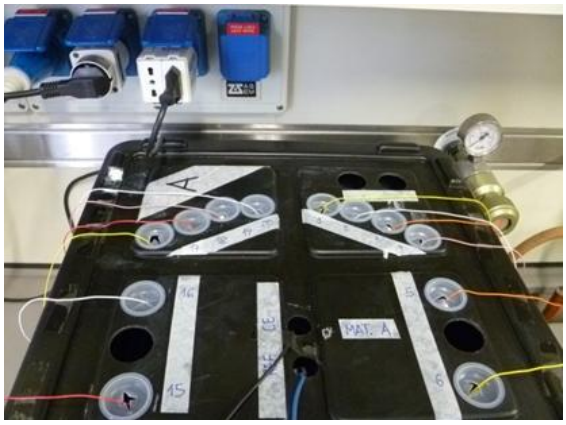

Figure 3.7- Cell cover with holes.

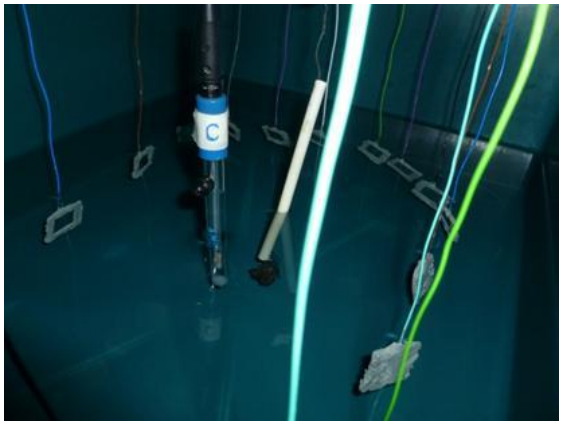

Figure 3.8- Reference electrode, counter electrode and samples in the test cell.

Fig. 3.9- Electrical connection of the electrochemical cells to the potentiostat.

3.3.3 Experimental procedure

The first week three tanks (one for each material) were filled with a room temperature test solution: in order to obtain an initial solution of 100 mg/L Cl^-, 0,17 g/L NaCl were added to 20 L of distilled water. Samples were kept 24 h in free corrosion condition until steady state potential was measured (E_{corr}). They were anodically polarized at E_1= + 50 mV vs E_{corr}, as summarized in Table 3.1. The value of the ohmic drop on the shunts was monitored daily (Fig. 3.9) and registered on an Excel Word file:

- if this value was zero, the specimen was still in passive condition.
- if the value was greater than 5 mV, the sample was considered in corrosion condition.
- if the measure of the ohmic drop was exceeding 5 mV for two consecutive days, the sample was detatched from the test circuit.

An ohmic drop of 5 mV corresponds to a circulating current density of 1,25 mA/m^2, as shown in Equation 3.1.

Eq. 3.1 $$i = \frac{I}{S} = \frac{V}{R \cdot S} = \frac{0{,}005V}{10^{-4}\Omega \cdot 4 \cdot 10^{-4} m^2} = 1{,}25 \frac{mA}{m^2}$$

Where V is the voltage measured across the resistor (V), R is the resistance value (Ω) and S is the sample surface (4 cm^2). The value 5 mV has been chosen on the basis of corrosion test experience: when corrosion starts the measured ohmic drop is immediately of the order of 200 mV and for conservative reasons the upper limit of passivity condition is chosen to be that corresponding to an ohmic drop of 5 mV.

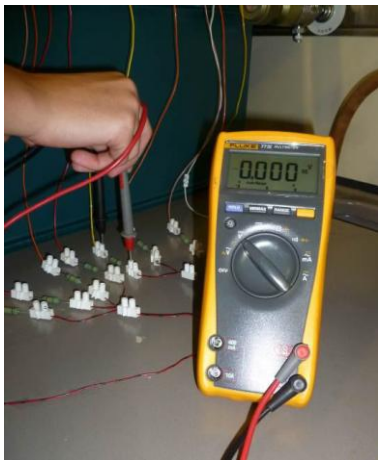

Figure 3.10- Ohmic drop on the resistance measurement.

At the end of the week the percentage of corroded samples was calculated and they were replaced with new specimens. Still passive samples were not replaced: this experiment is based on the assumption that pitting corrosion is a Markov process and, therefore, samples have no memory of their past history. The chlorides content was increased to 300 mg/L, adding 0,33 g/L NaCl to the solution and keeping the temperature constant.

The ohmic drops value on the shunt was monitored daily for a week and corroding samples were detatched as previously described. At the end of the week the corroded samples were replaced with new specimens. The chlorides content was increased to 1000 mg/L, adding 1,16 g/L NaCl to the solution and keeping the temperature constant.

The monitoring and the detachment procedure occured in the same way also during the third week.

Table 3.2- Experimental condition, 20°C, $\mathbf{E_1}$

Material	Temperature	Chlorides (mg/L)	E_{corr} (V SSC)	E_1 (V SSC)
AISI 430	25	100, 300, 1000	-0,110	-0,060
AISI 304	25	100, 300, 1000	0,050	0,100
470LI	25	100, 300, 1000	-0,100	-0,050

The potentiostatic test at polarization potential E_2= +0,150 V vs E_{corr} have been carried out with the same procedure described above and summarized in Table 3.3.

Table 3.3- Experimental conditions 20°C, **E_2**

Material	Temperature	Chlorides (mg/L)	E_{corr} (V SSC)	E_2 (V SSC)
AISI 430	25	100, 300, 1000	0,050	0,200
AISI 304	25	100, 300, 1000	0,060	0,210
470 LI	25	100, 300, 1000	0,050	0,200

Similarly, also 40°C tests start: three tanks are assembled as described in section 3.2.2 and with the aid of a thermostat, the temperature of a 100 mg/L Cl^- solution is raised to 40 °C. The samples are left 24 h in free corrosion and the open circuit potential is measured and registered. The specimens are polarized to E_1= +50 mV vs E_{corr} (Table 3.4), the ohmic drops across the resistors are monitored daily and corroding samples detached from the circuit. After a week corroded samples are replaced and the chlorides concentration is increased to 300 mg/L. Likewise, the following week the chlorides content is raised 1000 mg/L. Each week the corroded specimens percentage is calculated. Table 3.4 summarizes the experimental conditions.

Table 3.4- Experimental conditions 40°C, **E_1**

Material	Temperature	Chlorides (mg/L)	E_{corr} (V SSC)	E_1 (V SSC)
AISI 430	40	100, 300, 1000	-0,020	0,030
AISI 304	40	100, 300, 1000	-0,020	0,030
470 LI	40	100, 300, 1000	0,000	0,050

The same experimental set up and monitoring is carried out for three weeks at 40 °C polarized to E_2*= +300 mV vs E_{corr}, as summarized in Table 3.5.

Table 3.5- Experimental conditions 40°C, **E_2***

Material	Temperature	Chlorides (mg/L)	E_{corr} (V SSC)	E_2* (V SSC)
AISI 430	40	100, 300, 1000	0,025	0,325
AISI 304	40	100, 300, 1000	0,000	0,300
470 LI	40	100, 300, 1000	0,000	0,300

3.4 RESULTS AND DISCUSSION

Tables 3.5, 3.6 and 3.7 show the results of the potentiostatic polarization tests. For each experimental condition the percentage of corroded specimens (Eq. 3.2) is computed.

Eq. 3.2 $$P_c = \frac{n}{N} \cdot 100$$

Where n is the number of corroded samples and N is equal to 20.

Table 3.5- Results of potentiostatic test at E_1 and E_2 on AISI 430 at 25 and 40°C

Material	**T (°C)**	**Polarization level vs E_{corr}**	**E (V SSC)**	**Chlorides (mg/L)**		
				100	300	1000
				Week 1	Week 2	Week 3
AISI 430	25	+50 mV	-0,060	**0%**	0%	**0%**
		+150 mV	0,200	**10%**	5%	**60%**
	40	+50 mV	0,030	**0%**	0%	**0%**
		+300 mV	0,325	**95%**	100%	**100%**

Table 3.6- Results of potentiostatic test at E_1 and E_2 on AISI 304 at 25 and 40°C

Material	**T (°C)**	**Polarization level vs E_{corr}**	**E (V SSC)**	**Chlorides (mg/L)**		
				100	300	1000
				Week 1	Week 2	Week 3
AISI 304	25	+50 mV	0,100	**0%**	0%	**0%**
		+150 mV	0,210	**15%**	0%	**10%**
	40	+50 mV	0,030	**0%**	0%	**0%**
		+300 mV	0,300	**10%**	0%	**25%**

Table 3.7- Results of potentiostatic test at E_1 and E_2 on 470LI stainless steel at 25 and 40°C

Material	**T (°C)**	**Polarization level vs E_{corr}**	**E (V SSC)**	**Chlorides (mg/L)**		
				100	300	1000
				Week 1	Week 2	Week 3
470LI	25	+50 mV	-0,050	**0%**	0%	**0%**
		+150 mV	0,200	**5%**	5%	**15%**
	40	+50 mV	0,050	**0%**	0%	**0%**
		+300 mV	0,300	**5%**	0%	**10%**

The results obtained from the laboratory tests are compared from those arising from MATLAB® implementation of the five-steps Markov model. The comparison is shown in Tables 3.8, 3.9 and 3.10 and in the corresponding histograms; Tables also show the transitional probabilities dependence on the input parameters.

It's clear that a large discrepancy exists between experimental and Markov model results; anyway, this gap seems to decrease as the testing condition becomes more aggressive (higher potential, higher temperature and chlorides concentration), expecially for AISI 430 stainless steel. This will be the starting observation for the model revision of the following chapters. Before that, some consideration should be done on both, experimental set up and Markov model state of art: corrosion data obtained by laboratory tests question the common engineering knowledge of stainless steels corrosion behavior; on the other hand the results of this five-steps Markov model can lead to too conservative materials selection criteria. Test design and experimental procedure have been carried out properly, but also corrosion data must be interpreted carefully: for example, environmental conditions, as potential, solution temperature, pH and chemistry, are homogeneous in space and controlled in time during laboratory tests; this does not occur in field conditions, where temperature and aggressive species concentration vary in time and are not homogeneous all over the metal surface, biofilm and pollutant are present, exposed surfaces are larger and contain higher density of pitting initiation sites. Furthermore, in real cases, to which Markov model applies, materials lie in corrosive environment for years while this potentiostatic tests last three weeks. As underlined in [2], corrosion laboratory tests are frequently the best available source of data for materials selection: since most equipment is intended to perform for many years, whereas the time available for prior testing is short, accelerating test are often necessary; if the acceleration (higher temperature, higher stress, lower pH, higher chlorides concentration, or, as in this case, application of an anodic polarization potential) produce the same mode of failure that is expected under non-accelerated nominal and longer term conditions, results from such testing provide credibility to prediction. Despite the commonly agreed reliability of accelerated corrosion test results, one can doubt on the choice of this potentiostatic test duration asking if a week is sufficient for pit initiation. Corrosion engineers experience suggest that pits start in a few days after immersion in aggressive solution and practical consideration have lead to the previously described experimental design.

The equations of transitional probabilities of Markov model, described in Chapter 2, are empirical and based on engineering knowledge of corrosion behavior of stainless steels. An attempt to justify and modify these equations through literature data elaboration and laboratory tests is made in the following chapters.

Table 3.8- AISI 430 (PREN 17) experimental corrosion probability and Markov probabilities.

T (°C)	pH	Cl (mg/L)	E (V SCE)	Pc EXP	1-R Markov	R	p	m
20	7	100	-0,001	**0%**	**42%**	0,0317	0,1776	0,8856
		300		**0%**	**84%**	0,0317	0,1776	0,5145
		1000		**0%**	**96%**	0,0317	0,1776	0,1949
		100	-0,156	**10%**	**64%**	0,0317	0,4372	0,8856
		300		**5%**	**93%**	0,0317	0,4372	0,5145
		1000		**60%**	**98%**	0,0317	0,4372	0,1949
40	7	100	-0,014	**0%**	**97%**	0,0317	0,2587	0,1949
		300		**0%**	**99%**	0,0317	0,2587	0,0697
		1000		**0%**	**100%**	0,0317	0,2587	0,0214
		100	0,281	**95%**	**99%**	0,0317	0,5869	0,1949
		300		**100%**	**100%**	0,0317	0,5869	0,0697
		1000		**100%**	**100%**	0,0317	0,5869	0,0214

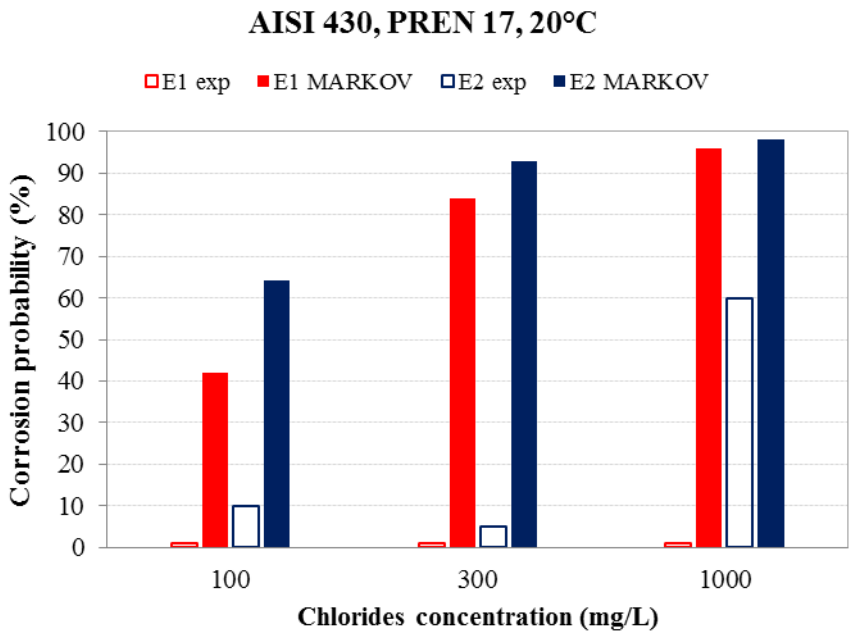

Plot 3.1- Experimental and theoretical corrosion probability comparison for AISI 430 at 20°C.

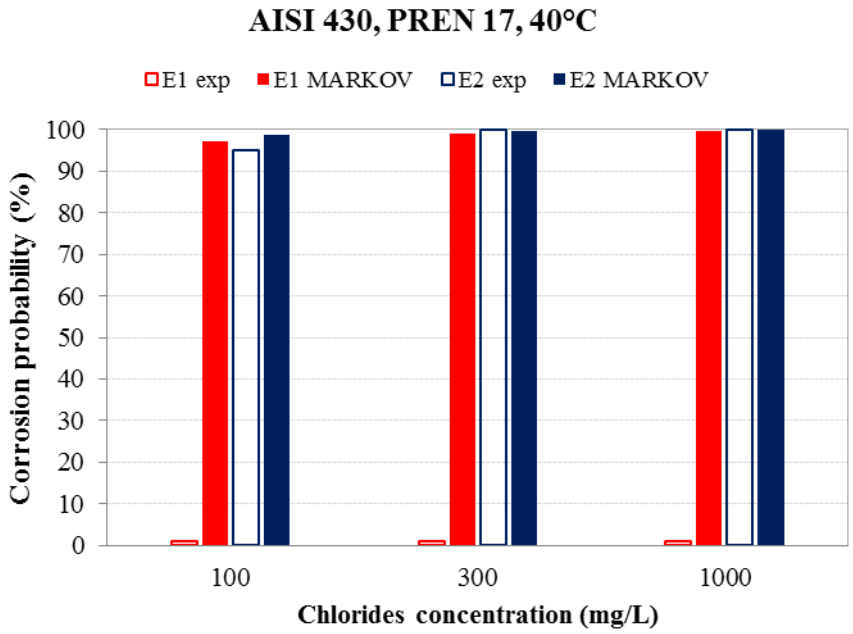

Plot 3.2- Experimental and theoretical corrosion probability comparison for AISI 430 at 40°C.

Table 3.9- AISI 304 (PREN 18) experimental corrosion probability and Markov probabilities.

T (°C)	pH	Cl (mg/L)	E (V SCE)	Pc EXP	1-R Markov	r	p	m
20	7	100	0,056	**0%**	**34%**	0,0318	0,3079	0,9392
		300		**0%**	**84%**	0,0318	0,3079	0,6068
		1000		**0%**	**96%**	0,0318	0,3079	0,2442
		100	0,166	**15%**	**42%**	0,0318	0,4258	0,9392
		300		**0%**	**88%**	0,0318	0,4258	0,6068
		1000		**10%**	**97%**	0,0318	0,4258	0,2442
40	7	100	-0,014	**0%**	**95%**	0,038	0,2398	0,2442
		300		**0%**	**98%**	0,038	0,2398	0,0891
		1000		**0%**	**100%**	0,038	0,2398	0,0276
		100	0,256	**15%**	**98%**	0,038	0,5313	0,2442
		300		**0%**	**99%**	0,038	0,5313	0,0891
		1000		**25%**	**100%**	0,038	0,5313	0,0276

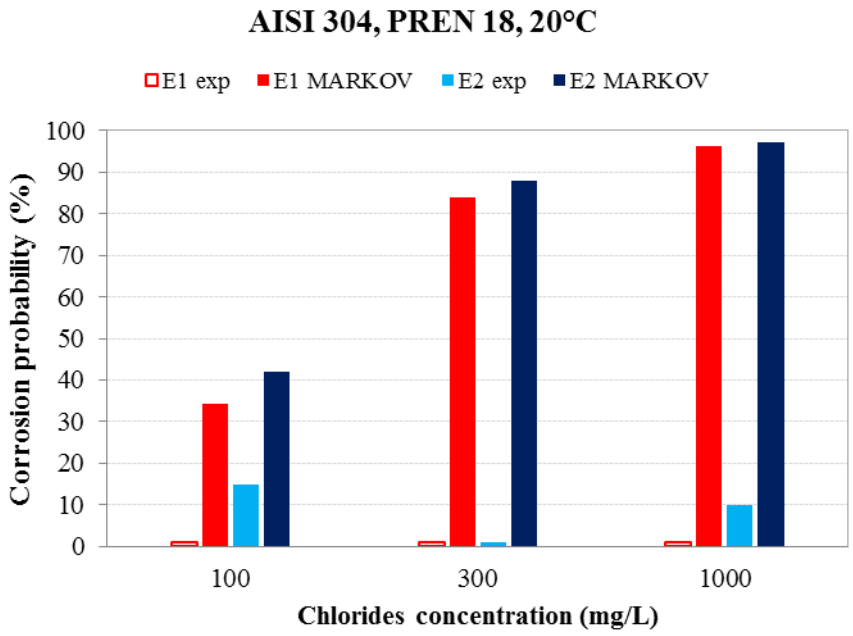

Plot 3.3- Experimental and theoretical corrosion probability comparison for AISI 304 at 20°C.

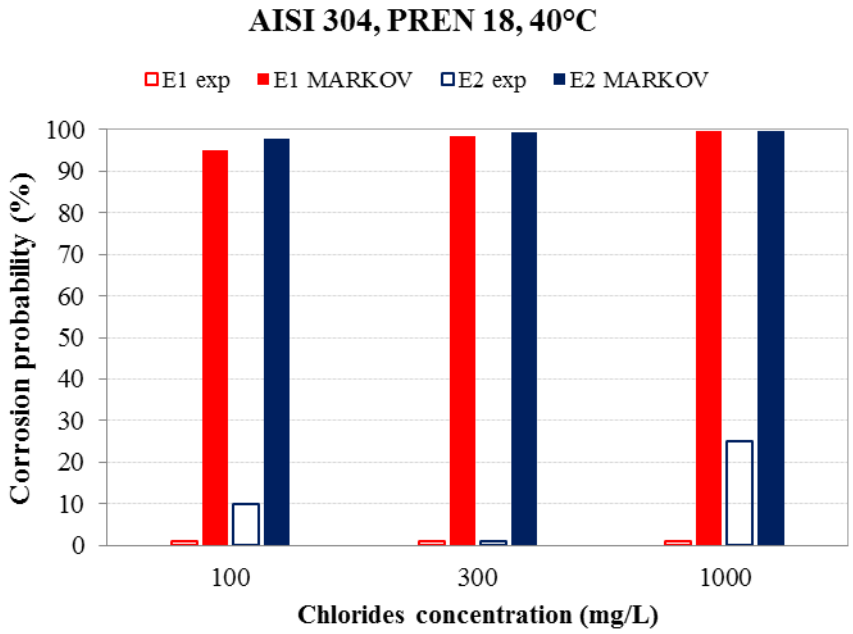

Plot 3.4- Experimental and theoretical corrosion probability comparison for AISI 304 at 40°C.

Table 3.10- 470 LI (PREN 24) experimental corrosion probability and Markov probabilities.

T (°C)	pH	Cl (mg/L)	E (V SCE)	Pc EXP	1-R Markov	r	p	m
20	7	100	-0,094	**0%**	**0%**	0,0955	0,0802	1
		300		**0%**	**1%**	0,0955	0,0802	0,9869
		1000		**0%**	**24%**	0,0955	0,0802	0,7274
		100	0,156	**5%**	**0%**	0,0955	0,2879	1
		300		**5%**	**4%**	0,0955	0,2879	0,9869
		1000		**15%**	**96%**	0,0955	0,2879	0,7274
40	7	100	0,006	**0%**	**38%**	0,0955	0,1529	0,7274
		300		**0%**	**75%**	0,0955	0,1529	0,3516
		1000		**0%**	**92%**	0,0955	0,1529	0,1219
		100	0,246	**5%**	**60%**	0,0955	0,3815	0,7274
		300		**0%**	**88%**	0,0955	0,3815	0,3516
		1000		**10%**	**97%**	0,0955	0,3815	0,1219

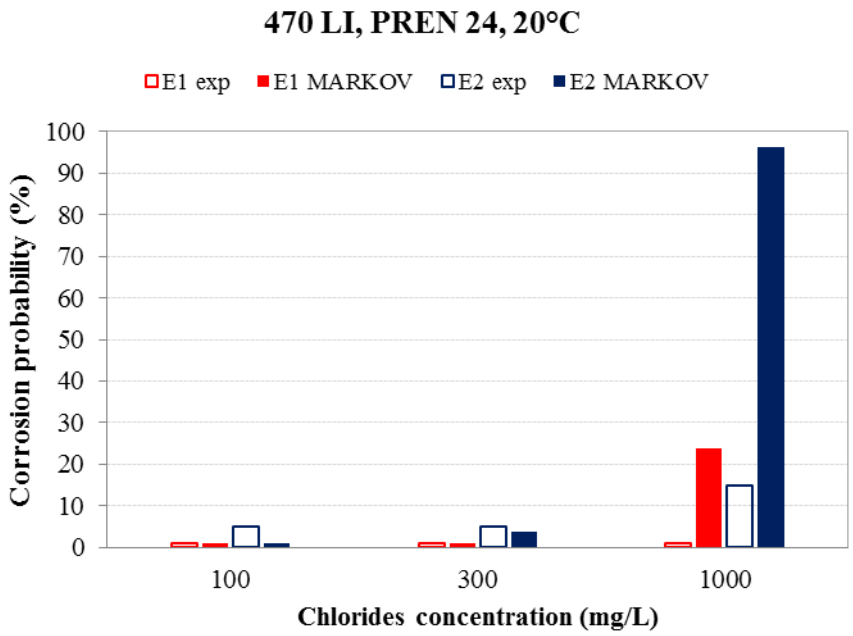

Plot 3.5- Experimental and theoretical corrosion probability comparison for 470 LI at 20°C.

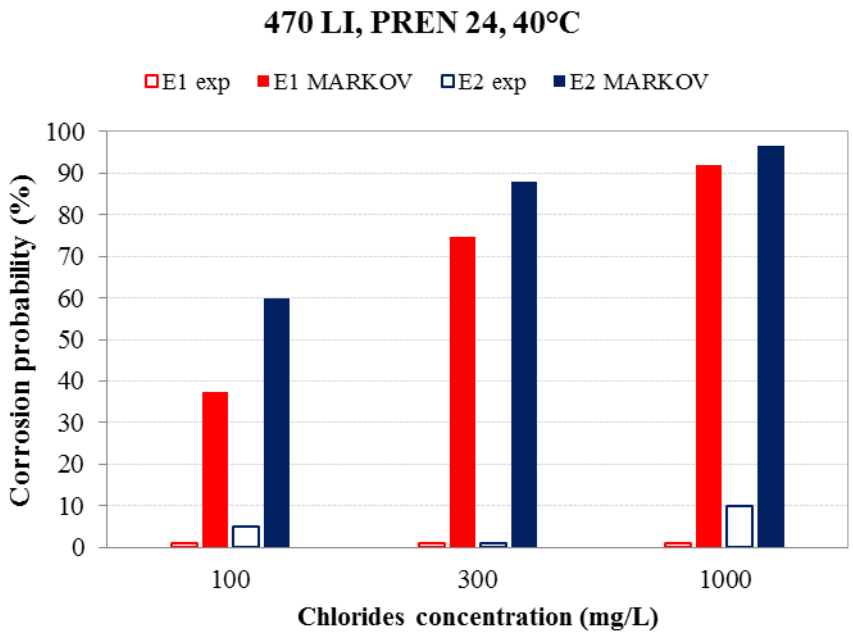

Plot 3.6- Experimental and theoretical corrosion probability comparison for 470 LI at 40°C.

Chapter 4

p-PROBABILITY: A REVIEW OF THE META-PITTING TO PITTING TRANSITION

4.1 INTRODUCTION

The transitional probability *p* is the probability that the system moves from the metapitting state to the pitting absorbing state. If *p*-probability is zero, pitting corrosion would not occur: the only condition that allows this to happen with certainty is the cathodic protection. Therefore, *p* is chosen to be dependent on the difference between the potential of the metal in a specific environment and the protection potential, defined as the repassivation potential. The protection potential is assumed to be linearly dependent on the PREN but independent on the chloride concentration of the solution. The *p*-probability equations and the *p*-probability-potential trend (Fig. 4.1), already discussed in section 2.4.4, are reported below:

Eq. 4.1
$$\begin{cases} p=0 & \text{if } E \leq E_{prot} \\ p=\left(E-E_{prot}\right)^{3/2} & \text{if } E \geq E_{prot} \end{cases}$$

Eq. 4.2
$$E_{prot} = -0{,}760 + \frac{PREN}{50}$$

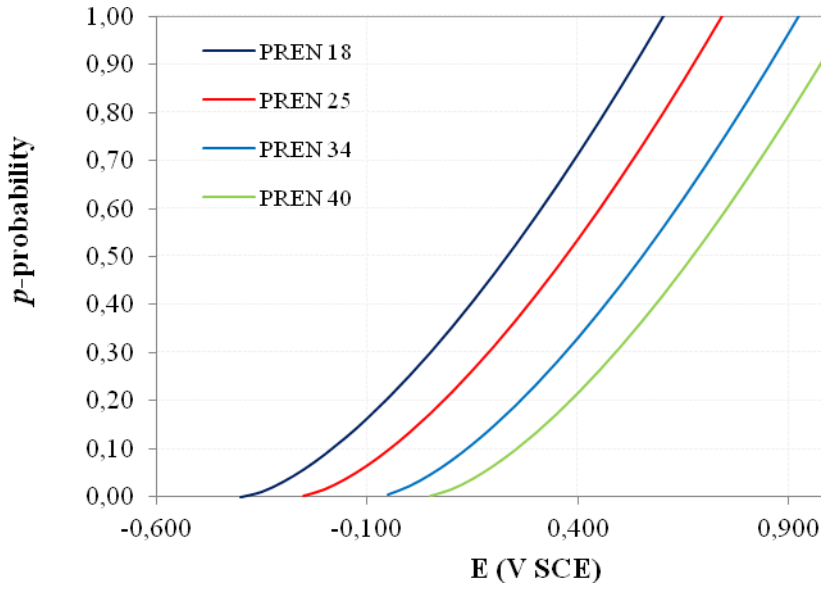

Figure 4.1- Potential dependence of *p* probability.

As widely discussed, Markov model equations were proposed on the basis of the engineering knowledge in the field of materials selection, where localized corrosion represents a risk for materials service life. In this work a bibliographic research and experimental tests were carried out in order to confirm (or modify) the equations initially proposed. The compare between experimental and theoretical corrosion probability, proposed in section 3.4, suggests that, since, the gap between the results diminishes increasing the potential, the first consideration should be done about the shape of the *p*-probability curve: for low potential *p*-probability should be lower than that predicted by the existing Markov model. Furthermore, an asymptotic behavior should be taken into account: it's reasonable to think that pitting probability does not increase indefinitely with potential but tends to one asymptotically; indeed, the *p*-probability expression for potential higher than protection potential should be modified. On the contrary, the condition p= 0 if $E \leq E_{prot}$ should be not changed because set its basis on thermodynamic reasoning (section 2.4.4).

Moreover, the E_{prot}-PREN relation (Eq. 4.2) must be checked with literature data and experimental results. For sake of simplicity, the linear dependence will be considered still valid; considering carbon steel protection potential as that corresponding to a zero PREN stainless steel is a reasonable and useful starting point.

4.2 STATISTICAL ELABORATION OF LITERATURE DATA

4.2.1 Pitting potential distribution

A significant amount of literature data is available on pitting potential of various stainless steels in environment with different chlorides concentration. Otherwise, there is a lack of data on protection potential values. For these reasons, *p*-equations rework starts from pitting potential data collection. Pitting potential values for different materials are extrapolated from tables and graphs of books [1, 2, 11] and articles [13, 15, 35, 36] and tabulated. Chlorides concentration solution above 10 g/L, room temperature and neutral pH conditions are taken into account (Appendix A). The attention, then, has been focused on graph of Figure 4.2, which shows pitting potential trend varying with chromium content, main element which defines PREN (Eq.1.1). Plot 4.1 shows an acceptable match between selected data and trend derived from Figure 4.2; furthermore, it shows the scattering of pitting potential values: the probabilistic approach is, then, mandatory.

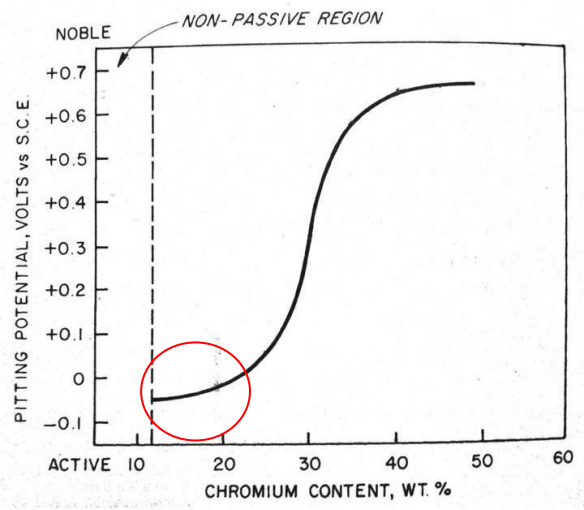

Figure 4.2- Effect of chromium content on pitting potential of iron-chromium alloys [2].

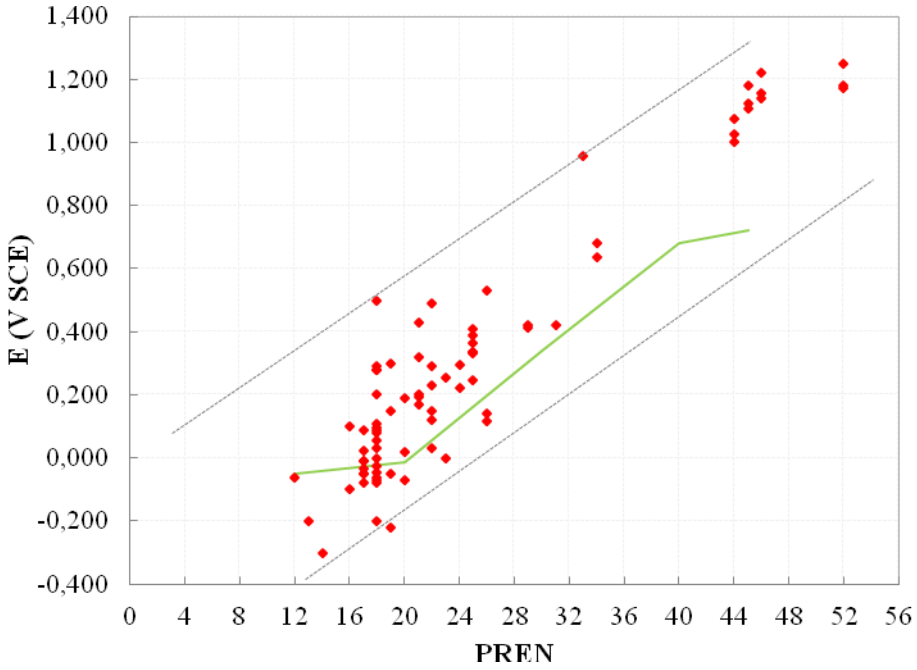

Plot 4.1- Selected data are reported on a potential-PREN graph, compared with curve of Figure 4.2 and values scattering is underlined.

As shown in Figure 4.2 (red circle), pitting potential does not vary dramatically for stainless steels with PREN between 17 and 20, hence, only data concerning these materials are selected and elaborated. From this point forward no more restriction on chlorides content are made but, again, only room temperature and neutral pH conditions are considered (Appendix A, bold highlighted values).

Pitting potential obey Gaussian distribution (section 2.5.1); accordingly, normal and cumulative probability functions are calculated for the selected data, known the mean and the standard deviation (Eq. 2.14 and 2.15): the curves are reported in Plot 4.2 and 4.3 and the values in Appendix B. The pitting potential for PREN 17 stainless steel has been chosen as that corresponding to P= 0,10: the probability that pitting occurs for lower potential is 10% (Plot 4.2).

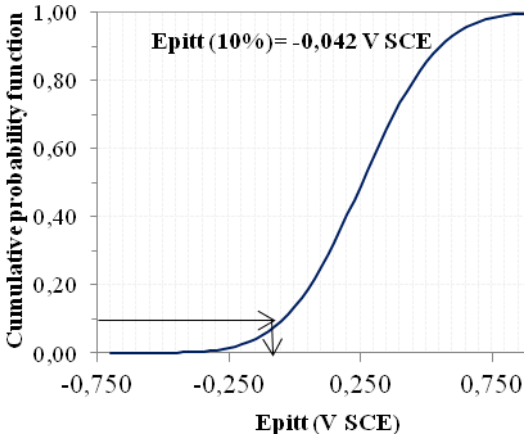

Plot 4.2- Cumulative probability function curve and definition of pitting potential.

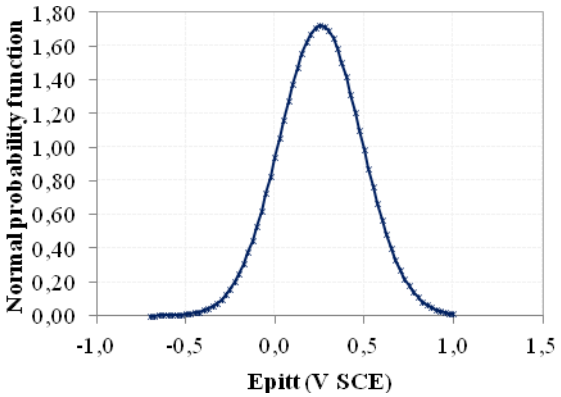

Plot 4.3- Normal distribution function curve of pitting potential.

4.2.2 Protection potential determination

The assumptions of linear dependence of protection potential with PREN and of independence on chlorides concentration are considered still valid. Chlorides independence may be a strong assumption but the whole model, in which each transitional probability is affected by different parameters, must be considered: the real system is described by the transition matrix and the distribution vectors (section 2.2), which interconnect transitional probabilities and their influence factors.

Considering engineering experience on corrosion and cathodic protection [4], it is assumed that the protection potential value is 300 mV lower than the pitting potential. Plot 4.4 shows this consideration applied to the theoretical curve, derived from Fig. 4.2.

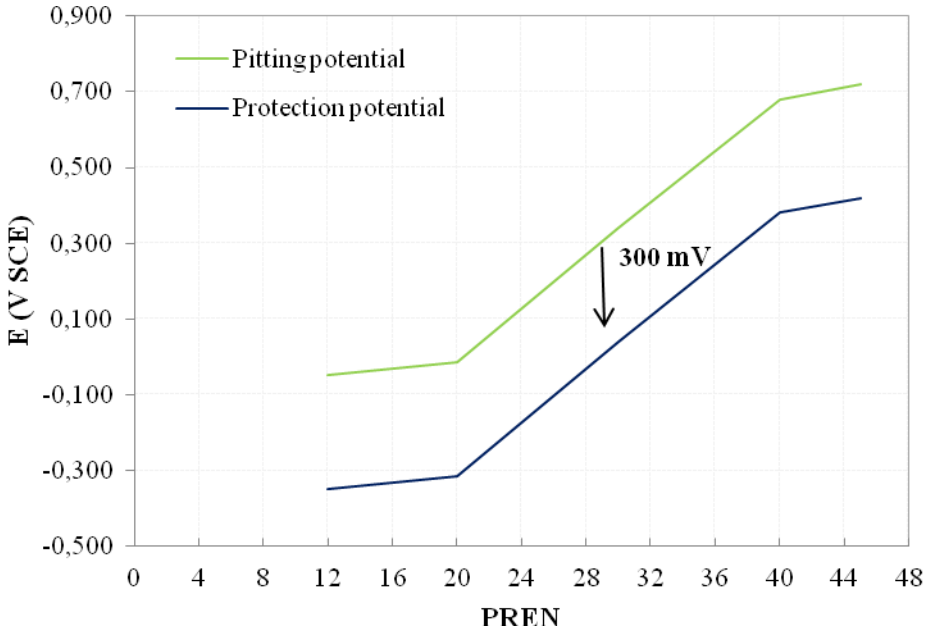

Plot 4.4- Protection potential determination.

Then, for PREN 17 stainless steels the protection potential is:

Eq. 4.3 $E_{prot}(V\ SCE)=E_{pitt}(10\%)- 0,300= -0,042 - 0,300= -0,342\ V\ SCE$

Since carbon steel (which is considered a 0 PREN stainless steel) protection potential is -0,760 V SCE and PREN 17 protection potential is -0,342 V SCE (Eq. 4.3), the slope of the straight line E_{prot}-PREN would be $\frac{1}{40}$.

Eq. 4.4 $$E_{prot} = -0,760 + \frac{PREN}{40}$$

Plot 4.5 shows the old-Markov model and the new-Markov model straight lines compared with the "literature" curve, obtained from Plot 4.4: a good match is observed between the reviewed trend and the theoretical curve.

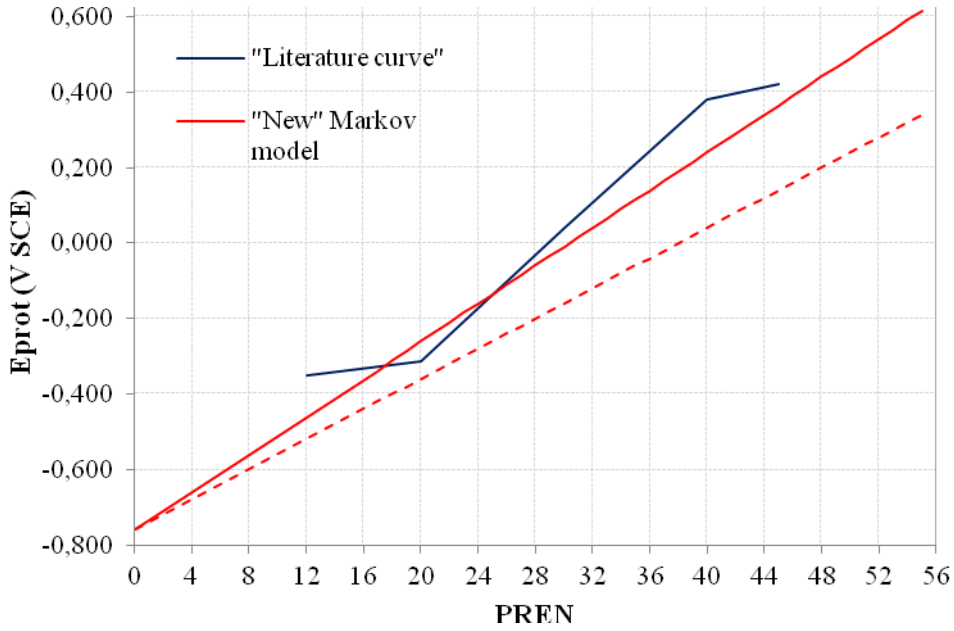

Plot 4.5- E_{prot}-PREN trend.

4.2.3 Calculation of p-probability

As widely discussed, *p*-probability depends on the difference between the potential assumed by the material in a specific environment and the protection potential. The idea is to modify the shape of the *p*-probability curve (Eq. 4.5), taking into account an asymptotic behavior and the prediction of lower probability for low potential (section 4.1).

Eq. 4.5
$$\begin{cases} p=0 & \text{if } E \le E_{prot} \\ p=1-\exp[-A\cdot(E-E_{prot})]^{B} & \text{if } E \ge E_{prot} \end{cases}$$

The cumulative probability function of the pitting potential distribution, which gives the probability of occurrence, is used as model curve: for each probability value, E_{pitt} is substituted with $E-E_{prot}$, where E_{prot} is the mean value between the new Markov model protection potential of stainless steels with PREN from 17 to 20 (Appendix B). A and B constant (Eq 4.5) are calculated as the parameters which minimize the difference between

the cumulative distribution and the *p*-probability curve. The resulting values are A= $\frac{3}{2}$ and B= 3:

Eq. 4.6 $$p = 1 - \exp\left[-\frac{3}{2}\left(E - E_{prot}\right)\right]^3$$

Plot 4.6 shows the "old" Markov model *p*-probability curve (dashed line) and the reviewed one, which satisfies the requirement of asymptotic behavior and prediction of lower probabilities for low potential.

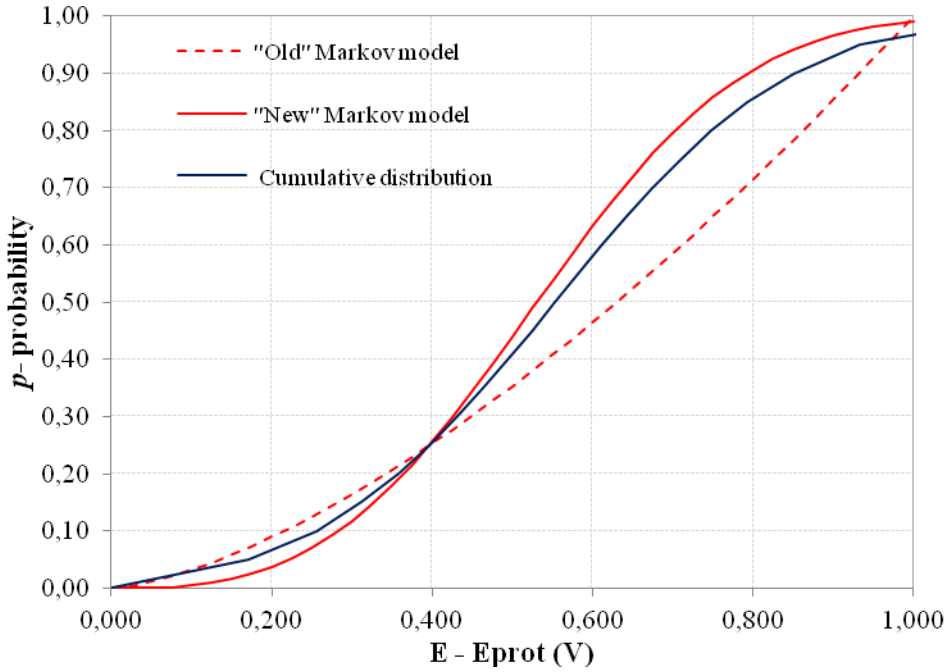

Plot 4.6- *p* probability- (E- E_{prot}) trend.

Finally, *p*-probability-potential curves for different stainless steels are shown in Plot 4.7: a first improvement in the equation revision has been made: the new curves are shifted on the right with respect the old curves, then predicting lower probabilities; for example, at potential of 100 mV SCE, *p*-probability for AISI 304 for the "old" model was 35% while decreases to 20% for the reviewed model.

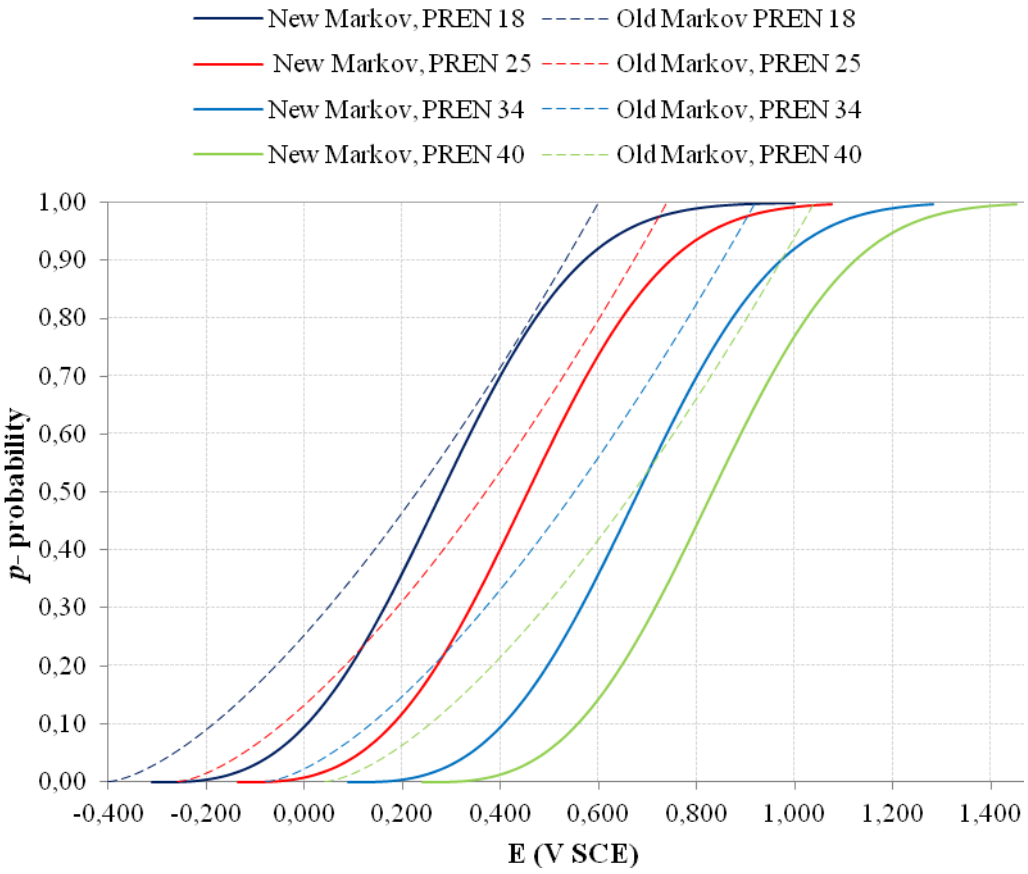

Plot 4.7- *p* probability-potential trend for different stainless steels: comparison between new and old Markov model.

4.3 CYCLIC POTENTIODYNAMIC POLARIZATION TESTS

p-probability equations (Eq. 4.4 and 4.5) were obtained through literature data elaboration; with the aim of confirm them, laboratory tests were carried out in order to obtain, in specific experimental condition, pitting and protection potential.

The relative susceptibility to localized corrosion for iron-, nickel-, or cobalt-based alloys is usually determined through cyclic potentiodynamic polarization measurements. ASTM G61 [40] covers the procedure for conducting them and the experimental procedure which can be used to check experimental techniques and instrumentation.

The voltage applied between the working electrode and the inert counter electrode is ramped at a continuous slow rate (0,6 V/h) relative to a reference electrode using a potentiostat. The voltage is first increased in the anodic direction (forward scan); then, the voltage scan direction is reversed at some chosen current or voltage (ASTM G61 suggests when current reaches 5 mA). The scan is terminated at another chosen voltage, usually either the corrosion potential [40] or some potential lower than corrosion potential [2]. The potential at which the scan is started is the corrosion potential measured when the corrosion process reaches the steady state; ASTM G61 suggests to start the potential scan one hour after specimen immersion. The procedure, as outlined in the standards, is not the only or even necessarily the best way to generate the polarization scan in all situations [1].
Though the generation of the polarization scan is simple, its interpretation can be difficult. Features identified as important for determining the propensity for localized corrosion are the *protection* or *repassivating* potential and the *pitting* or *breakdown* potential (Fig. 4.3).

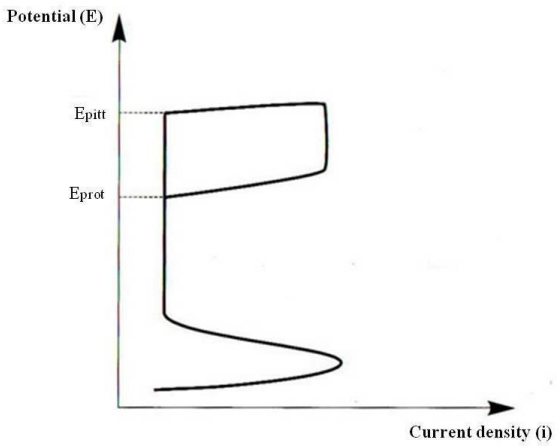

Figure 4.3- Cyclic polarization curve for a passive metal.

The potential at which the anodic current increases significantly with the applied potential is the pitting potential. In general, the more noble is the pitting potential, obtained at fixed scan rate, the less susceptible the alloy is to the initiation of the localized attack.
The second parameter of great interest is the potential at which the hysteresis loop is completed during reverse polarization scan after localized corrosion propagation. This potential is taken as the repassivation, E_{rp}, or protection potential, E_{prot}. In general, once initiated, localized corrosion can propagate only at potential more positive than the protection potential [7]; in other words, even after pitting initiation, repassivation will

occur at more negative potential. At potential between E_{pitt} and E_{prot}, sites that have initiated can propagate.

Although the cyclic method is a reasonable method for checking relative susceptibility of alloys to pitting corrosion in different environment, it has been found to have a number of shortcomings [7]. The major problem concerns the effect of the potential scan rate; the values of both E_{pitt} and E_{prot} are strong function of the manner in which the tests are performed, particularly the potential scan rate used; experimental values of E_{pitt} are linked to the induction time required for pitting: pitting potential obtained from slow scan rate test are lower than that from higher scan rate test because the attack has more time to occur and to propagate. Another complication arises from allowing too much pitting propagation to occur before reversing the scan direction: the more attack that has been allowed to occur, the more negative is the E_{prot} value.

Due to the statistical nature of pitting nucleation, the scatter in the data obtained from different polarization curves of the same material is expected especially in the forward scan. The reverse scans are more reproducible, because the local chemistry controls the repassivation [7].

4.3.1 Experimental set up

Cyclic potentiodynamic polarization tests have been performed on different materials in order to compare experimental protection potential and new-Markov model protection potential values. The electrochemical cell scheme is shown in Fig. 4.4: the reference electrode is SSC_{sat}, the counter electrode Ti-MMC and the working electrode is the test material sample. Test parameters are reported in Table 4.1.

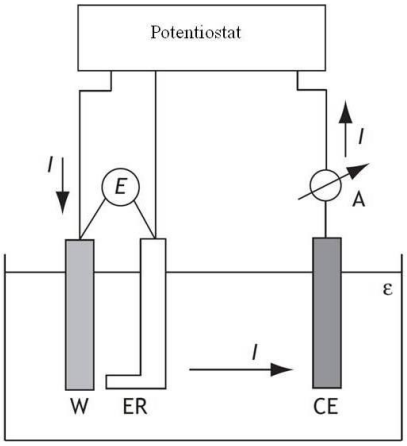

Fig. 4.4- Electrochemical cell.

Table 4.1- Test parameters.

Exposed surface	0,0001 m^2
Chloride concentration	20 g/L
Temperature	20 °C
pH	7
Scan rate	0,166 mV/s
Reversal scan current	3 mA

4.3.2 Results and discussion

4.3.2.1 AISI 430 stainless steel

Several test have been performed on AISI 430 stainless steel and experimental cyclic potentiodynamic curves are shown in Plot 4.8.

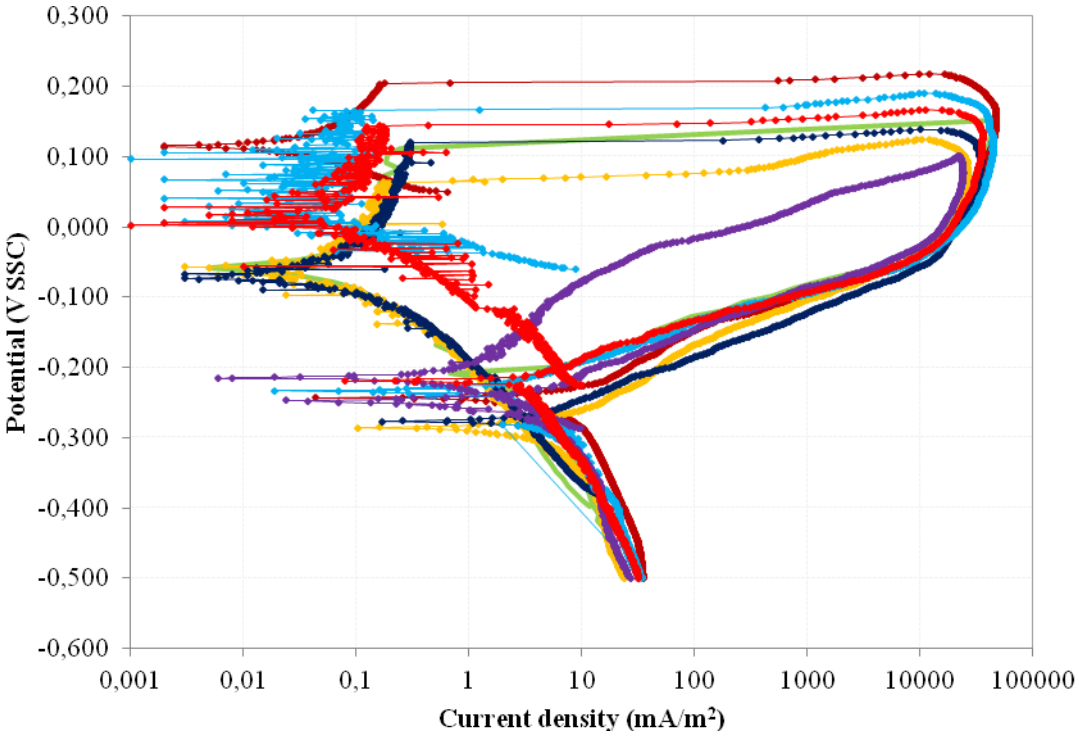

Plot 4.8- Cyclic potentio8ynamic curve for AISI 430 (PREN 17) in 20 g/L NaCl solution.

Plot 4.8 shows that the curves obtained from different tests are similar, which guarantees the reliability of results, and also shows the expected statistical variability of pitting and protection potential; furthermore, it's worth to notice that E_{prot} are not "passivity" protection potential, as in Fig. 4.3, but repassivation is achieved for immunity condition. In Table 4.2 are reported the experimental values of each test and in Table 4.3 are shown experimental mean values of pitting and protection potential and the comparison with old (Eq. 4.7) and new (Eq. 4.8) Markov model values (M* notation indicates new Markov model).

Eq. 4.7 $$E_{prot}(M) = -0{,}760 + \frac{17}{50} = -0{,}420\,\text{V SCE}$$

Eq. 4.8 $$E_{prot}(M^*) = -0{,}760 + \frac{17}{40} = -0{,}335\ \text{V SCE}$$

Experimental results show a good agreement with the new-Markov model equations: the discrepancy between Markov model protection potential and experimental values

decreases if equation is modified. Furthermore, the assumption $E_{prot}= E_{pitt} - 300$ mV is justified.

Table 4.2- Experimental values of pitting and protection potential.

Material	PREN	Test	E_{pitt} (V SCE)	E_{prot} (V SCE)
AISI 430	17	1	0,068	-0,252
		2	0,160	-0,287
		3	0,019	-0,330
		4	0,076	-0,321
		5	0,117	-0,277
		6	-0,077	-0,291
		7	0,102	-0,263

Table 4.3- Mean experimental values and Markov model values for AISI 430 stainless steel.

	Experimental	"Old" Markov model	"New" Markov model
E_{pitt} (V SCE)	0,066	-	-
E_{prot} (V SCE)	-0,289	-0,420	-0,335
$E_{pitt} - E_{prot}$ (V)	0,335	0,046	0,131

4.3.2.2 AISI 304 stainless steel

Several test have been performed on AISI 304 stainless steels and cyclic potentiodynamic curves are shown in Plot 4.9: the consideration done for AISI 304 are still valid.

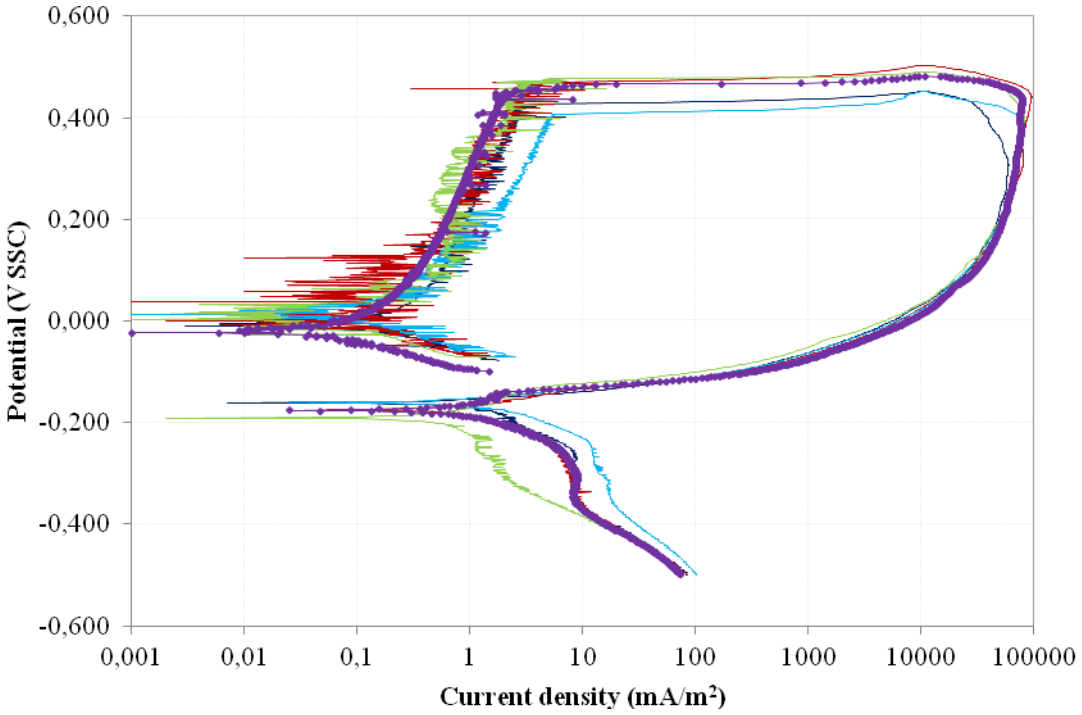

Plot 4.9- Potentiodynamic curve for AISI 304 in 20 g/L NaCl solution.

Experimental pitting and protection potential are reported in Table 4.4. Markov model protection potential are obtained from Eq. 4.9 (old-Markov model) and Eq. 4.10 (new-Markov model) and in Table 4.5 are compared with mean experimental values. Also for AISI 304 stainless steel the modification of the theoretical equation lead to a better match with experimental results.

Eq. 4.9 $E_{prot}(M) = -0{,}760 + \frac{18}{50} = -0{,}400$ V SCE

Eq. 4.10 $E_{prot}(M^*) = -0{,}760 + \frac{18}{40} = -0{,}310$ V SCE

Table 4.4- Experimental values of pitting and protection potential.

Material	PREN	Test	E_{pitt} (V SCE)	E_{prot} (V SCE)
AISI 304	**18**	**1**	0,385	-0,205
		2	0,428	-0,219
		3	0,364	-0,204
		4	0,434	-0,235
		5	0,417	-0,220

Table 4.5- Mean experimental values and Markov model values for AISI 304 stainless steel.

	Experimental	"Old" Markov model	"New" Markov model
E_{pitt} (V SCE)	0,406	-	-
E_{prot} (V SCE)	-0,217	-0,400	0,310
E_{pitt} - E_{prot} (V)	0,622	0,183	0,093

4.3.2.3 AISI 470LI stainless steel

Plot 4.10 shows the cyclic curves obtained from potentiodynamic test carried out on 470 LI stainless steel. Experimental results are reported in Table 4.6 but they seems not to be reliable or useful for the compare with Markov model values. This can be explained considering the fact that these cyclic potentiodynamic curves have features difficult to interpret: a lot of instability phenomena occur during forward scan, pitting potential seems to be of the order of oxygen evolution potential and it is not easy to determine where the hysteresis loop is completed and, then, the protection potential. Further laboratory tests should be made in order to get reliable values of pitting and protection potentials for high PREN stainless steels, like cyclic potentiodynamic polarization tests in deareated solutions or potentiostatic scratch tests [7].

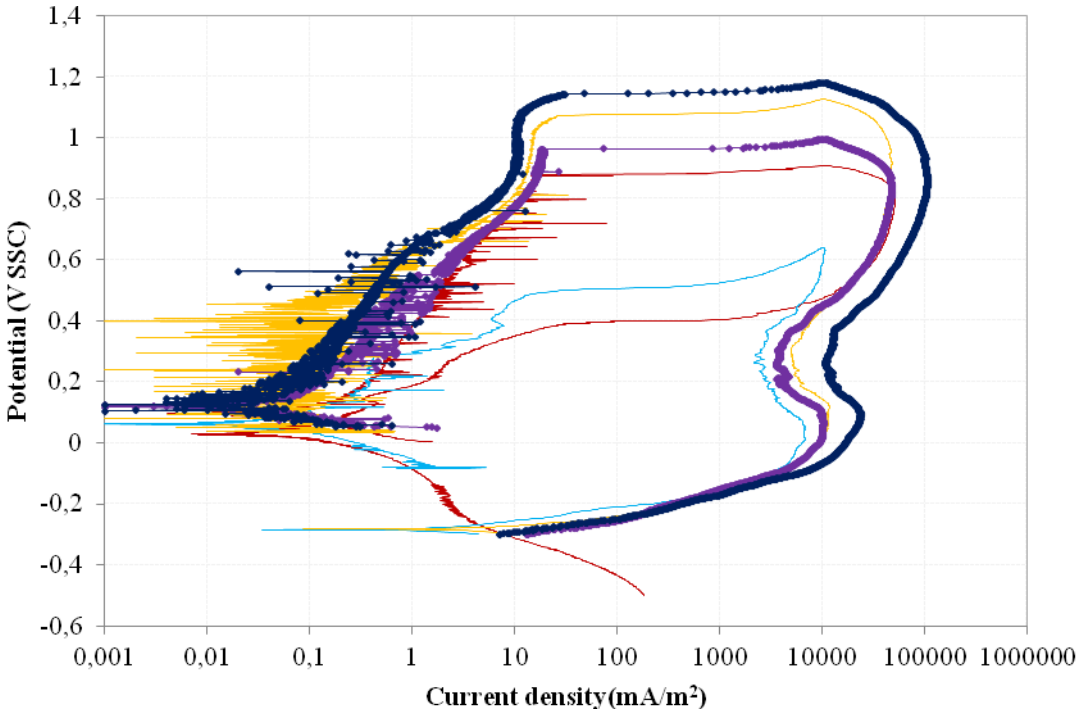

Plot 4.10- Potentiodynamic curve for AISI 470LI in 20 g/L NaCl solution.

Table 4.6- Experimental values of pitting and protection potential.

Material	PREN	Prova	E_{pitt} (V SCE]	E_{prot} (V SCE)
470LI	24	1	0,825	-0,015
		2	0,436	-0,329
		3	0,945	-0,324
		4	0,894	-0,344
		5	1,008	-0,322

Min	0,436	-0,344
Max	1,008	-0,015
Mean	0,822	-0,267

4.3.2.4 Protection potential-PREN curve: experimental and theoretical values comparison.

Protection potential values obtained from potentiodynamic tests are checked with Markov model curves. Low PREN stainless steels experimental values show a good agreement with the reviewed Markov model, as shown in Plot 4.11. For the *p*-probability curves comparison will be, then, considered only AISI 304 and 430 stainless steels.

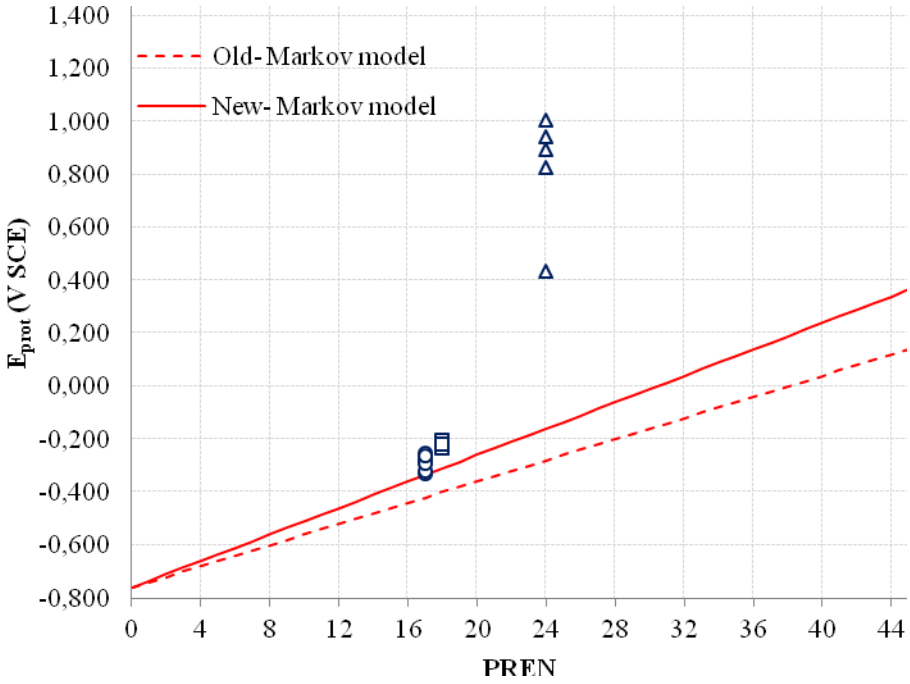

Plot 4.11- E_{prot}-PREN trend: theoretical and experimental comparison.

4.4 p-PROBABILITY CURVE: EXPERIMENTAL AND THEORETICAL VALUES COMPARISON

On the following plots, *p*-probability curves are calculated using experimental results and are compared with theoretical values. The reviewed Markov model *p*-probability curve is obtained using in Eq. 4.6 protection potential values obtained from Eq. 4.4; experimental *p*-probability values are obtained entering experimental protection potential in Eq.4.6: as

shown in Plot 4.12 and 4.13, they are reasonable, mostly considering that accelerated tests are conducted under controlled procedures and in controlled environment; accordingly, they predict lower pitting probability than theoretical model. Furthermore, mean values of E_{pitt} and E_{prot} are reported on the graphs (red circles) and compared with the reviewed Markov model curve; a good match is obtained: at potential equal to mean experimental protection potential a perfect match is obtained for both AISI 430 and 304 (pitting does not propagate and *p* is equal to zero); at pitting potential a better match is obtained for AISI 304 but the results must be observed keeping in mind that the final pitting probability is 1-R of Eq. 2.15, which takes into account also the chlorides concentration of the solution. Indeed, at 20 g/L (Table 4.1) and at potential equal to 0, 066 V SCE, the pitting probability 1-R for AISI 430, calculated with Matlab®, is 99%.

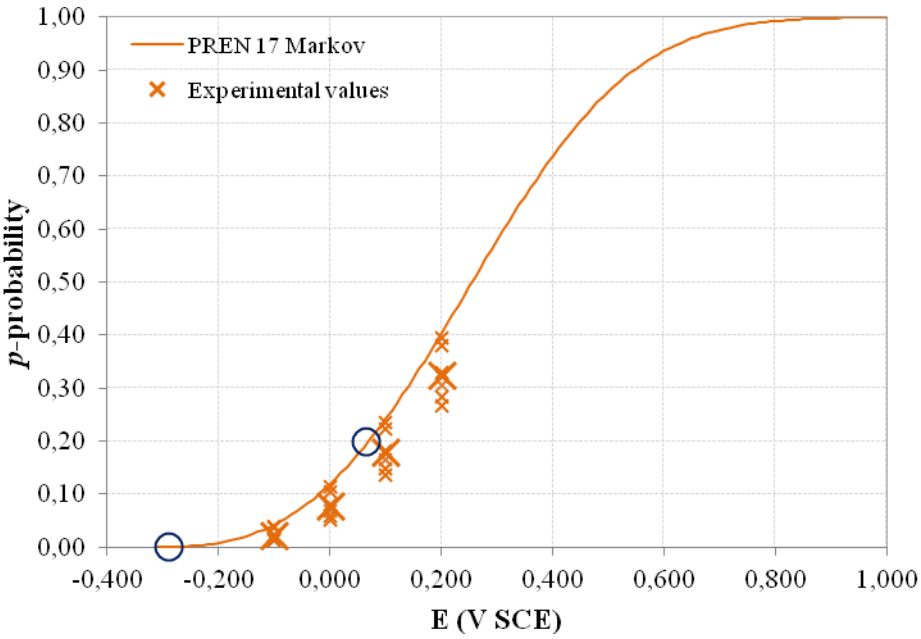

Plot 4.12- *p*-probability curve for AISI 430 stainless steel and experimental values.

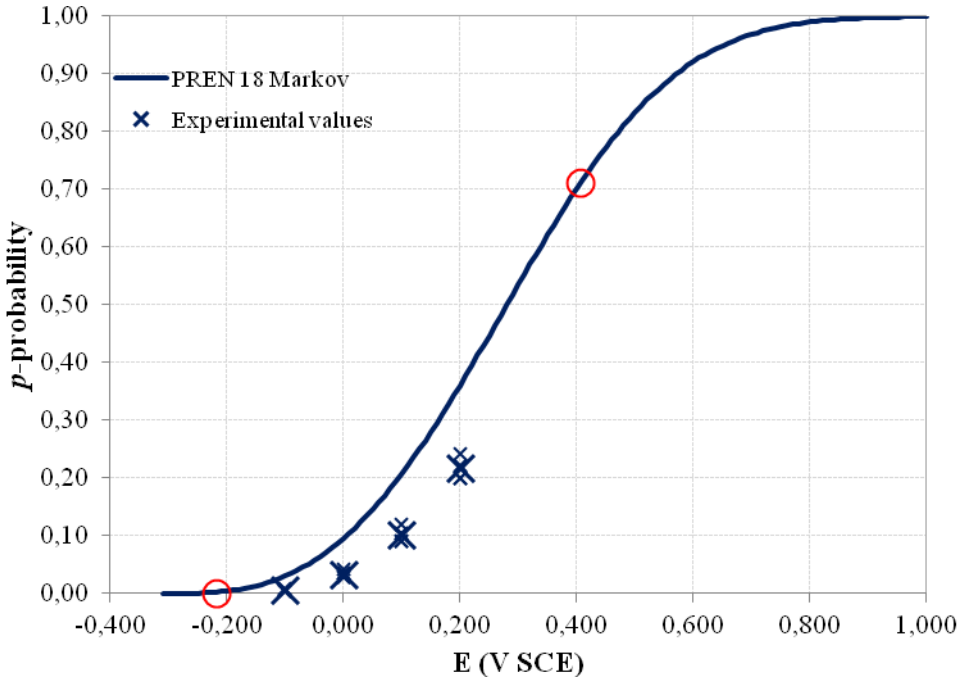

Plot 4.13- *p*-probability curve for AISI 304 stainless steel and experimental values.

Chapter 5

m-PROBABILITY: A REVIEW OF THE META-STABLE TO META-PASSIVE TRANSITION

5.1 INTRODUCTION

The transitional probability *m* is the probability that a stainless steel in a specific environment moves from the initial state of metastability to the condition of metapassivity. *m*-probability depends on the ratio between chlorides concentration in the environment ($[Cl^-]$) and critical chlorides threshold of the stainless steel ($[Cl^-]_{cr}$):

Eq. 5.1 $$m = 1 - \exp\left(-\frac{2{,}8}{k}\right)$$

Eq. 5.2 $$k = \frac{[Cl^-]}{[Cl^-]_{cr}}$$

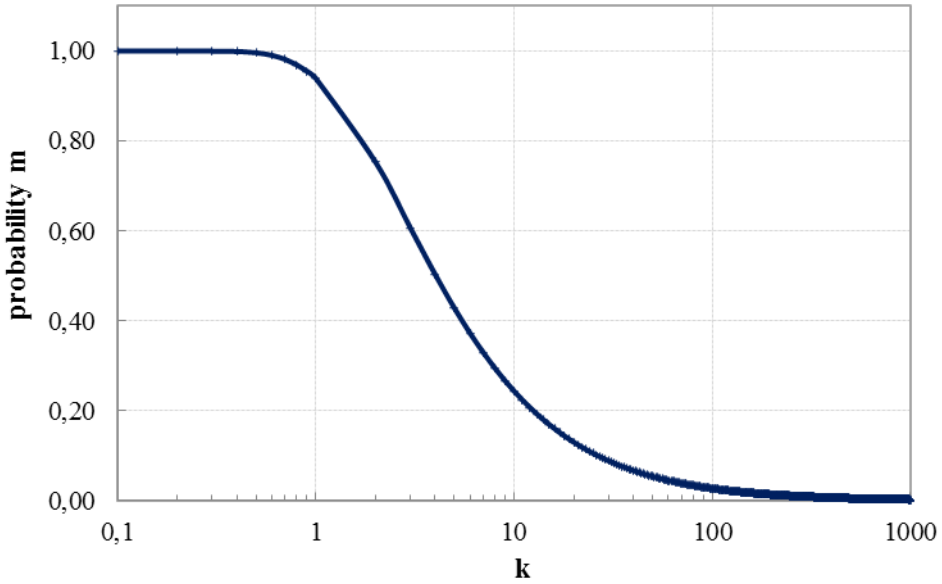

Figure 5.1- k dependence of *m*-probability.

Figure 5.1 shows the dependence of *m*-probability on k: if the solution chlorides concentration is, for example, 10 times higher than the critical chlorides threshold, *m* tends quickly to zero; if $[Cl^-]$ is, instead, equal or lower than $[Cl^-]_{cr}$ *m*-probability is between 0,90 and 1. The breakdown of the passive film is more likely to occur as the chloride concentration of the solution approaches the critical chloride content. Equation 5.3 shows the relationship between critical chloride threshold and metallurgical, environmental and geometrical factors (section 2.4.2):

Eq. 5.3
$$\log[Cl]_{cr} = \left[\frac{PREN}{9} - \frac{7 - pH}{3{,}5} - \frac{T - 20}{20\left(1 - \frac{1}{4} k_{crevice}\right)} - 0{,}3 k_{crevice} \right]$$

Since the relation between critical chlorides threshold and PREN is widespread among corrosion engineers, the attention has been focused on pH and temperature dependence. Experiments have been designed to get the critical chlorides concentration at three different pH (2, 7 and 12) and at two different temperatures (20 °C and 40 °C) in order to subsequently check them with Markov model trends (Figure 5.2 and 5.3).

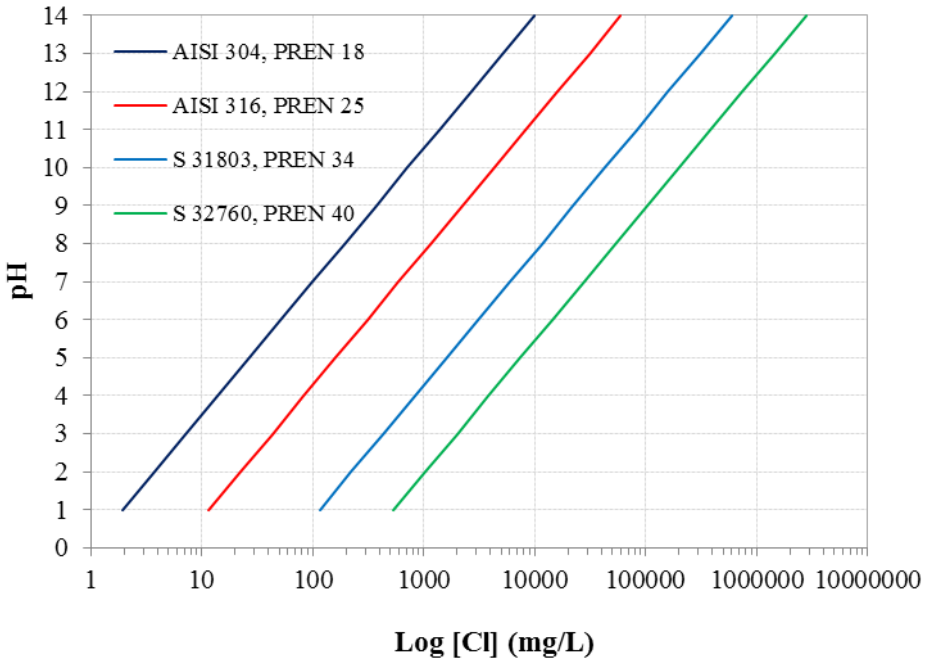

Figure 5.2- Critical chlorides threshold dependence of pH: theoretical curves predicted by Markov model for different stainless steel at 20°C and k_{cr}= 0.

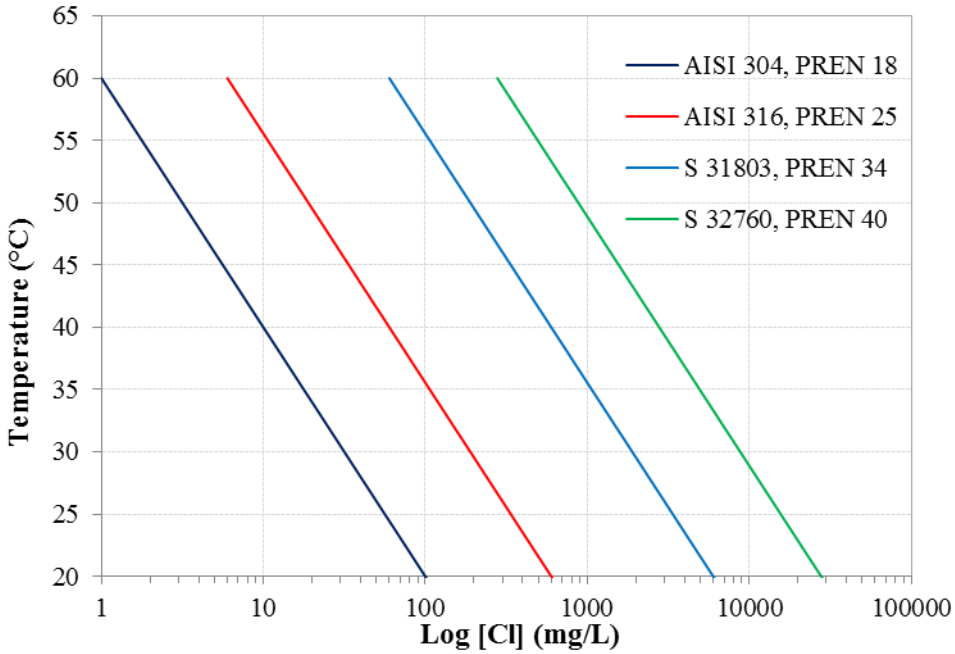

Figure 5.3- Critical chlorides threshold dependence of temperature: theoretical curves predicted by Markov model for different stainless steels at pH 7 and K_{cr} equal to zero.

5.2 LINEAR POLARIZATION RESISTANCE TEST

Corrosion initiation is always associated with an increase of current density with respect to that of the passive state; Linear Polarization Resistance (LPR) monitoring is an effective electrochemical method of measuring corrosion current by means of a potentiostat and a three-electrode electrochemical cell, shown in Figure 5.4 and described in section 3.2. Between the sample (working electrode) and the reference electrode is applied a potential which is scanned at constant rate (0,166 mV/s) from -10 mV vs E_{corr} to +10 mV vs E_{corr} and the circulating current is measured and normalized with respect to the surface area [7].

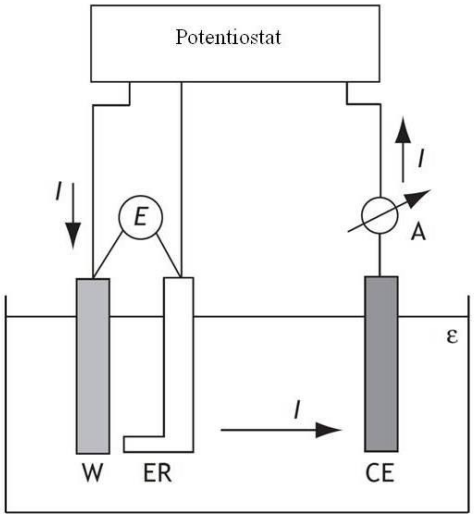

Figure 5.4- Schematic representation of the electrochemical cell: CE is the counter electrode (Ti-MMO), W the working electrode (stainless steel sample) and ER the reference electrode (SSCsat).

At potential very close to E_{corr} the slope of the potential-current curve, $\left(\frac{\Delta E}{\Delta i}\right)$, is approximately linear (Fig. 5.5) and has the units of resistance (Eq. 5.4)

Eq. 5.4 $$LPR = \frac{\Delta E}{\Delta i} \ [\Omega] \qquad \text{if } (E\text{-}Ecorr) \rightarrow 0$$

The measured resistance is inversely related to the corrosion current:

Eq. 5.5 $$i_{corr} = \frac{\Delta i}{2{,}3\Delta E} \frac{\beta_a \beta_c}{\beta_a + \beta_c} = \frac{B}{LRP}$$

Where βa and βc are anodic and cathodic Tafel slopes and B is the Stern-Geary coefficient.

Representing the polarization curve as a linear potential-current density plot, the polarization resistance LPR is determined as the tangent of the curve at *i*=0.

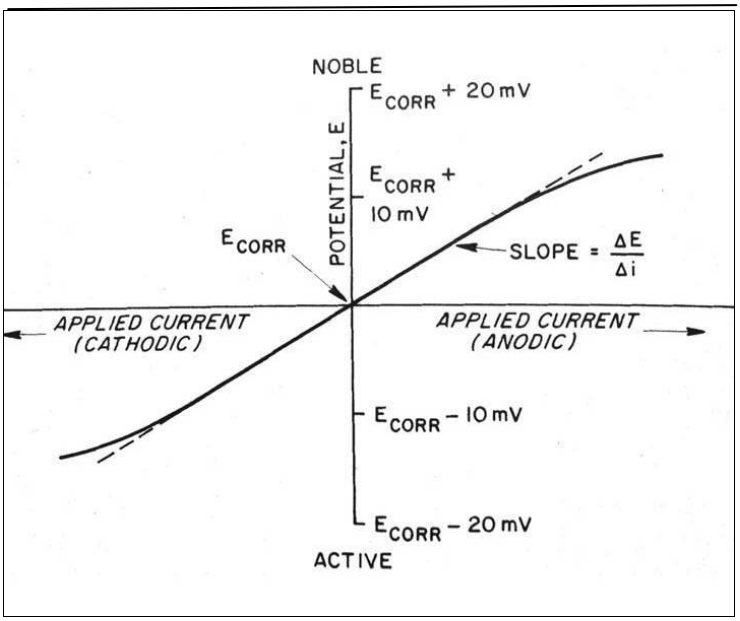

Figure 5.5 Measurement of i_{corr} by linear polarization [2].

Polarization resistance and corrosion potential monitoring provides information about pitting corrosion. A simultaneously drop of LPR and potential suggests passive layer breakdown and increase of corrosion rate. This is explained considering the inverse proportionality between polarization resistance and current density (Eq 5.5); furthermore, Figure 5.6 shows that a lower corrosion potential means an active behavior of stainless steel. If the system works at point A, the material is passive and characterized by noble potential and low corrosion current density; when the passive film breakdown occurs, stainless steel anodic curve is like that of an active material (Fig. 5.6, dashed line) and the working point of the system becomes B: the potential drop from A to B is matched with an increase of current density.

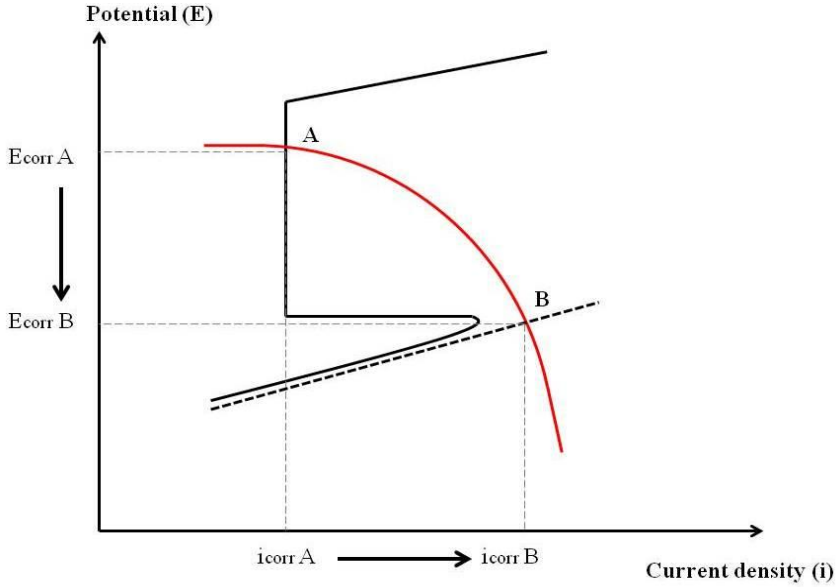

Figure 5.6- Schematic illustration of the electrochemical concept of potential decrease.

5.3 EFFECT OF pH ON CRITICAL CHLORIDES THRESHOLD

5.3.1 Aim of the test

In order to get the pH-critical chlorides concentration trend, the following experiment has been designed. Three tanks, containing NaCl solution, were set up: one at pH 2, one at pH 7 and one at pH 12. In each tank were immersed five samples of AISI 304 stainless steel, whose potential and LPR variation in time was monitored. Every 48 hours the chlorides concentration was increased until a simultaneous decrease of potential and LPR occurs: the chlorides content corresponding to this simultaneous variation is the critical chlorides threshold.

5.3.2 Experimental set-up

Fifteen AISI 304 stainless steel samples (size 1 x 1 cm) were cut from sheets of dimensions 18 x 27 x 0.1 cm. They were electrically connected to an insulated electrical cable by spot welding of the back surface. The sample surface, which will be exposed to the solution, was then positioned to the bottom of a lubricated teflon couvette and the back surface was

covered with an epoxy resin (Fig. 5.7). After 24 hours, the sample was extracted from the sample-holder and the exposed surface finished with abrasive papers. The sample is shown in Figure 5.8.

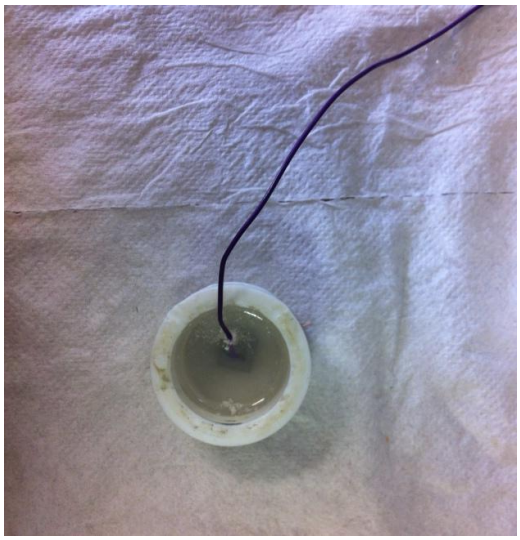

Figure 5.7- Sample in the teflon couvette.

Figure 5.8- Finished sample.

The test solutions were prepared with 2 L of distilled water and different concentration of sodium chlorides, depending on the pH. The initial chlorides concentration were: 50 mg/L at pH 7, 10 mg/L at pH 2 and 300 mg/L at pH 12. Acid solution was obtained adding 0,981 g of H_2SO_4; alkaline solution adding 8 g of NaOH.

For each becker a cover with five holes for the samples and two holes for the reference and counter electrodes was prepared. Holes allow the passage of electric cables (Fig. 5.9). Five sample were immersed in each becker and a shunt was mounted at the end of each cable (Fig.5.10). Every 48 hours potential and LPR were monitored (Fig. 5.11) and chlorides concentration was increased by the addition of sodium chlorides to the solution.

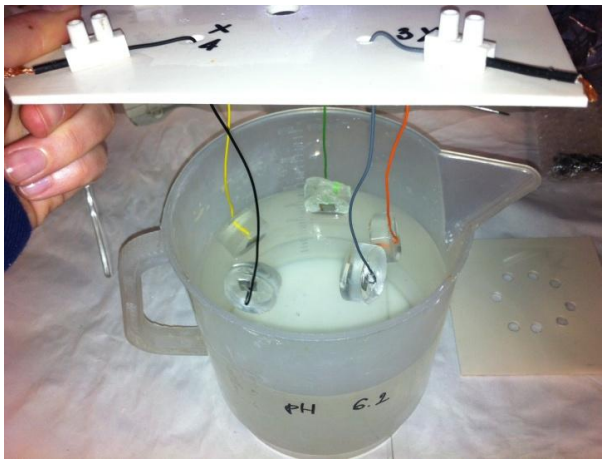

Fig. 5.9- Cables passage into cover holes and sample immersion.

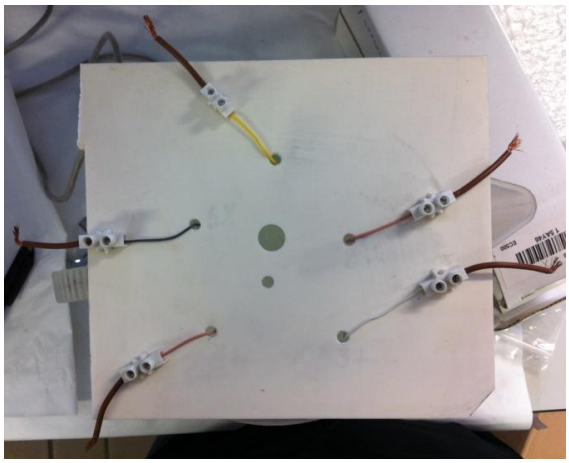

Fig. 5.10- Becker cover.

Fig. 5.11- Electrical connection and monitoring.

5.3.3 Results

5.3.3.1 pH= 2

Plot 5.1 and 5.2 show potential and LPR variation with time. Sample 1 and sample 5 are affected by a potential drop which, however, is not matched with a LPR drop; anyway, the determination of the critical chlorides content (corresponding to the day when a sensible decrease of potential and LPR occurs) is possible and reported in Table 5.1. The variation in the electrochemical behavior of sample 2, 3, and 4 is difficult to recognize: potential and polarization resistance trend is quite constant in time and corrosion current density is, since the first day after immersion, of the order of 10 mA/m^2; since, at pH 2, AISI 304 stainless steel may be subject of a corrosion attack uniformly distributed over the entire surface (see section 2.3.1); the idea, which agrees with experimental results, is that for samples 2, 3 and 4 general corrosion occurred.

Table 5.1- Critical chlorides threshold at pH 2.

pH	Sample	$[Cl]_{cr}$ (mg/L)	Mean value (mg/L)	Minimum value (mg/L)
2	1	4000	**2750**	1500
	2	-		
	3	-		
	4	-		
	5	1500		

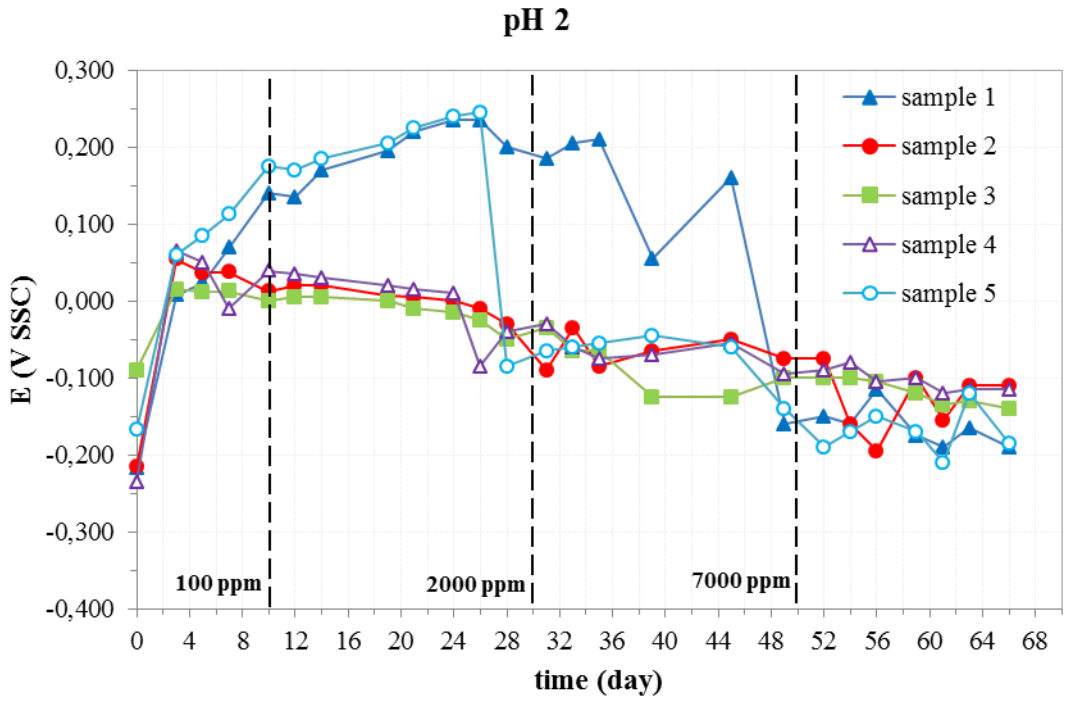

Plot 5.1- Potential- time trend at pH 2.

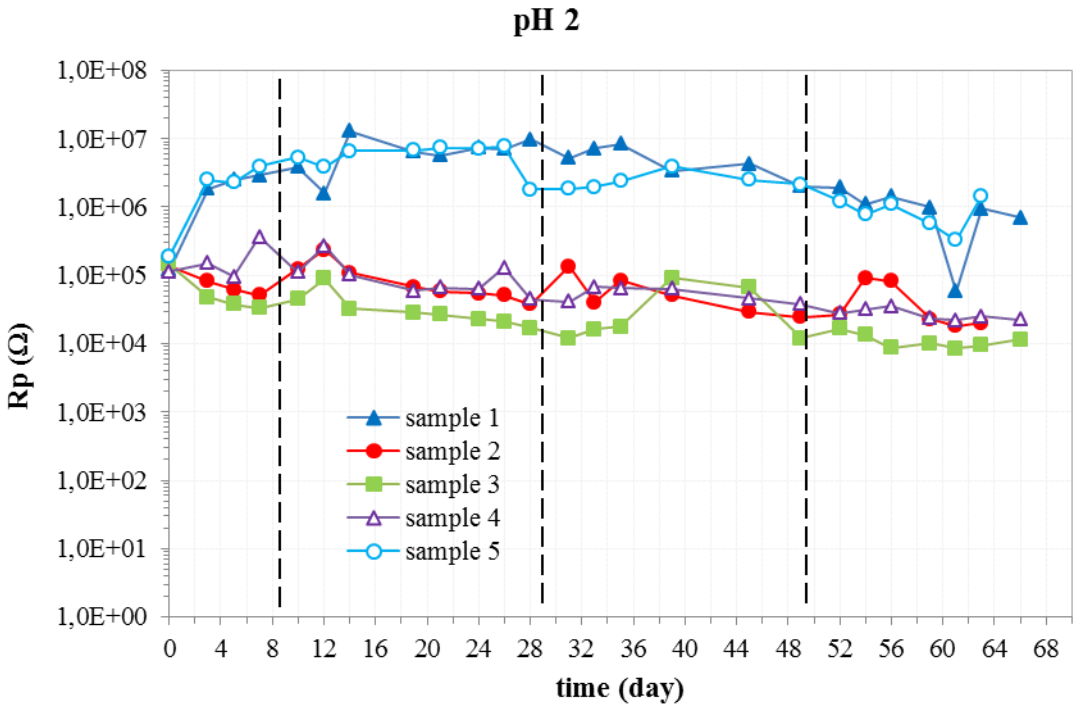

Plot 5.2- LPR-time trend at pH 2.

5.3.3.2 pH= 7

Plot 5.3 and 5.4 show potential and LPR variation with time for the five samples at pH 7 and Table 5.2 reports critical chlorides thresholds and their mean value. Also in this case, trends are difficult to interpret; instability phenomena, like metastable pits, may be occurred: this is shown by the "up and down" trend of both potential and LPR. Critical chlorides concentration is chosen to be that corresponding to potential and resistance stabilization to the lower values: potential decreases from about 100 mV SSC (passive condition) to -200 mV SSC (active condition), while LPR decreases from values of the order of 10^7 Ω, which corresponds to passive currents lower than 1 mA/m^2, to values of the order of 10^5 Ω, which corresponds to corrosion current higher than 2 mA/m^2.

Sample 5 has an anomalous behavior: potential of the order of -150 mV SSC, which remains stable in time, and LPR which decreases progressively from initial values of the order of 10^5 to values of the order of 10^4; this can be explained assuming a less stable passive film, maybe deriving by some inaccuracy during sample preparation.

Table 5.2- Critical chlorides threshold at pH 7.

pH	Sample	$[Cl]_{cr}$ (mg/L)	Mean value	Minimum value
7	1	30000	**17500**	10000
	2	15000		
	3	15000		
	4	10000		
	5	-		

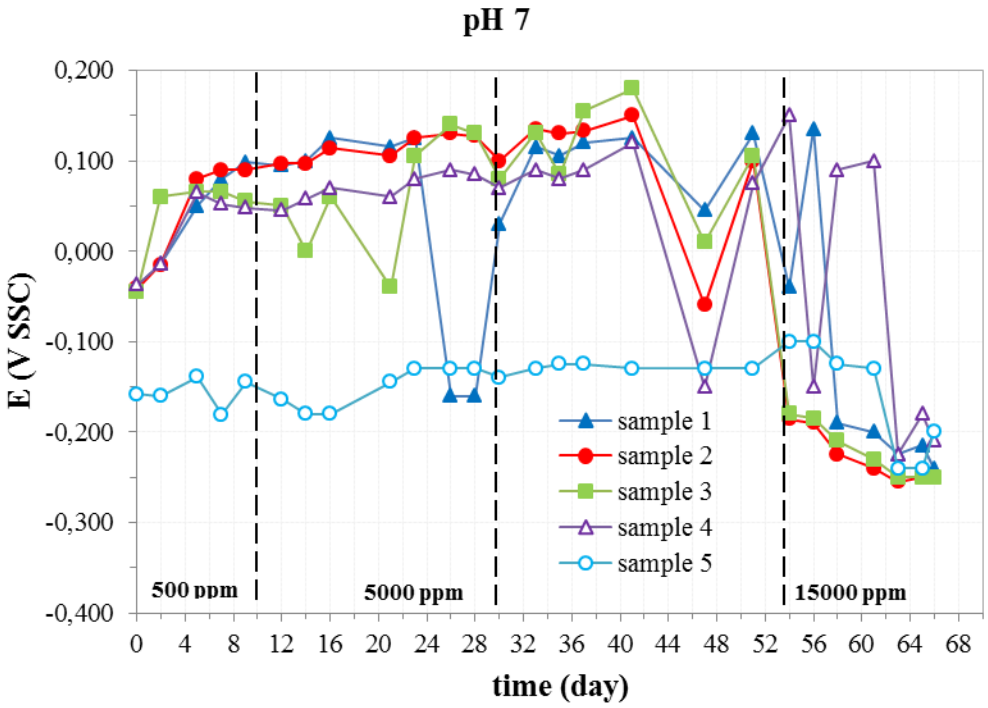

Plot 5.3- Potential-time trend at pH 7.

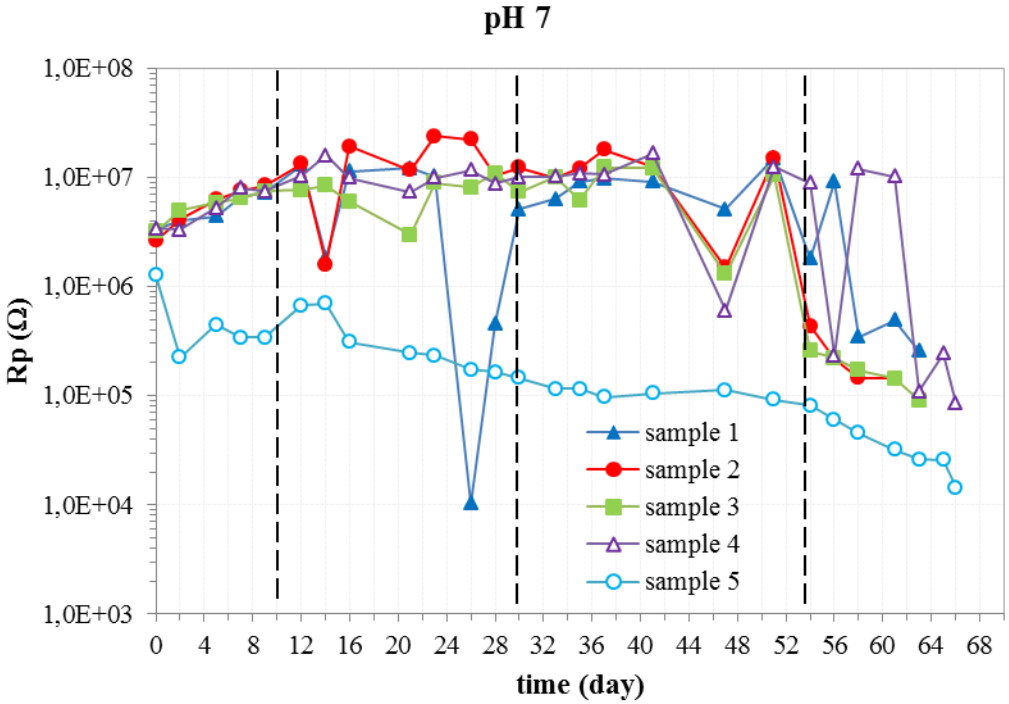

Plot 5.4- LPR-time trend at pH 7.

5.3.3.3 pH= 12

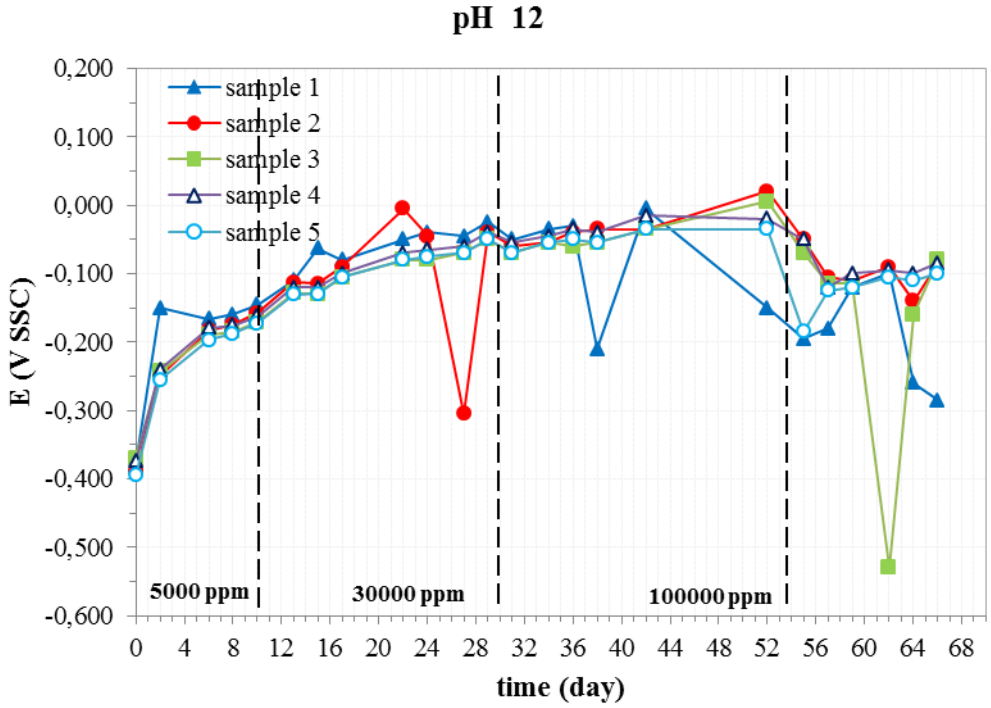

Plot 5.5- Potential-time trend at pH 12.

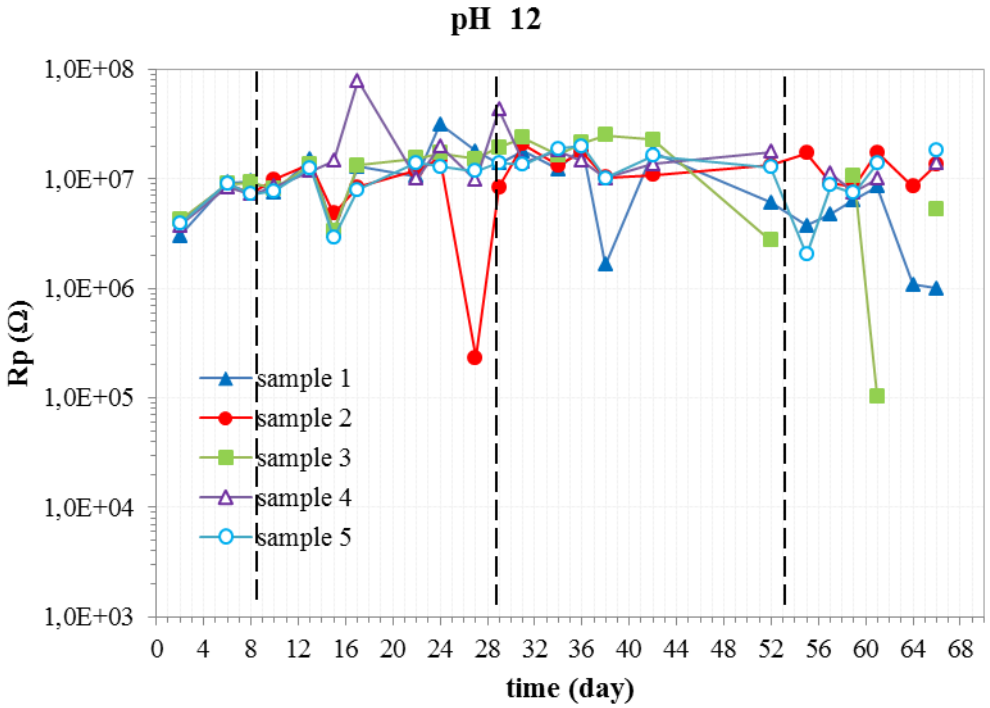

Plot 5.6- LPR-time trend at pH 12.

Plots 5.5 and 5.6 show potential and LPR variation with time for the five samples at pH 12. Also in this case, the "up and down" trend of both potential and LPR suggests that metastable pits may be started; anyway, the critical chlorides threshold cannot be identified because there is not an evident and permanent variation in the electrochemical behavior of the samples.

5.3.4 Discussion

The first consideration that must be done is about the absolute value of the critical chlorides threshold. It's evident that, for example, a critical chlorides threshold of 20.000 ppm at pH 7 is not reasonable: corrosion experience suggests that AISI 304 stainless steel critical chloride content at neutral pH, room temperature and stagnant condition is about 50-100 ppm. As already discussed in Chapter 3, it's important to take into account the limitation of laboratory experiments in order to interpret carefully the results of these tests. Laboratory experiments are carried out under controlled condition during which there isn't any temperature, pH or chlorides concentration variation; sample surface is small (1 cm^2) compared to exposed surface in real system components and then the probability to find pitting initiation sites (surface defects) decreases. Another critical point is experiments duration: initiation time for pits formation is a stochastic parameter very difficult to predict; laboratory experiments are accelerated test for practical reasons and, even if widespread accepted and used, may lead to misleading results. It follows that two days maybe are not sufficient to initiate corrosion at a fixed chlorides concentration.

For comparison purposes, the experimental pH-critical chlorides threshold trend and the Markov one (for PREN 18 stainless steel, at 20°C, and k_{cr} equal to zero) are reported on the same graph (Plot 5.7): as discussed, absolute values of chlorides threshold are not reliable but the linear trend is respected; the pH= 12 critical chlorides threshold reported on Plot 5.7 is the chlorides concentration of the last day of the experimental tests (200.000 mg/L).

As the slope of the old Markov model and experimental straight lines is quite different, the idea is to change the A constant of Eq. 5.4, which for Markov model is equal to 3,5:

Eq. 5.4 $$\log[Cl]_{cr} \propto \left(\frac{pH-7}{A}\right)$$

The experimental curve is then shifted toward lower values: the boundary condition is chlorides threshold at pH 7 equal to zero and the experimental straight line is then fixed at the point B. While old Markov model trend was that each 3,5 pH unit the critical threshold increased of one order of magnitude, the experimental trend shows that each 5 pH unit $[Cl^-]_{cr}$ increases of about one order of magnitude (Eq. 5.5); then, the new A constant is equal to 5:

Eq. 5.5 $$\log[Cl]_{cr} \propto \left(\frac{pH-7}{5}\right)$$

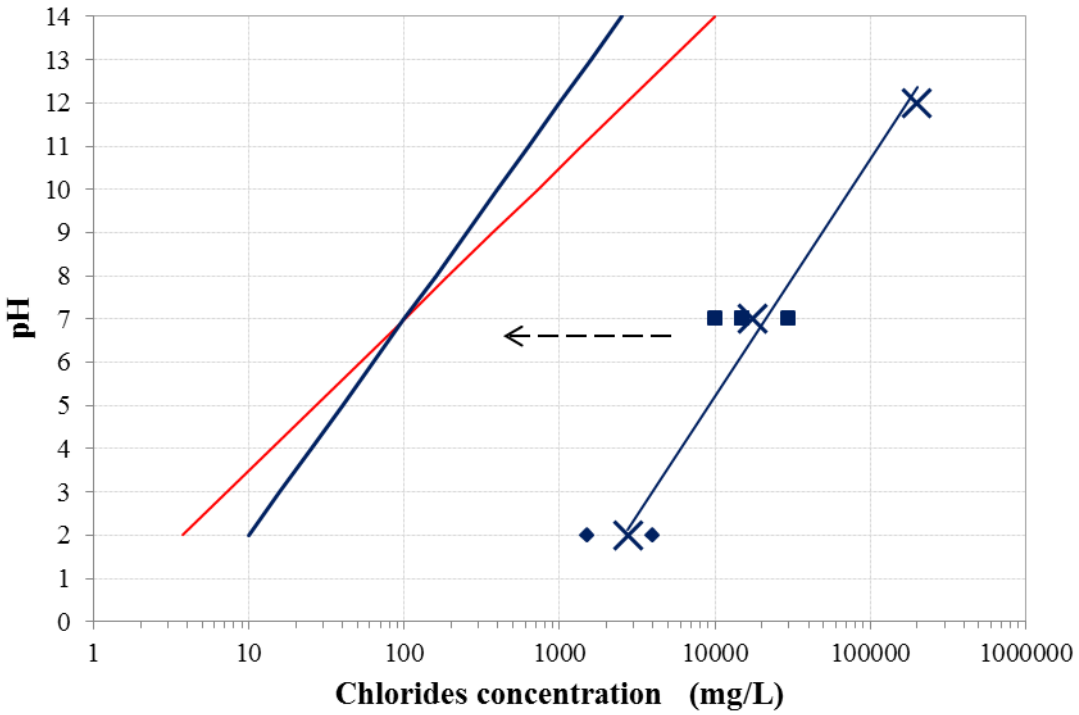

Plot 5.7- Experimental data elaboration: reviewed pH- chlorides threshold trend.

5.4 EFFECT OF TEMPERATURE ON CRITICAL CHLORIDES THRESHOLD

5.4.1 Aim of the test

In order to get the temperature-critical chlorides threshold trend, potential and LPR monitoring has been carried out for five samples at 40°C and neutral pH. The 20°C results are considered those at pH 7 of section 5.3.3.2.

5.4.2 Experimental set up

The test material is AISI 304 stainless steel and five samples were prepared as described in section 5.3.2. The test solution was prepared with 1,6 L of distilled water and an initial chlorides concentration of 100 mg/L. The cover with five holes for the sample electric cables and two holes for the reference and counter electrodes was prepared. Five sample were immersed in the glass becker and a shunt was mounted at the end of each cable, as already shown in Fig. 5.10.
In order to raise solution temperature to 40°C and maintain it during the experiment duration, an heating plate was used which had been connected with a Vertex, a digital thermoregulator for direct temperature control of the liquid (Fig. 5.12). Every 48 hours potential and LPR were monitored and chlorides concentration increased by the addition of sodium chlorides to the solution.

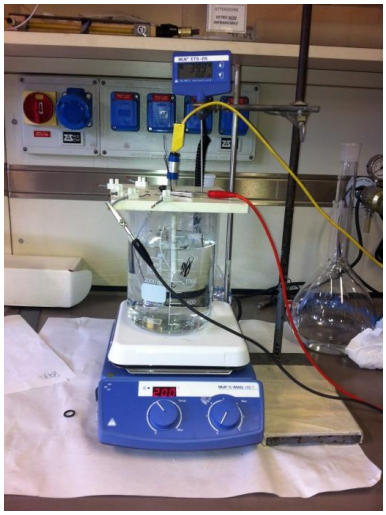

Fig. 5.12- 40° C test set up and cables for potential and LPR monitoring.

5.4.3 Results

Plots 5.8 and 5.9 show potential and LPR variation with time and in Table 5.3 are reported the critical chloride thresholds and their mean value. Also in this case the trends are difficult to interpret because there is not always an evident drop in potential and polarization resistance; anyway, sample 1 shows a 250 mV and samples 4 and 5 a 50 mV of potential drop matched with LPR decrease, which from values of the order of 10^6 Ω decreases to values of the order of 10^4-10^5 Ω; sample 2 and 3 show, instead, a potential stabilization in time to high potential values.

Table 5.3- Critical chlorides threshold at 40°C.

Temperature	Sample	[Cl]cr (mg/L)	Mean value	Minimum value
40	1	15000	7000	2000
	2	-		
	3	-		
	4	2000		
	5	5000		

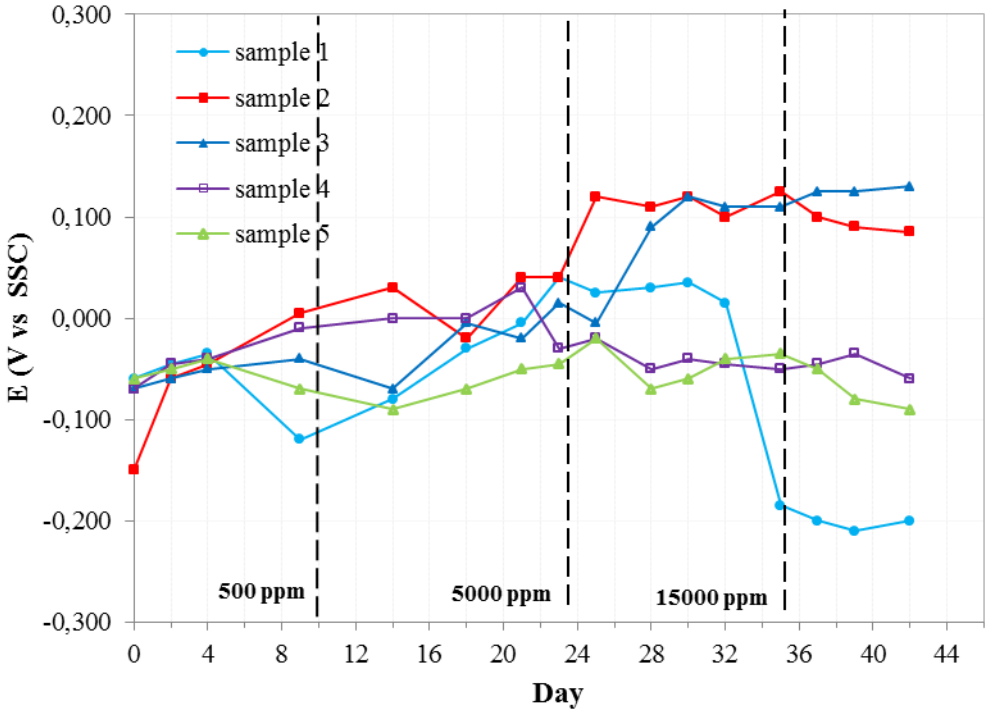

Plot 5.8- Potential-time trend at 40°C.

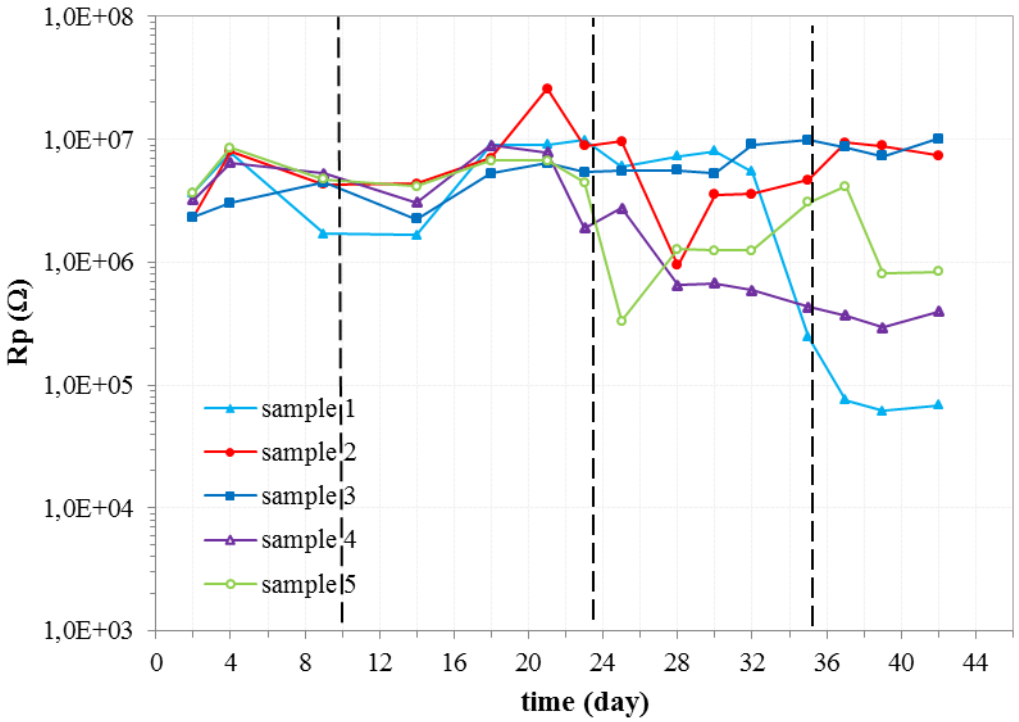

Plot 5.9- LPR-time trend at 40°C.

5.4.4 Discussion

The considerations done about experimental corrosion tests limitation (section 5.3.4) are relevant also in this case and the data elaboration which follows is methodologically similar to that realized for the pH trend. The experimental and the Markov model curves are compared in Plot 5.10: the critical chlorides threshold of 100 ppm for PREN 18 stainless steel at 20°C and pH 7 is chosen again as boundary condition; then, the curve is shifted to lower values and fixed at point B; the aim is to evaluate the slope variation and change the A constant of Eq. 5.6, which, for Markov model, is equal to 20:

Eq. 5.6 $$\log[Cl]_{cr} \propto \left(\frac{20-T}{A}\right)$$

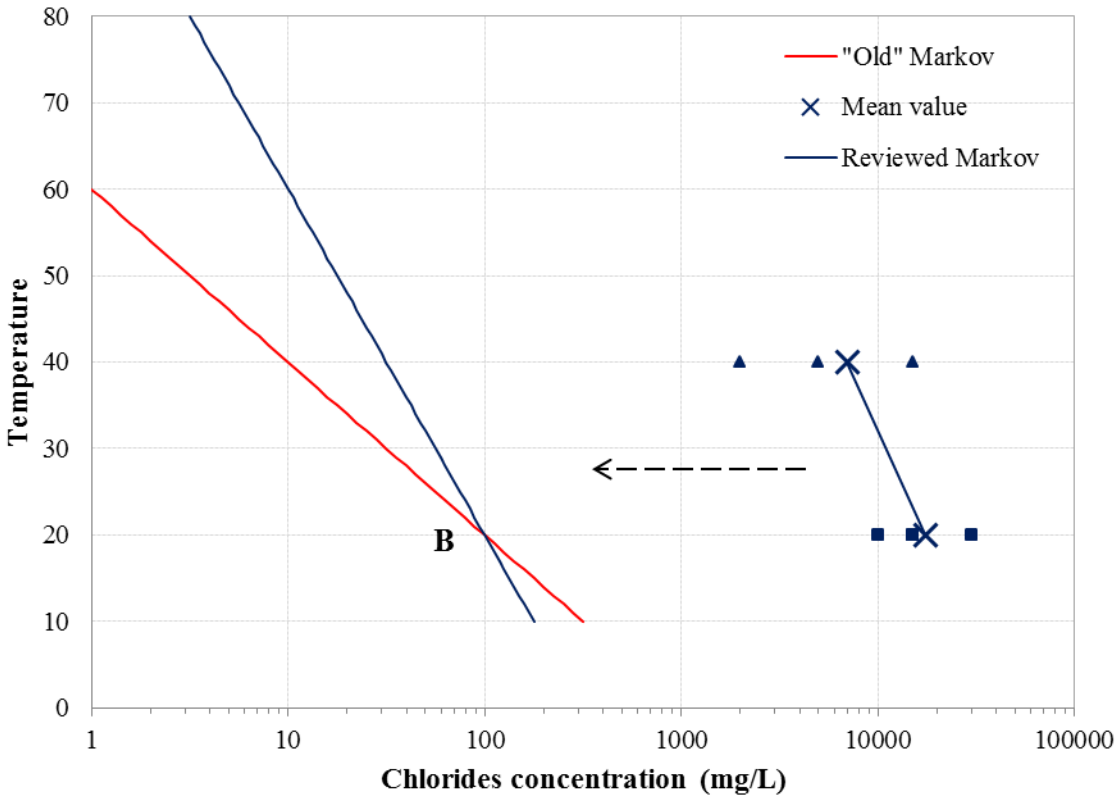

Plot 5.10- Experimental data elaboration: reviewed temperature- critical chlorides threshold trend.

Experimental data show that critical chlorides threshold decreases one order of magnitude each 40°C increase (Eq. 5.7), instead each 20°C as predicted by the old Markov model; A constant is then equal to 40, as shown in Eq. 5.7.

Eq. 5.7 $$\log[Cl]_{cr} \propto \left(\frac{20-T}{40}\right)$$

5.5 CALCULATION OF *m*-PROBABILITY

As already discussed, the PREN dependence of critical chlorides threshold has not been modified because widespread among corrosion engineers and the crevice parameter has not been studied yet. The *m*-probability equation becomes:

Eq. 5.8 $$\log[Cl]_{cr} = \left[\frac{PREN}{9} - \frac{7-pH}{5} - \frac{T-20}{40\left(1-\frac{1}{4}k_{crevice}\right)} - 0{,}3k_{crevice}\right]$$

Table 5.5 shows how *m*-probability changes varying pH and the reviewed probability is compared with the old one. Values are obtained through Matlab® elaboration.

Table 5.5- pH dependence of old Markov and new Markov model *m*-probability.

PREN	Temperature (°C)	Chlorides (mg/L)	pH	m-probability old Markov	m-probability new Markov
18	20	1000	**2**	0,0104	0,0276
			7	0,2442	0,2442
			12	0,9995	0,9392

As expected, *m*-probability (meta-stable to meta-passive transition) increases as pH increases because alkaline condition favors repassivation. Reviewed *m*-probability at pH 2 is higher than that of Markov model: laboratory tests results show an high resistance to pitting for samples at pH 2. At neutral pH (and 20°C) *m*-probability does not change respect to "old" Markov model because of the choice of the boundary condition for data

elaboration (section 5.3.4). At alkaline pH reviewed *m*-probability results lower because of the change in the slope of the pH-critical chlorides threshold straight line (Plot 5.7).
The effect of temperature on *m*-probability is shown in Table 5.6: *m*-probability decreases as the temperature increases, as expected. The reviewed probabilities are higher than the "old" because experimental tests show an higher pitting resistance of the material. This trend changes for temperature lower than 20°C because of the slope of the temperature-critical threshold straight line.

Table 5.6- Temperature dependence of old Markov and new Markov model m-probability.

PREN	Temperature (°C)	Chlorides (mg/L)	pH	m-probability old Markov	m-probability new Markov
18	**20**	1000	6	0,1350	0,1619
	40			0,0144	0,0543
	60			0,0014	0,0028

Table 5.7- Chlorides concentration dependence of old and new Markov model m-probability.

PREN	Temperature (°C)	Chlorides (mg/L)	pH	m-probability old Markov	m-probability new Markov
18	40	**100**	6	0,1350	0,4280
		1000		0,0144	0,0543
		20000		0,00072	0,0028

Table 5.7 shows a decrease of meta-stable to meta-passive transition probability as chlorides concentration increases because higher chlorides lead to less strong passive film. The reviewed probabilities, as expected, are higher.
Plot 5.11 shows a compare of old Markov and new Markov model *m*-probability curve for three different stainless steels at pH 6, 25°C and k_{cr} equal to zero. It shows an higher metastable to metapassive transition probability: for example, for PREN 18 stainless steel at 100 ppm chlorides the old Markov *m*-probability was 55% while the new one is 73%; a PREN 40 duplex stainless steel shows an *m*-probability equal to one until about 8000 ppm chlorides; it decreases to 70% at 25000 ppm for the old model and 30000 ppm for the new one; one can also observe that increasing the PREN, the difference between the two model decreases.

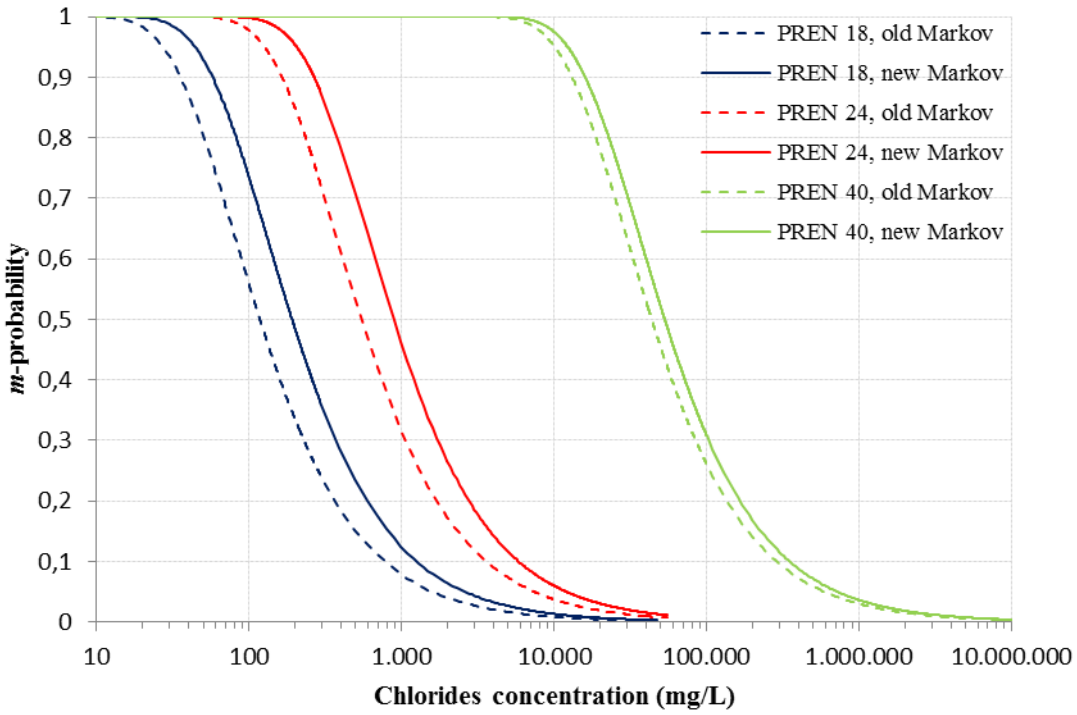

Plot 5.11- Compare between old and new Markov m-probability dependence for different stainless steel at pH 6, 25°C and kcr equal to zero on chlorides concentration.

In order to complete the *m*-probability review, crevice effect must be studied; furthermore, some consideration about Eq. 5.1 should be done. Considering what already examined and modified, in the following and last chapter a compare between reviewed, old Markov and experimental pitting probabilities (1-R) is shown.

Chapter 6

CONCLUSION

In the industrial field, localized corrosion of stainless steels, as pitting and crevice, is a critical issue. Since, once pits initiate, their propagation is fast and generally unstoppable, the major effort of corrosion engineers is focused on the prediction of the initiation time. Pitting corrosion and its initiation are intrinsically stochastic phenomena and for their description a probabilistic approach is mandatory. In this work is proposed a Markov chain's mathematical model which assumes that pitting retains no memory of its past history and is characterized by two absorbing states (pitting and repassivation) and three transitional states (metastable, metapassive, metapitting), as shown in Fig. 6.1; the model takes into account metallurgical and environmental factors, as material composition (PREN), chlorides concentration, pH, temperature, fluidodynamic condition and oxidant power of the system, with the aim to calculate the corrosion probability of stainless steels in environments. By means of literature data elaboration and laboratory tests, the equations, which relates the aforementioned parameters with the transitional probabilities (in particular *m* and *p*), initially empirical expressions based on engineering knowledge of corrosion behavior of stainless steels, are revised and partly modified. The new equations are reported in the following.

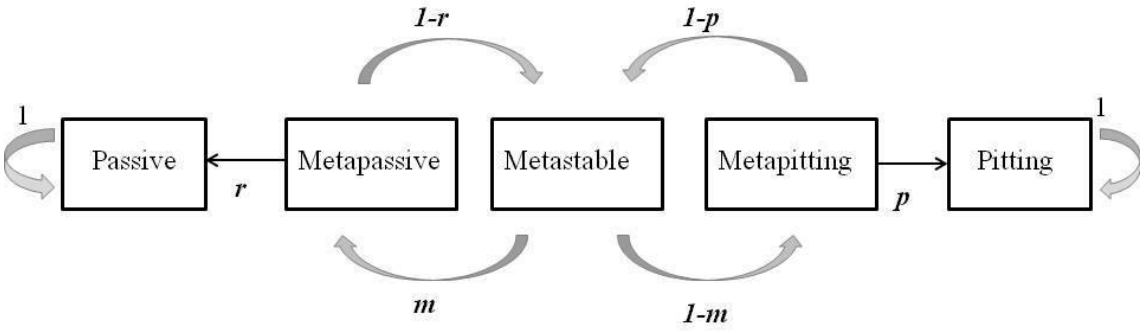

Fig. 6.1- Five-step Markov model.

6.1 p-probability: new Markov model equation

The probability to move from the metapitting state to the pitting absorbing state depends on the difference between the potential of the material in a specific environment and the protection potential (Eq. 6.1). If the system is on cathodic protection ($E \le E_{prot}$) *p*-probability is equal to zero because corrosion is not thermodynamically possible.

Eq. 6.1
$$\begin{cases} p = 0 & E \le E_{prot} \\ p = 1 - \exp\left[-\frac{3}{2}\left(E - E_{prot}\right) \right]^3 & E \ge E_{prot} \end{cases}$$

The protection potential is assumed to be linear dependent on PREN (Eq. 6.2) but independent on the chlorides concentration, which plays an important role in defining, instead, *m*-probability.

Eq. 6.2
$$E_{prot} = -0{,}760 + \frac{PREN}{40} \text{ V SCE}$$

6.2 m-probability: new Markov model equation

The probability that the system evolves from the metastable condition to the metapassive state depends on the ratio *k* between the solution chlorides concentration $[Cl^-]$ and the critical chlorides threshold $[Cl^-]_{cr}$ (Eq. 6.3).

Eq. 6.3
$$m = 1 - \exp\left(-\frac{2{,}8}{k} \right), \text{ where}$$

Eq. 6.4
$$k = \frac{[Cl^-]}{[Cl^-]_{cr}}$$

Eq. 6.5 shows the relationship between critical chloride content and metallurgical, environmental and geometrical factors; in this work, the elaboration was focused on temperature and pH dependence.

$$\text{Eq. 6.5} \qquad \log[Cl]_{cr} = \left[\frac{PREN}{9} - \frac{7 - pH}{5} - \frac{T - 20}{40\left(1 - \frac{1}{4} k_{crevice}\right)} - 0{,}3 k_{crevice} \right]$$

6.3 r-probability: the existing Markov model equation

The probability *r* is the probability that a stainless steel in a specific environment moves from the metapassive condition to the absorbing state of passivity. It depends on the fluidodynamic condition of the system (fluid velocity) and on stainless steel PREN; these dependence have not been study and Equations 6.6 and 6.7 are the originals:

$$\text{Eq. 6.6} \qquad r = 1 - (1 - r_{min}) \exp\left(-0{,}2 v^4\right)$$

$$\text{Eq. 6.7} \qquad r_{min} = \left(\frac{PREN}{50} \right)^{3,2}$$

6.4 Final consideration and future perspective

In Tables 6.1, 6.2 and 6.3 the experimental corrosion probabilities for AISI 430, 304 and 470LI stainless steels are compared with the old Markov model pitting probabilities and with those reviewed (calculated by means of Matlab®): especially for the less aggressive conditions, the gap between experimental and Markov model corrosion probabilities is decreased. For example for AISI 430 at 20°C and pH 7 the corrosion probability decreases from 42% to 14%; at polarization potential + 0,300 mV vs E_{corr} and 1000 mg/L Cl^- it remains unchanged for low PREN stainless steels and decreases, instead, from 96% to 28% for PREN 24 stainless steel.

Table 6.1- AISI 430 (PREN 17) experimental corrosion probability and Markov probabilities.

T (°C)	pH	Cl (mg/L)	E (V SCE)	Pc EXP	1-R Old Markov model	1-R Reviewed Markov model
20	7	100	-0,014	**0%**	42%	**14%**
		300		**0%**	84%	**55%**
		1000		**0%**	96%	**84%**
		100	-0,156	**10%**	64%	**57%**
		300		**5%**	93%	**91%**
		1000		**60%**	98%	**98%**
40	7	100	-0,014	**0%**	97%	**77%**
		300		**0%**	99%	**93%**
		1000		**0%**	100%	**98%**
		100	0,281	**95%**	99%	**95%**
		300		**100%**	100%	**99%**
		1000		**100%**	100%	**100%**

Table 6.2- AISI 304 (PREN 18) experimental corrosion probability and Markov probabilities.

T (°C)	pH	Cl (mg/L)	E (V SCE)	Pc EXP	1-R Old Markov model	1-R Reviewed Markov model
20	7	100	0,056	**0%**	34%	**21%**
		300		**0%**	84%	**72%**
		1000		**0%**	96%	**93%**
		100	0,166	**15%**	42%	**34%**
		300		**0%**	88%	**84%**
		1000		**10%**	97%	**96%**
40	7	100	-0,014	**0%**	95%	**61%**
		300		**0%**	98%	**97%**
		1000		**0%**	100%	**96%**
		100	0,256	**15%**	98%	**89%**
		300		**0%**	99%	**97%**
		1000		**25%**	100%	**99%**

Table 6.3- 470LI (PREN 24) experimental corrosion probability and Markov probabilities.

T (°C)	pH	Cl (mg/L)	E (V SCE)	Pc EXP	1-R Old Markov model	1-R Reviewed Markov model
20	**7**	100	-0,094	**0%**	0%	**0%**
		300		**0%**	1%	**0%**
		1000		**0%**	24%	**2%**
		100	0,156	**5%**	0%	**0%**
		300		**5%**	4%	**1%**
		1000		**15%**	96%	**28%**
40	**7**	100	0,006	**0%**	38%	**3%**
		300		**0%**	75%	**52%**
		1000		**0%**	92%	**24%**
		100	0,246	**5%**	60%	**3%**
		300		**0%**	88%	**42%**
		1000		**10%**	97%	**81%**

More work should be made to improve this five-steps Markov model, as laboratory tests, in order to obtain reliable values of protection potential for high PREN stainless steels (as potentiodynamic tests in deareated solution and potentiostatic scratch tests), and field tests, in order to compare "in field" corrosion probabilities to that predicted by Markov model. Furthermore, the crevice dependence of the critical chlorides threshold (Eq. 6.5) and *r*-probability dependence on fluidodynamic condition of the system (Eq. 6.6 and 6.7) must be studied.

APPENDIX A: Literature data collection.

PREN	Cl (mg/L)	Epitt (V SCE)	Reference
12	21000	-0,060	[2]
13	21000	-0,200	[11]
14	21000	-0,300	[11]
16	21000	0,100	[11]
16	21000	-0,100	[11]
17	**21000**	**0,025**	[1]
17	**21000**	**-0,080**	[1]
17	**17000**	**0,090**	[1]
17	**26000**	**-0,010**	[1]
17	**35000**	**-0,050**	[1]
17	**18000**	**-0,050**	[1]
17	**18000**	**-0,010**	[1]
17	**30000**	**-0,034**	[37]
18	**21000**	**0,110**	[35]
18	**30000**	**-0,024**	[37]
18	**21000**	**-0,045**	[11]
18	**21000**	**-0,080**	[11]
18	**21000**	**-0,070**	[11]
18	**35000**	**0,200**	[1]
18	**35000**	**0,500**	[1]
18	**21000**	**-0,060**	[11]
18	**21000**	**0,000**	[11]
18	**35000**	**-0,200**	[11]
18	**21000**	**0,280**	[35]
18	**21000**	**0,290**	[1]
18	**18000**	**0,030**	[1]
18	**18000**	**0,080**	[1]
18	**30000**	**0,056**	[37]
18	**21000**	**0,280**	[35]
18	**35000**	**0,090**	[1]
18	**35000**	**0,095**	[1]
19	**17500**	**0,300**	[1]
19	**26000**	**0,150**	[1]
19	**35000**	**-0,050**	[1]
19	**21000**	**-0,220**	[1]
20	**17500**	**0,190**	[1]
20	**26000**	**0,020**	[1]
20	**35000**	**-0,070**	[1]

PREN	Cl (mg/L)	Epitt (V SCE)	Reference
21	17500	0,430	[1]
21	26000	0,320	[1]
21	35000	0,202	[1]
21	35000	0,195	[1]
21	35000	0,170	[1]
22	21000	0,120	[11]
22	21000	0,150	[11]
22	35000	0,030	[11]
22	21000	0,490	[36]
22	18000	0,290	[1]
22	18000	0,230	[1]
23	30000	0,256	[37]
23	21000	0,000	[11]
24	35000	0,297	[1]
24	35000	0,224	[1]
25	19000	0,388	[36]
25	21000	0,410	[35]
25	22000	0,365	[36]
25	25000	0,332	[36]
25	6000	0,335	[11]
25	20000	0,335	[11]
25	90000	0,245	[11]
26	30000	0,116	[37]
26	21000	0,530	[35]
26	21000	0,140	[11]
29	35000	0,423	[1]
29	35000	0,413	[1]
31	21000	0,420	[11]
33	30000	0,956	[37]
34	35000	0,637	[1]
34	35000	0,680	[1]
44	19000	1,075	[36]
44	22000	1,025	[36]
44	25000	1,002	[36]
45	19000	1,182	[36]
45	22000	1,125	[36]
45	25000	1,108	[36]
46	19000	1,221	[36]

PREN	Cl (mg/L)	Epitt (V SCE)	Reference
46	22000	1,158	[36]
46	25000	1,139	[36]
52	19000	1,249	[36]
52	22000	1,182	[36]
52	25000	1,174	[36]

APPENDIX B: Density and cumulative distribution of the collected pitting potential.

Mean E_{pitt} (V SCE)	0,255
St. dev. (V SCE)	0,232

E (V SCE)	Density	Cumulative
-0,700	0,000	0,000
-0,675	0,001	0,000
-0,650	0,001	0,000
-0,625	0,001	0,000
-0,600	0,002	0,000
-0,575	0,003	0,000
-0,550	0,004	0,000
-0,525	0,006	0,000
-0,500	0,009	0,001
-0,475	0,012	0,001
-0,450	0,017	0,001
-0,425	0,023	0,002
-0,400	0,032	0,002
-0,375	0,043	0,003
-0,350	0,057	0,005
-0,325	0,075	0,006
-0,300	0,098	0,008
-0,275	0,126	0,011
-0,250	0,160	0,015
-0,225	0,201	0,019
-0,200	0,250	0,025
-0,175	0,307	0,032
-0,150	0,373	0,040
-0,125	0,448	0,050
-0,100	0,532	0,063
-0,075	0,624	0,077
-0,050	0,723	0,094
-0,025	0,829	0,113
0,000	0,939	0,135
0,025	1,051	0,160
0,050	1,164	0,188
0,075	1,273	0,218
0,100	1,376	0,252

E (V SCE)	Density	Cumulative
0,125	1,471	0,287
0,150	1,553	0,325
0,175	1,622	0,365
0,200	1,674	0,406
0,225	1,707	0,448
0,250	1,721	0,491
0,275	1,715	0,534
0,300	1,690	0,577
0,325	1,645	0,618
0,350	1,583	0,659
0,375	1,506	0,698
0,400	1,416	0,734
0,425	1,316	0,768
0,450	1,209	0,800
0,475	1,098	0,829
0,500	0,985	0,855
0,525	0,874	0,878
0,550	0,766	0,898
0,575	0,664	0,916
0,600	0,569	0,932
0,625	0,482	0,945
0,650	0,403	0,956
0,675	0,333	0,965
0,700	0,273	0,973
0,725	0,220	0,979
0,750	0,176	0,984
0,775	0,139	0,988
0,800	0,108	0,991
0,825	0,084	0,993
0,850	0,064	0,995
0,875	0,048	0,996
0,900	0,036	0,997
0,925	0,026	0,998
0,950	0,019	0,999
0,975	0,014	0,999
1,000	0,010	0,999

Pitting potential cumulative distribution.

P%	Epitt
5%	-0,126
10%	**-0,042**
15%	0,015
20%	0,060
25%	0,099
30%	0,134
35%	0,166
40%	0,196
45%	0,226
50%	0,255
55%	0,284
60%	0,314
65%	0,344
70%	0,377
75%	0,411
80%	0,450
85%	0,495
90%	0,552
95%	0,636
99%	0,794

Cumulative function used as model curve.

Eprot	-0,298	V SCE

P	E (V SCE)	E-Eprot
0,05	-0,126	0,172
0,1	-0,042	0,256
0,15	0,015	0,312
0,2	0,060	0,358
0,25	0,099	0,396
0,3	0,134	0,431
0,35	0,166	0,463
0,4	0,196	0,494
0,45	0,226	0,524
0,5	0,255	0,553
0,55	0,284	0,582
0,6	0,314	0,611
0,65	0,344	0,642
0,7	0,377	0,674
0,75	0,411	0,709
0,8	0,450	0,748
0,85	0,495	0,793
0,9	0,552	0,850
0,95	0,636	0,934
0,99	0,794	1,092

REFERENCES

[1] A. J. Sedriks, *Corrosion of stainless steels*, Wiley, 1979, pp. 282.

[2] *Austenitic stainless steels*, ASM International, Material Park, Ohio, USA.

[3] R. W. Revie, *Uhlig's corrosion handbook*, 2nd Ed., Wiley, 2000, pp. 1302.

[4] P. Pedeferri, *Corrosione e protezione dei materiali metallici*, Polipress, 2007, pp. 408.

[5] M. Pourbaix, *Atlas of electrochemical equilibria in aqueous solutions*, 2nd Ed., Houston: National association of corrosion engineers, 1974, pp. 644.

[6] G.S. Frankel, *Localized corrosion of metals: a review of the rate controlling factors in initiation and growth*, Electrochemical Society Proceedings, Vol. 99-42, pp. 445-475.

[7] J.R. Scully, *Corrosion tests and standards manual*, 2nd Ed., R. Baboian Editor, 2005, pp. 882.

[8] P. Pedeferri, *Metodi di prevenzione e protezione*, Corso di corrosione e protezione dei materiali 2004-2005, Politecnico di Milano.

[9] V. Boneschi, M. Boniardi, *Gli acciai inox e la resistenza alla corrosione*, Lamiera, 2008, pp. 124-131.

[10] W. Nicodemi, *Metallurgia, Principi generali*, 2nd Ed., Zanichelli, 2007, pp. 352.

[11] L.L Sheir, R.A. Jarman and G.T Burstein, *Corrosion Metal/Environment reactions*, 3rd Ed.,Vol.1, Butterworth Heinemann, 2000, pp. 3:35-3:77.

[12] G. Salvago, G. Fumagalli, *Valutazione degli effetti delle condizioni metallurgiche e della finitura superficiali sulla probabilità di attacco localizzato di acciai inossidabili*, Atti, Giornate nazionali sulla corrosione e protezione, 24-25 Maggio 1994, pp. 225-232.

[13] L. Magagnin, G. Salvago, *Statistical evaluation of localized corrosion for stainless steels ranking*, Corrosion Reviews, Vol. 19, Nos 3-4, 2001, pp. 347-366.

[14] A. Pardo, E. Otero, M.C. Merino, M.D. López, M.V. Utrilla, F. Moreno, *Influence of pH and chloride concentration on the pitting and crevice corrosion behavior of high-alloy stainless steels*, Corrosion engineering section, 2000, pp. 411-418.

[15] H. M. Ezuber, *Metallurgical and environmental factors affecting the pitting behavior of UNS S32205 duplex stainless steel in chloride solutions*, Materials and Corrosion No. 2, 2012, pp. 111-118..

[16] S. Ravasio, *Modello statistico a catena di Markov per la previsione dell'innesco del pitting su acciai inossidabili*, Tesi di laurea di primo livello, Politecnico di Milano, 2008, pp. 51.

[17] L. Lazzari, M. Ormellese, S. Ravasio, *Modello a matrici di Markov per la previsione dell'innesco del pitting di acciai inossidabili*, Politecnico di Milano.

[18] T. Shibata, *Statistical and stochastic approaches to localized corrosion*, W.R. Whitney Award Lecture, 1996, pp. 813-829.

[19] R. Fratesi, *Statistical estimate of the pitting potential of AISI 319L stainless steel in 3.5% NaCl measured by means of two electrochemical methods*, Corrosion NACE, Vol. 41, 1985, pp. 114-117.

[20] G. Salvago, G. Fumagalli, *The distribution of the breakdown potential of stainless steels: effects of test repetition, specimen exposure surfaces and threshold current*, Corrosion science, Vol. 37, No 8, 1995, 1303-1311.

[21] J. W. Provan, E. S. Rodrguez III, *Part I: Development of a Markov description of pitting corrosion*, Corrosion, 1989, pp. 177-192.

[22] ASTM G46, *Standard guide for examination and evaluation of pitting corrosion*, Reapproved 2005.

[23] P. Citti, G. Arcidiacono, G. Campatelli, *Fondamenti di affidabilità*, McGraw-Hill, 2003, pp. 192.

[24] F. Caleyo, J.C. Velazquez, A. Valor, J.M. Hallen, *Markov chain modelling of pitting corrosion in underground pipelines*, Corrosion Science, Vol. 51, 2009, pp. 2197-2207.

[25] E. S. Rodriguez III, *On a new Markov model for the pitting corrosion process and its application to reliability*, Work of thesis, McGill university, Montreal, 1986, pp. 273.

[26] C. M. Grinstead, J.L. Snell, *Introduction to probability*, 2nd Ed., American mathematical society, 2006, pp. 405-470.

[27] H. P. Hong, *Application of the stochastic process to pitting corrosion*, Corrosion, 1999, pp. 10-16.

[28] F. Caleyo, J.C. Velazquez, A. Valor, J.M. Hallen, *Markov chain modelling of pitting corrosion in underground pipelines*, Corrosion Science, Vol. 51, 2009, pp. 2197-2207.

[29] A. Valor, F. Caleyo, L. Alfonso, D. Rivas, J.M. Hallen, *Stochastic modelling of pitting corrosion: a new model for initiation and growth of multiple corrosion pits*, Corrosion Science, Vol. 49, 2007, pp. 559-579.

[30] F. Bolzoni, P. Fassina, G. Fumagalli, L. Lazzari, E. Mazzola, *Application of probabilistic models to localized corrosion study*, Metallurgia Italiana 98, 2006, pp. 9-15.

[31] G. Contreras, P. Fassina, G. Fumagalli, S. Goidanich, L. Lazzari, E. Mazzola, *A study on metastability phenomena of passive films for corrosion resistant alloys*, Electrochemical acta, 2007, pp. 1-22.

[32] C. Alonso, M. Castellote, C. Andrade, Chloride *threshold dependence of pitting potential of reinforcements*, Electrochimica Acta, Vol. 47, 2002, pp. 3469-3481.

[33] T. Shibata, *Corrosion probability and statistical evaluation of corrosion data*, Uhlig's corrosion handbook, 2nd Ed., Wiley, 2000, pp. 367-391.

[34] ASTM G31, *Standard practice for laboratory immersion corrosion testing of metals*, 2012.

[35] L. Felloni, R. Fratesi, O. Ruggeri, G. Sambogna, *Pitting ad crevice corrosion potentials of sola1 panel stainless steels in seawater and 0.6M NaCl*, Corrosion NACE, Vol. 41, 1985, pp. 169-177.

[36] G. Latha, S. Rajeswari, *Pitting and crevice corrosion behavior of superaustenitic stainless steel in sea water cooling system*, Corrosion Reviews, Vol.18, No.6, 2000, pp. 429-456.

[37] R.W. Staehle, B.F. Brown, *Localized corrosion*, NACE 1, 1974, pp. 749.

[38] ASTM G61, *Standard test method for conducting cyclic potentiodynamic polarization measurements for localized corrosion susceptibility of iron-, nickel-, or cobalt-based alloy*s, Reapproved 2009.